2008-12

Adaptive filter techniques for optical beam jitter control and target tracking

Beerer, Michael J.

Monterey, California. Naval Postgraduate School

NAVAL POSTGRADUATE SCHOOL

MONTEREY, CALIFORNIA

THESIS

ADAPTIVE FILTER TECHNIQUES FOR OPTICAL BEAM JITTER CONTROL AND TARGET TRACKING

by

Michael J. Beerer

December 2008

Thesis Advisor:	Brij N. Agrawal
Co-Advisor:	Andres Larraza
Second Reader:	Hyungjoon Yoon

Approved for public release; distribution is unlimited

THIS PAGE INTENTIONALLY LEFT BLANK

REPORT DOCUMENTATION PAGE			Form Approved OMB No. 0704-0188
Public reporting burden for this collection of information is estimated to average 1 hour per response, including the time for reviewing instruction, searching existing data sources, gathering and maintaining the data needed, and completing and reviewing the collection of information. Send comments regarding this burden estimate or any other aspect of this collection of information, including suggestions for reducing this burden, to Washington headquarters Services, Directorate for Information Operations and Reports, 1215 Jefferson Davis Highway, Suite 1204, Arlington, VA 22202-4302, and to the Office of Management and Budget, Paperwork Reduction Project (0704-0188) Washington DC 20503.			
1. AGENCY USE ONLY *(Leave blank)*	**2. REPORT DATE** December 2008	**3. REPORT TYPE AND DATES COVERED** Master's Thesis	
4. TITLE AND SUBTITLE Adaptive Filter Techniques for Optical Beam Jitter Control and Target Tracking		**5. FUNDING NUMBERS**	
6. AUTHOR(S) Michael J. Beerer			
7. PERFORMING ORGANIZATION NAME(S) AND ADDRESS(ES) Naval Postgraduate School Monterey, CA 93943-5000		**8. PERFORMING ORGANIZATION REPORT NUMBER**	
9. SPONSORING /MONITORING AGENCY NAME(S) AND ADDRESS(ES) N/A		**10. SPONSORING/MONITORING AGENCY REPORT NUMBER**	
11. SUPPLEMENTARY NOTES The views expressed in this thesis are those of the author and do not reflect the official policy or position of the Department of Defense or the U.S. Government.			
12a. DISTRIBUTION / AVAILABILITY STATEMENT Approved for public release; distribution is unlimited.		**12b. DISTRIBUTION CODE**	

13. ABSTRACT (maximum 200 words)

The objective of this research is to develop advanced control methods to attenuate laser beam jitter using a fast-steering mirror. Adaptive filter controllers using Filtered-X Least Mean Square (FX-LMS) and Filtered-X Recursive Least Square (FX-RLS) algorithms are explored. The disturbances that cause beam jitter include mechanical vibrations on the optical platform (narrowband) and atmospheric turbulence (broadband). Both feedforward filters (with the use of auxiliary reference sensor(s)) and feedback filters (with only output feedback) are investigated. Hybrid adaptive filters, which are a combination of feedback and feedforward, are also examined. For situations when obtaining a coherent feedforward reference signal is not possible, methods for incorporating multiple semi-coherent reference signals into the control law are developed. The controllers are tested on a jitter control testbed to prove their functionality for beam pointing at static and dynamic targets. The testbed is equipped with shakers mounted to the optical platform and a disturbance fast-steering mirror to simulate the effects of atmospheric propagation. Experimental results showed that the developed control laws (multiple reference feedforward, feedback and hybrid) had superior performance to the fully coherent reference feedforward adaptive filter controller.

14. SUBJECT TERMS Adaptive Filter, Filtered-X, Least Mean Square, Recursive Least Square, Jitter Control, Beam Control, Target Tracking, Beam Pointing			**15. NUMBER OF PAGES** 117
			16. PRICE CODE
17. SECURITY CLASSIFICATION OF REPORT Unclassified	**18. SECURITY CLASSIFICATION OF THIS PAGE** Unclassified	**19. SECURITY CLASSIFICATION OF ABSTRACT** Unclassified	**20. LIMITATION OF ABSTRACT** UU

NSN 7540-01-280-5500 Standard Form 298 (Rev. 2-89)
Prescribed by ANSI Std. 239-18

THIS PAGE INTENTIONALLY LEFT BLANK

Approved for public release; distribution is unlimited

ADAPTIVE FILTER TECHNIQUES FOR OPTICAL BEAM JITTER CONTROL AND TARGET TRACKING

Michael J. Beerer
Civilian, United States Air Force
B.S., University of California Irvine, 2006

Submitted in partial fulfillment of the
requirements for the degree of

MASTER OF SCIENCE IN APPLIED PHYSICS

from the

NAVAL POSTGRADUATE SCHOOL
December 2008

Author: Michael J. Beerer

Approved by: Brij N. Agrawal
Thesis Advisor

Andres Larraza
Co-Advisor

Hyungjoon Yoon
Second Reader

James H. Luscombe
Chairman, Department of Physics

THIS PAGE INTENTIONALLY LEFT BLANK

ABSTRACT

The objective of this research is to develop advanced control methods to attenuate laser beam jitter using a fast-steering mirror. Adaptive filter controllers using Filtered-X Least Mean Square (FX-LMS) and Filtered-X Recursive Least Square (FX-RLS) algorithms are explored. The disturbances that cause beam jitter include mechanical vibrations on the optical platform (narrowband) and atmospheric turbulence (broadband). Both feedforward filters (with the use of auxiliary reference sensor(s)) and feedback filters (with only output feedback) are investigated. Hybrid adaptive filters, which are a combination of feedback and feedforward, are also examined. For situations when obtaining a coherent feedforward reference signal is not possible, methods for incorporating multiple semi-coherent reference signals into the control law are developed. The controllers are tested on a jitter control testbed to prove their functionality for beam pointing at static and dynamic targets. The testbed is equipped with shakers mounted to the optical platform and a disturbance fast-steering mirror to simulate the effects of atmospheric propagation. Experimental results showed that the developed control laws (multiple reference feedforward, feedback and hybrid) had superior performance to the fully coherent reference feedforward adaptive filter.

THIS PAGE INTENTIONALLY LEFT BLANK

TABLE OF CONTENTS

THIS PAGE INTENTIONALLY LEFT BLANK

LIST OF FIGURES

LIST OF TABLES

THIS PAGE INTENTIONALLY LEFT BLANK

EXECUTIVE SUMMARY

The objective of this research is to develop advanced control methods to attenuate laser beam jitter using a fast-steering mirror. The intent is to point an optical beam accurately at a target in the presence of jitter. The disturbances that cause beam jitter can be time-varying and include mechanical vibrations on the optical platform as well as jitter induced by propagation through a turbulent atmosphere. Mechanical vibrations caused by rotary or repetitive devices (engines, actuators, electric motors, etc) onboard the optics platform cause narrowband jitter. Jitter caused by atmospheric propagation is spread over a wide range of frequencies causing broadband jitter. Methods for attenuating these disturbances must be developed in order to allow high precision optical devices to operate.

In order to study improved techniques for jitter control, the Jitter Control Testbed was developed at Naval Postgraduate School. Optical components are mounted on a floating platform used to simulate a spacecraft/aircraft's vibrational environment. Multiple shakers are mounted on the platform to create narrowband vibrations along different axes of the platform and a 3-axis accelerometer provides signals correlated with the shaker disturbances. A fast-steering mirror is also mounted on the platform and attempts to cancel out the beam jitter.

Adaptive control techniques have shown the greatest potential over linear time-invariant controllers. The characteristics of atmospheric turbulence and optical payloads can change and thus fixed-parameter control algorithms cannot effectively attenuate this time-varying jitter. In this thesis, adaptive filter controllers using Filtered-X Least Mean Square (FX-LMS) and Filtered-X Recursive Least Square (FX-RLS) algorithms are investigated with various application scenarios. Both feedforward filters (with the use of auxiliary reference sensor(s)) and feedback filters (with only output feedback) are examined.

The feedfoward control method requires a reference signal that is highly correlated with the disturbances. Obtaining such a signal is often not possible in practice,

however, other signals may be available that are correlated with only portions of the total beam jitter. Methods for incorporating multiple semi-coherent reference signals into the feedforward control law are developed. Feedback techniques, which do not require a reference signal, and hybrid adaptive filters, which combine the feedforward and feedback methods, are also examined.

The controllers are tested on the Jitter Control Testbed to prove their functionality for beam pointing at static and dynamic targets. Experimental results showed that the multiple reference signal feedforward controller preformed as well as or better than the single reference controller. The feedback and hybrid controllers provided the best overall performance.

ACKNOWLEDGMENTS

I would like to thank my advisor, Professor Brij Agrawal, for providing me the opportunity to work in the state-of-the-art Spacecraft Research and Design Center (SRDC) at NPS. Professor Agrawal obtained all the necessary funding and provided the essential resources needed to conduct this research. The entire SRDC staff was extremely supportive of my efforts. I thank Professor Andres Larraza for co-advising this thesis. Professor Larraza was also extremely helpful when I was first applying to NPS. His actions were implemental for my sponsor to grant me an additional quarter of study at NPS.

I thank Dr. Hyungjoon Yoon for his invaluable guidance and support while conducting this research. During my first few months of research, Dr. Yoon gave me weekly lessons on advanced control theory and instruction on the jitter control testbed hardware and software. Once I was more or less acquainted with adaptive filter theory and the testbed, Dr. Yoon met with me almost daily to discuss the direction of the jitter control research and assist me in applying the theory to the testbed. Dr. Yoon encouraged me to solve problems and overcome obstacles on my own, and for that, I am truly grateful.

I thank my sponsor, the USAF Civilian Palace Acquire program, for paying me to go to school for the past year and granting me additional time to study, which made all the difference when writing this thesis. I consider myself extremely fortunate to have had the chance to pursue a Master's degree while working for the Air Force. I thank my home office, the Electronic Warfare Group at Edwards Air Force Base, for providing me this great opportunity and giving me much support while I was away.

Finally, I thank all my friends and family, for without them, all else is meaningless. Even optical beam jitter control!

THIS PAGE INTENTIONALLY LEFT BLANK

I. INTRODUCTION

A. MOTIVATION

Optical beam jitter control has become a topic of great interest with applications in directed energy weapons, free-space laser communications and adaptive optics. The objective of this research is to point a laser beam accurately at a target in the presence of jitter. Optical beam jitter is defined as rotational motion (pitch and yaw) of an optical beam away from line of sight. It is generally an angular quantity (measured in radians), but the errors are manifested when the beam strikes some two-dimensional surface, such as a CCD array, and is then measured as a distance or number of pixels [1].

The disturbances that cause beam jitter can be time-varying and include mechanical vibrations on the optical platform as well as jitter induced by propagation through a turbulent atmosphere. Mechanical vibrations caused by rotary or repetitive devices (engines, actuators, electric motors, etc) onboard the optics platform cause narrowband jitter. Jitter caused by atmospheric propagation is spread over a wide range of frequencies causing broadband jitter. Methods for attenuating these disturbances must be developed in order to allow high precision optical devices to operate.

The primary tools used for controlling the optical beam are a fast-steering mirror and beam position sensors. The sensors feed information to a control computer that in turn commands the steering mirror to tip and tilt to remove the jitter from the beam. Due to the complex nature of the disturbances, advanced control techniques are essential. These control techniques, specifically adaptive filter methods, are the focus of this thesis.

Many methods to control optical beam jitter using a fast-steering mirror have been proposed in the literature. Classical feedback control techniques such as proportional-integral-derivative (PID) control and linear-quadratic-Gaussian (LQG) control have difficulty handling the time-varying nature of the disturbances [2]-[4]. The gains of linear time-invariant controllers can only be tuned to specific disturbance characteristics.

Adaptive control techniques, specifically adaptive filters, have shown the greatest potential for controlling optical beam jitter. Professor Gibson and his research team at UCLA have published several papers on beam jitter control using a feedback multichannel recursive-least-squares (RLS) lattice filter algorithm [5] - [11]. McEver et al. proposed adaptive feedback control using the *Q*-parameterization method [12].

Feedforward adaptive filter control methods have been the main focus of study at Naval Postgraduate School (NPS) [2], [3], [4] and [13]. This technique may be used when a reference signal, which is correlated with the disturbance(s), is available. Watkins and Agrawal proposed a Filtered-X Least Mean Square (FX-LMS) adaptive feedforward controller [2], [3]. Yoon et al. proposed a Filtered-X Recursive Least Square (FX-RLS) controller with an integrated bias estimator for canceling time-varying optical beam jitter [13]. Outside of NPS, this technique has also been studied by Anderson et al. at CSA Engineering [1].

While feedforward adaptive control has shown great promise, it has one major disadvantage in that it requires a reference signal. The reference signal must be highly correlated (coherent) with the disturbance(s) and is fed forward to the controller [14]. An auxiliary reference sensor measures the disturbance and provides the reference signal. In many real-life applications, it is not possible to obtain a single reference signal that is correlated with the entire frequency content of the disturbance(s).

In this thesis, we develop adaptive filter methods that do not require a single fully coherent reference signal. First, feedforward techniques are developed that fuse together information from multiple semi-coherent reference signals. In these situations, reference signals are available that are only correlated with some component of the total disturbance. We also develop feedback adaptive filter methods that do not require any reference signal and hybrid feedback/feedforward techniques that combine both methods. These modifications give the adaptive filter control technique more functionality in applications where a single coherent reference signal (and corresponding sensor) is not available.

The developed control techniques are tested on a jitter control testbed to prove their functionality for beam pointing at static and dynamic targets. The results are compared with those from [2], [3], [4] and [13], where feedforward adaptive filter techniques were studied using a single fully coherent reference signal.

B. THESIS OVERVIEW

Chapter II describes the set-up on the Jitter Control Testbed at Naval Postgraduate School.

Chapter III summarizes the topic of active noise control and its application for optical beam jitter control.

Chapter IV provides a review of adaptive filter theory including the Wiener filter, FX-LMS and FX-RLS algorithms. In addition, the multiple reference signal feedforward, feedback and hybrids method are presented.

Chapter V briefly explains system identification and the methods used to obtain the plant model on the JCT.

Chapter VI describes the disturbance sources on the jitter control testbed in detail and summarizes a study on the degree of correlation between the various disturbance sources and the individual reference sensors.

Chapter VII provides the results of the jitter rejection experiments where the developed control techniques are tested and compared.

Chapter VIII demonstrates the use of adaptive filter algorithms for dynamic target tracking and beam pointing.

THIS PAGE INTENTIONALLY LEFT BLANK

II. EXPERIMENTAL SETUP

The Jitter Control Testbed (JCT) at the Spacecraft Research and Design Center (SRDC), at Naval Postgraduate School, Monterey, CA was used for this research. The testbed contains a laser source, 3-axis accelerometer, beam splitter, two inertial actuators (shakers), two position sensing detectors (PSD, referred to as OT-1 and OT-2) and two fast-steering mirrors, a control fast-steering mirror (CFSM) and a disturbance fast-steering mirror (DFSM). These components are mounted on a floating platform that is used to simulate a spacecraft/aircraft's vibrational environment. Two shakers are mounted orthogonally to one another to create vibrations along different axes of the platform. A 3-axis accelerometer is mounted near the shakers to provide signals correlated with the shaker disturbances.

A. JITTER CONTROL TESTBED OVERVIEW

A 5 mW He-Ne laser on JCT propagates from the source to the DFSM where both axes are given a band-limited broadband disturbance (0-200 Hz) to simulate the effects of atmospheric turbulence. The beam passes onto the vibration platform and to the CFSM where control inputs are applied to the beam from the control computer. The beam then propagates to the target PSD (OT-2) that is providing an error signal (the difference between the desired beam location and the actual location) to the control computer. The goal is to point the beam accurately at the target sensor in the presence of the disturbances. In order to simulate various beam control scenarios, the target sensor (OT-2) was mounted both on-board and off-board the vibration platform during the experiments. A beam splitter redirects the beam onto the reference signal PSD (OT-1). All of the optics on-board the vibration platform are subjected to the shaker disturbances. The beam position at the PSDs is reported in the Axis-1 and Axis-2 coordinate frame while the accelerometer signals are reported in X, Y and Z coordinates, both shown in Figure 1.

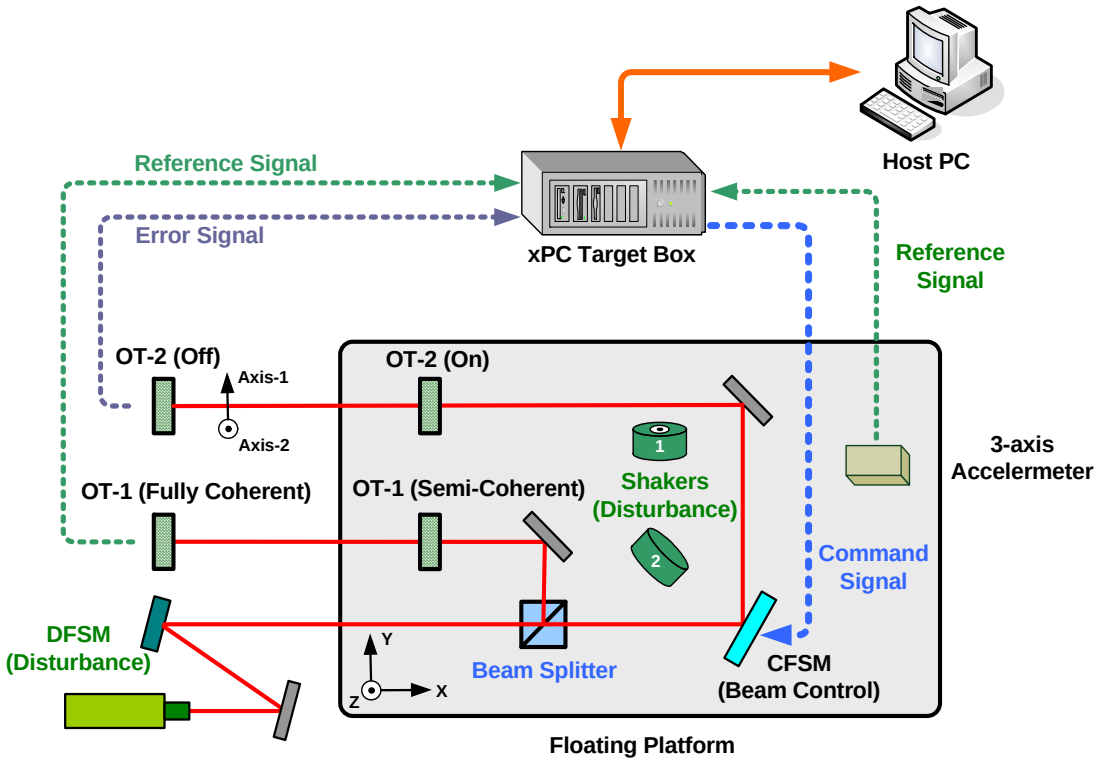

Figure 1. Experimental setup.

The position sensor OT-1 is one of the feedforward reference sensors on the JCT. When OT-1 is mounted off the vibration platform, as in [2], [3], [4] and [13], it provides a fully coherent reference signal that is highly correlated with both the disturbances from the DFSM and the shakers. This configuration, however, may not reflect real spacecraft/aircraft applications. When OT-1 is mounted on the vibration platform and subjected to the shaker disturbance, it continues to provide a signal correlated with the DFSM disturbance but its correlation with the shaker disturbances is degraded. In this configuration, an additional reference sensor with shaker correlation (provided by the accelerometer) is necessary to carry out feedforward control. The degree of correlation between the various reference sensors and the disturbances is addressed in Chapter VI.

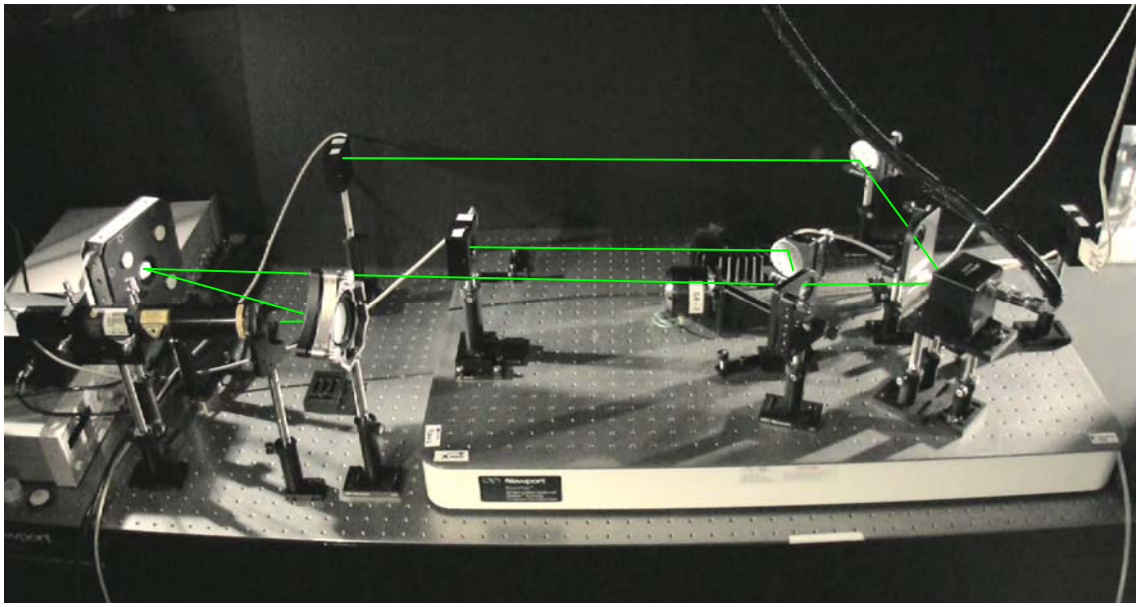

Figure 2. Jitter Control Testbed

B. POSITION SENSING DETECTORS

The position sensing detectors used for the experiments are On-Trak PSM2-10 position sensing modules with OT-301 amplifiers. The 10 mm by 10 mm detectors are photodiodes that provide an analog output directly proportional to the beam centroid Axis-1 and Axis-2 positions. The amplifier output range is ±10 V corresponding to ± 5 mm from the center of the detector. The amplifier has a noise level of 1 mV, and therefore, a minimum resolution of 0.5 μm. The frequency response of the sensor is approximately 15 kHz [3].

Figure 3. On-Trak Position Sensing Detector

C. FAST-STEERING MIRRORS

1. Control Mirror – Newport Fast-Steering Mirror

The control mirror is a Newport FSM200 with a FSM-CD-100 controller box. The two inch diameter mirror is mounted on four voice coils that steer the mirror on two axes. An analog voltage input, in the range of ±10 V, commands the mirror to tip and tilt. The mirror has a control bandwidth of approximately 800 Hz and a throw of ±26.2 milliradians. The controller box allows both open-loop and closed-loop control of the mirror and also outputs the mirror position. For these experiments, the mirror was used in the internal closed-loop mode and the mirror position information was not utilized. The mirror is suspended by very weak springs to minimize the necessary current to move the mirror. As a result, the internal closed-loop controller is necessary to stabilize the mirror position [3].

Figure 4. Newport Control Fast-Steering Mirror

2. Disturbance Mirror – Baker Fast-Steering

The disturbance mirror is a Baker "Light Force One" fast-steering mirror. The one inch diameter mirror is suspended by stiffer springs than the Newport mirror and operates in an open-loop mode. The Baker mirror has a control bandwidth of 3 kHz.

Figure 5. Baker Disturbance Fast-Steering Mirror

D. INERTIAL ACTUATORS

1. Shaker 1 – Aura Pro Bass Shaker

Shaker 1 is an Aura AST-2B-4 Pro Bass Shaker. The intended use for this device is to provide extra thump for high-end audio entertainment systems. The shaker has a usable bandwidth of 20 to 80 Hz and a resonance frequency of 40 Hz. The shaker is mounted along the Z axis of the table and testing with the accelerometer showed that it created vibration primarily along the Z axis. The sinusoidal signals that drive both shakers are amplified by Kepco, model BOP 20-10M, amplifier/power supplies.

2. Shaker 2 – CSA Engineering Inertial Actuator

Shaker 2 is a CSA, model SA-5, inertial actuator that can provide a force of 5 lbf in the bandwidth of 20 to 1000 Hz. The shaker has a resonance frequency of approximately 60 Hz. The intended use for this device is to be an actuator for active vibration control, a possible topic of future study on the JCT. The shaker has an electromagnetic circuit with a moving magnet that delivers the force along the cylindrical axis [3]. For this experiment the shaker was mounted horizontally to the platform in order to provide vibrations along the X and Y axes. Testing with the accelerometer showed that this position actually created vibrational motion along all three axes of the platform.

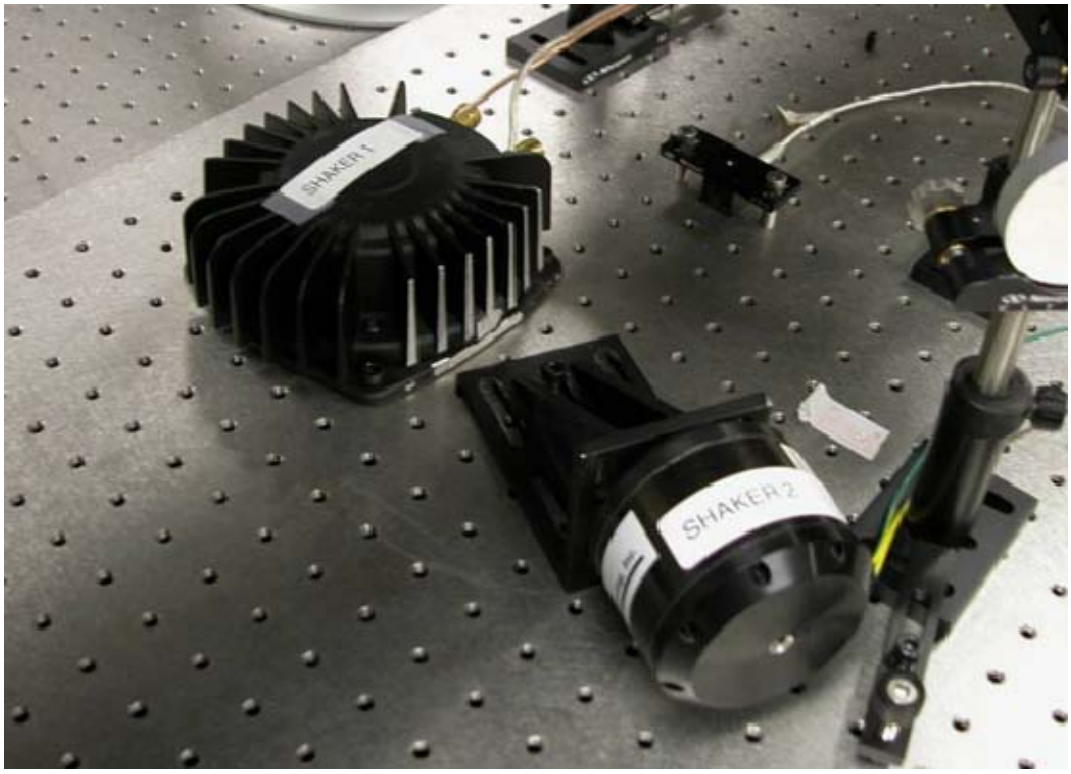

Figure 6. Aura (Shaker 1) and CSA (Shaker 2) inertial actuators.

E. ACCELEROMETER

A Kistler model 8690C10 3-axis accelerometer driven by a Kistler Piezotron Coupler, model 5124A, is used to measure the disturbance generated by the two shakers. The accelerometer outputs an analog ± 5 V signal for the X, Y and Z axes. The device has a ± 10 g range and 5 kHz frequency response.

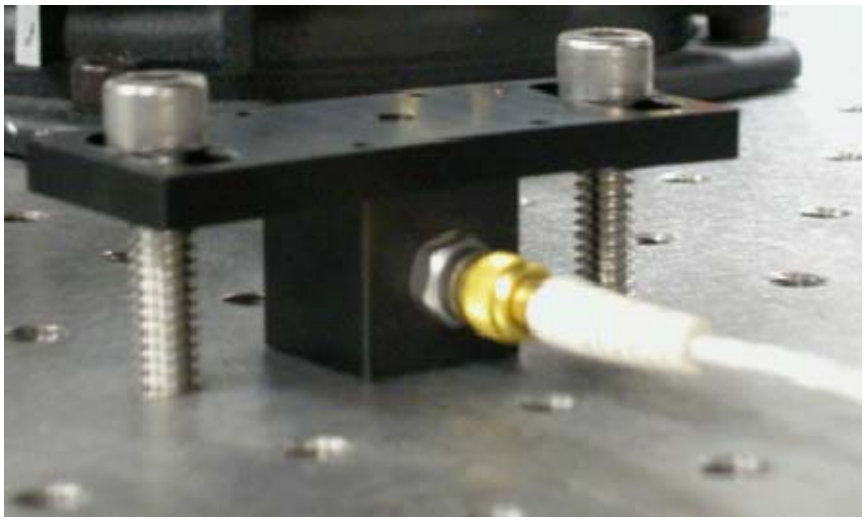

Figure 7. Kistler Accelerometer mounted on the vibration platform.

F. VIBRATION ISOLATION PLATFORMS

1. Newport Optical Table

The jitter control testbed sits on a Newport RS4000 Breadboard optical table mounted on four Newport I-2000 vibration isolators. The table is used to provide a vibration free environment for the vibration platform to rest on.

2. Newport Vibration Isolation Platform

A Newport BenchTop, model BT-2436, vibration isolation platform is mounted on top of the optical bench. The two shakers, CFSM, on-board PSDs, turning mirrors and accelerometer are mounted on the platform which simulates an aircraft/spacecraft's vibrational environment. This platform was originally designed to isolate the breadboard

from ground vibrations. In this experiment, the system is used in reverse, isolating the optical bench below from the shaker disturbances on the platform. The feasibility of this configuration was addressed by a previous researcher and found to be viable [3].

G. COMPUTER CONTROL SYSTEM AND SOFTWARE

Two computers are used on the testbed, a host PC and an xPC targetbox. Control algorithms are created in the host PC using MATLAB, version R2007b, Simulink with Real-Time Workshop and xPC Target. The algorithms are compiled by the host PC and downloaded to the xPC targetbox to be run in real-time on the JCT. Data acquisition and control commands on the xPC targetbox (control computer) are executed at 2 kHz.

The host PC is a Dell Precision 490 Workstation with dual-core 2.00 GHz Intel Xenon processor and 2.0 GB of RAM. The xPC targetbox is a Dell Precision 390 Workstation with an Intel Xenon quad-core 2.66 GHz processor and 3.5 GB of RAM. The targetbox is configured with a Measurement Computing PCI-DAS1602/16 A/D input board and PCIM-DDA06/16 D/A output board. The input board allows eight 16-bit analog inputs and the output board has six 16-bit analog outputs.

A signal flow diagram is shown in Figure 8. The host PC and targetbox communicate via a direct network connection using a crossover Ethernet cable.

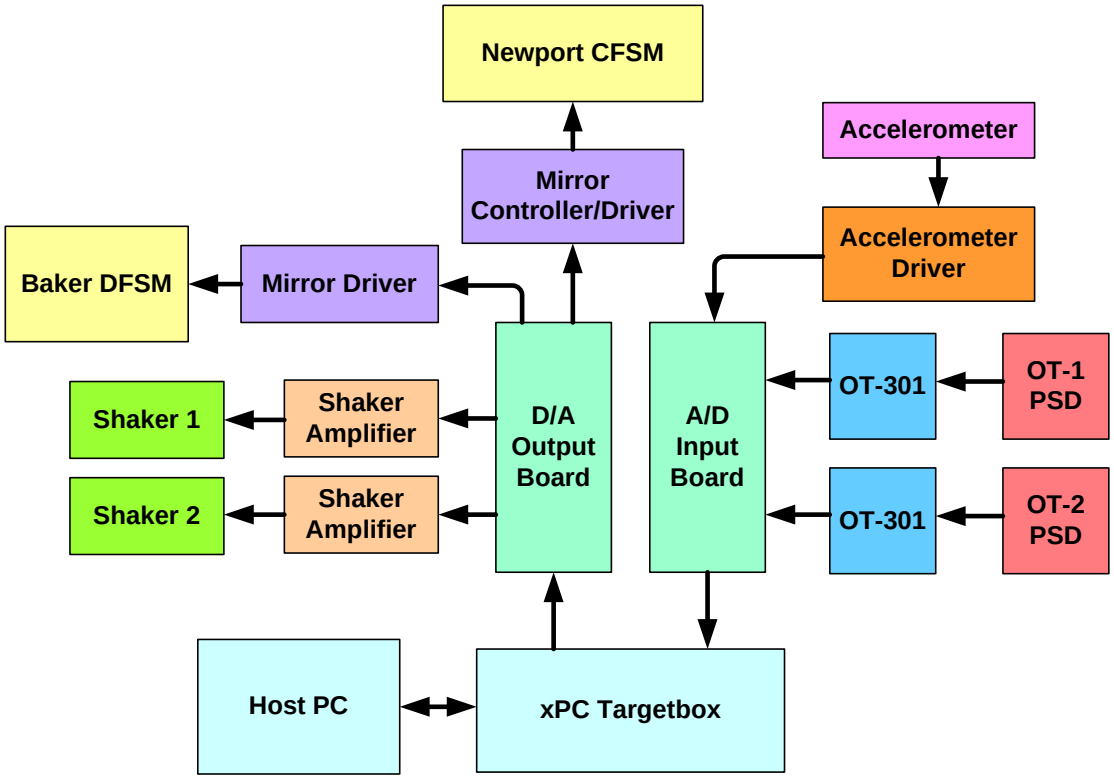

Figure 8. Signal Flow Diagram.

III. ACTIVE-NOISE CONTROL

The subject of Active Noise Control (ANC) was first developed in the field of acoustics and has only recently been adapted to optical beam control applications. In fact, most beam control systems still use classical control theory because its performance characteristics are well understood. Active noise control theory using adaptive filters is on the cutting edge of beam jitter control methods and can mainly be found today in research laboratories. On the contrary, with the advent of high speed digital signal processing, adaptive filter theory for controlling acoustic noise has matured over the past 30 years with ongoing research. Active noise control has even found its way into many households in noise canceling headphones and Bluetooth headsets [14].

Active noise control is used when performance specifications cannot be met by purely passive techniques. Passive noise control techniques include silencers and noise barriers in acoustics or mass-spring-damper systems in vibration control. ANC works on the principle of superposition and produces an anti-noise signal to cancel the unwanted noise at the target or error sensor. ANC for acoustics applications uses a loud speaker as a control actuator. ANC can be applied to vibration control using an inertial actuator or optical beam control using a fast-steering mirror [14].

ANC is based on either *feedforward control*, where a coherent reference noise input is sensed before it propagates past the control actuator, or *feedback control*, where the active noise controller attempts to cancel the noise without the benefit of an "upstream" reference input [14]. In either case, an error sensor located at the target provides a signal that is the sum of the primary noise and the control input from the actuator. In acoustics, a microphone would be used as the error sensor while a position sensor (PSD) is used in beam control [14].

On the Jitter Control Testbed, the axes of the CFSM are uncoupled, and therefore, the control inputs are applied independently. In adaptive filter theory this configuration is

referred to as single channel. The analogous situation in acoustics is sound traveling in a one dimensional duct. This example is used to illustrate feedforward and feedback ANC in the following sections.

A. FEEDFORWARD ANC

In feedforward ANC, a reference sensor is placed upstream of the control actuator and error sensor to provide a reference signal correlated with the noise. In Figure 9, the ANC system directly uses the reference signal, $r(t)$, to generate a command signal, $y(t)$, for the canceling speaker. An adaptive filter in the ANC box attempts to minimize the residual noise at the target, $e(t)$ [14]. For good noise rejection, the reference input must be both coherent and casual with the disturbance source, $d(t)$ [14]. A coherent reference signal is one that contains the same frequency information as the disturbance and a casual reference signal senses the disturbance early enough for the controller to compensate for it [4].

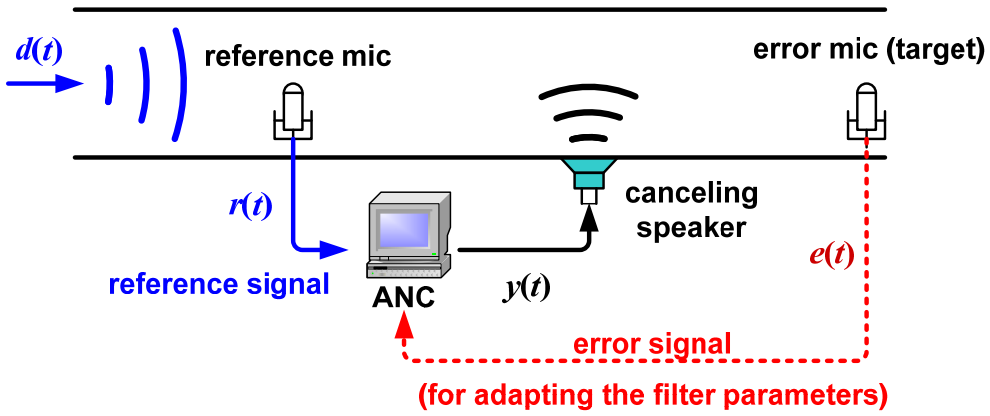

Figure 9. Feedforward ANC example.

An issue that affects most ANC applications is that the control signal, $y(t)$, cannot be directly added to the noise signal, $d(t)$, to find the error signal. The control signal must first pass through the actuator (loud speaker or CFSM) before its effect reaches the error sensor. In ANC lingo, $y(t)$ must first pass through the *secondary plant* dynamics of the

system before reaching the error sensor [14]. This fact has important implications in the analysis and design of the control system and will be addressed in Chapter IV.

B. FEEDBACK ANC

Feedback ANC does not have the reference sensor input, and therefore, must create control commands using only the error signal. The feedback methods employed in this thesis are developed in [14] and use an internally generated reference signal. This signal is created by summing the error signal, $e(t)$, and the control signal, $y(t)$. This technique (explained in more detail in Chapter IV) can be interpreted as using a linear predictor to estimate the noise source(s), $d(t)$, for use as a reference signal [14].

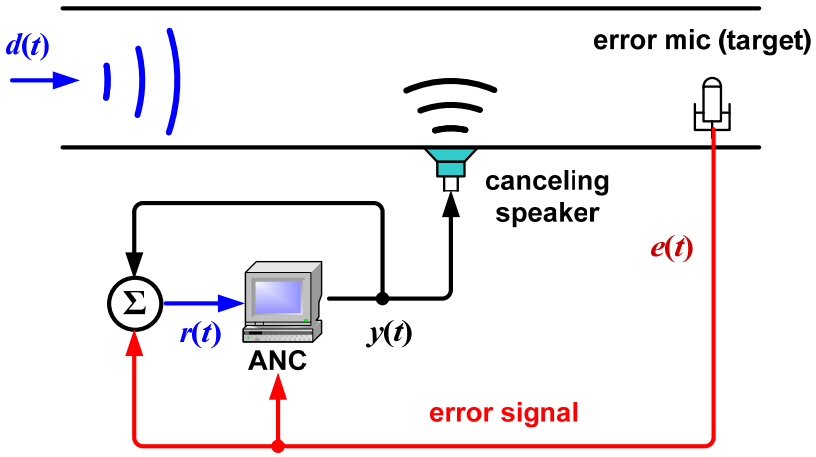

Figure 10. Feedback ANC example.

C. ANC APPLIED TO OPTICAL BEAM CONTROL

1. Broadband vs. Narrowband Disturbances

There are two categories of noise that can exist in the environment, broadband and narrowband. Broadband noise is caused by totally random processes, such as beam propagation through turbulence, and therefore, distributes its energy evenly across the frequency band. Narrowband noise concentrates most of its energy at specific frequencies.

This noise is usually related to rotating or repetitive devices. Broadband noise is referred to as *non-predictive* noise because of its random nature. On the contrary, narrowband noise is *predictive* because of its periodicity.

2. Causality Requirement

In [14], Kuo states that for feedforward broadband (non-predictive) noise cancellation, the reference input must give a sufficiently advanced indication of the approaching noise (causality requirement). For the case of optical beam control, this requirement cannot be met. Unlike the acoustics analogy, optical beams travel at light speed and the broadband disturbance from the DFSM reaches both the reference sensor and error sensor at virtually the same time. This results in a total loss of causality in the reference signal. However, some broadband disturbance can still be controlled if the disturbance is slowly changing compared to the controller bandwidth [4]. This is the case for the experiments in this thesis. The broadband disturbance (DFSM) is band-limited white noise between 0 and 200 Hz while the controller operates at 2 kHz.

3. Feedforward vs. Feedback ANC

In the acoustics field, feedback ANC has limitations because it does not use a reference signal to sample the disturbance before it impacts the error sensor. Without a reference sensor, Kuo refers to the feedback method as a narrowband (predictive) noise controller only [14]. However, we have just discovered that all ANC methods applied to optical beam control cannot meet the causality requirement. Therefore, we are limited to controlling only predictive noise and low frequency (relative to the control bandwidth) non-predictive noise. This fact brings to question the utility of the reference sensor. If the reference sensor cannot provide an advanced indication of approaching noise, then what good does it do?

In feedforward control, the disturbance is directly measured with a reference sensor; while in feedback control, the disturbance source is estimated. For optical beam

ANC, the superior method is the one that can produce the superior reference signal, i.e., the reference signal that is most correlated with the noise source. This, however, can be determined by experiment only.

Kuo also states that the feedforward method is generally more stable and robust than the feedback method [14]. These are other factors that weigh in on the superiority of either method, and also must be observed by experiment.

4. Reference Signals

A single reference feedforward adaptive filter requires a reference signal correlated with all disturbances. In [1], Anderson et al. demonstrate feedforward jitter control using the signal directly from the disturbance signal generator as a reference. By using such a signal, they are guaranteed that it is fully coherent. Such a set-up would obviously not work in practice because real disturbances are not created by signal generators.

On the Jitter Control Testbed, an off-board PSD (OT-1) can provide a reference signal that is correlated with both the broadband DFSM and narrowband shaker disturbances. The experiments on the jitter control testbed from [2], [3], [4] and [13] used such a signal.

For the experiments in this thesis, OT-1 is mounted on-board the vibration platform and only provides a signal correlated with the DFSM disturbance. In order to effectively do feedforward ANC, we additionally employ an accelerometer reference sensor. This second reference signal is correlated with the shaker disturbances. Methods for employing multiple reference signals in the control law will be developed in Chapter IV.

THIS PAGE INTENTIONALLY LEFT BLANK

IV. ADAPTIVE FILTER CONTROLLERS

Now that a basic overview of ANC techniques has been presented, it is possible to further discuss the control laws employed inside the ANC box from Figures 9 and 10. Prior research on the JCT demonstrated the superiority of adaptive controllers, particularly adaptive filters, when compared to classical linear time-invariant control laws [2], [3], [4], [13]. This thesis aims to further develop adaptive filter techniques so that they are more practical to implement in real-life beam control applications.

A. REVIEW OF DISCRETE-TIME CONTROL SYSTEMS

Discrete-time control systems are those that input and output non-continuous (sampled) values. For advanced control techniques, discrete (digital) controllers are preferred over continuous-time (analog) because they are easier to implement on modern digital signal processing devices. While fundamentally equivalent, there are several key differences between the two methods.

A continuous-time signal (or function) may always be represented by a sequence of samples that are derived by observing the signal at uniformly spaced intervals, Δt. We may thus represent a continuous-time signal $x(t)$ by the sequence $x(n)$, where $n = 0, \pm\Delta t$, $\pm 2\,\Delta t$ … [15]. For example, the function: $x(t) = sin(t)$, sampled at time intervals of $T_s = \pi/2$, becomes: $x(n) = [0\ 1\ 0\ -1\ 0\ 1\ ...]$ in discrete-time.

As with continuous-time control systems, the convolution operation is important for discrete-time control system analysis. The convolution operation in discrete-time is defined as the following:

$$[f * g](n) = \sum_{m=-\infty}^{\infty} f(m) \cdot g(n-m) \tag{1}$$

The analogous operation to the Laplace transform in continuous-time is the Z-transform in discrete-time and is defined as the following:

$$X(z) = Z\{x(n)\} = \sum_{n=0}^{\infty} x(n)z^{-n} \tag{2}$$

The Z-transform converts a discrete-time domain signal into a frequency domain representation where z is a complex variable. Therefore, $X(z)$ is the discrete-time transfer function of the impulse response function $x(n)$. The Z-transform ($Z\{\ \}$) and inverse Z-transform ($Z^{-1}\{\ \}$) are used to move back and forth between the time and frequency domains. Just as in continuous-time analysis, convolution in the time domain is equivalent to multiplication in the frequency domain. Figure 11 shows the parallel between continuous and discrete-time operations where $L\{\ \}$ and $L^{-1}\{\ \}$ represent the Laplace transform and inverse Laplace transform.

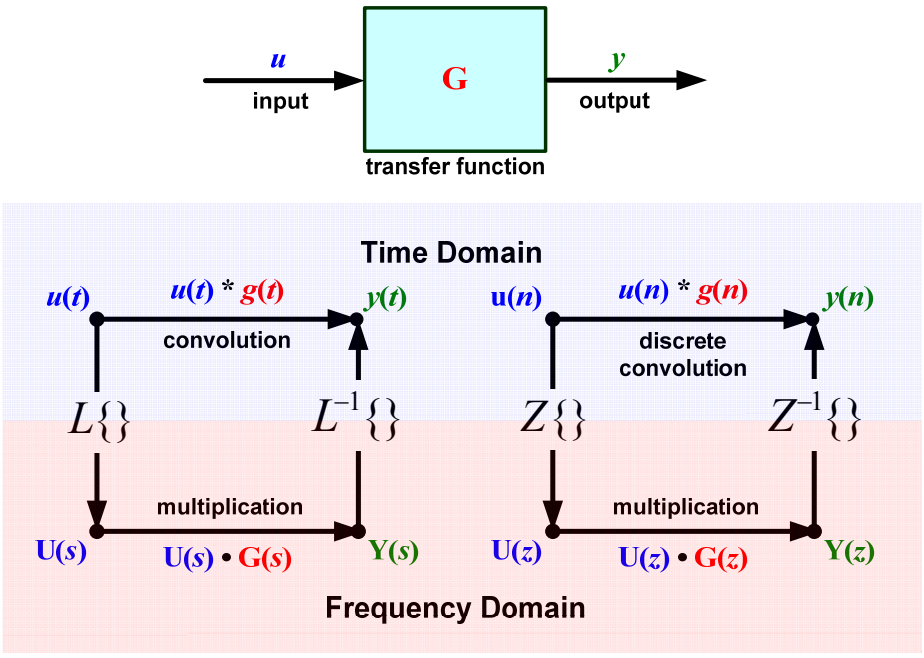

Figure 11. Comparison of continuous and discrete-time operations.

B. TRANSVERSAL FILTER

The primary tool of modern ANC systems is the adaptive filter. The focus of this research is to develop control techniques of the linear, discrete, finite impulse response, adaptive filter type. A filter is said to be linear if the output is a linear function of the observations applied to the filter input [15]. Linear discrete filters are classified as either

finite impulse response filters (FIR) or infinite impulse response filters (IIR), which are respectively characterized by finite memory and infinitely long, but fading memory [15]. The FIR type, also referred to as a transversal filter, is more practical to employ in a control system.

The goal of the jitter control algorithm is to estimate at each time step, n, the command, $y(n)$, for the CFSM that will produce the minimum jitter at the target PSD (OT-2). The signal from the target sensor represents the error between the desired beam location at the target and the actual location, and is referred to as the error signal, $e(n)$ [13].

A reference signal is input to a transversal filter, consisting of M stages. The output of the transversal filter is the control signal to the CFSM, $y(n)$ [13]. The reference signal, $r(n)$, is delayed one time step for each of the M stages, forming a vector of delayed inputs, $\mathbf{r}(n) = [r(n), r(n-1), \cdots, r(n-M+1)]^{\mathrm{T}} \in R^M$. The inner product of the vector of weights $\mathbf{w}(n) = [w_1(n), w_2(n) \cdots, w_M(n)]^{\mathrm{T}} \in R^M$ and the vector of reference signal inputs, $\mathbf{r}(n)$, produces the scalar output $y(n)$ [14]:

$$y(n) = \mathbf{w}^{\mathrm{T}}(n)\mathbf{r}(n) \tag{3}$$

The error signal at the target sensor is the difference between the disturbance and output from the controller, Equation 4. Bear in mind that the CFSM command signal, $y(n)$, must pass through the CFSM dynamics before its effect reaches the target. The transfer function between the CFSM input and the target sensor is referred to as the *secondary plant* dynamics of the system [14].

$$e(n) = d(n) - s(n) * y(n) \tag{4}$$

Where $d(n)$ is the disturbance at the target and $s(n)$ is the secondary plant dynamics. The asterisk represents a discrete-time convolution. Equations 3 and 4 are shown in block diagram form in Figure 12. $s(n)$ and the secondary plant dynamics transfer function, S(z), are Z-transform pairs.

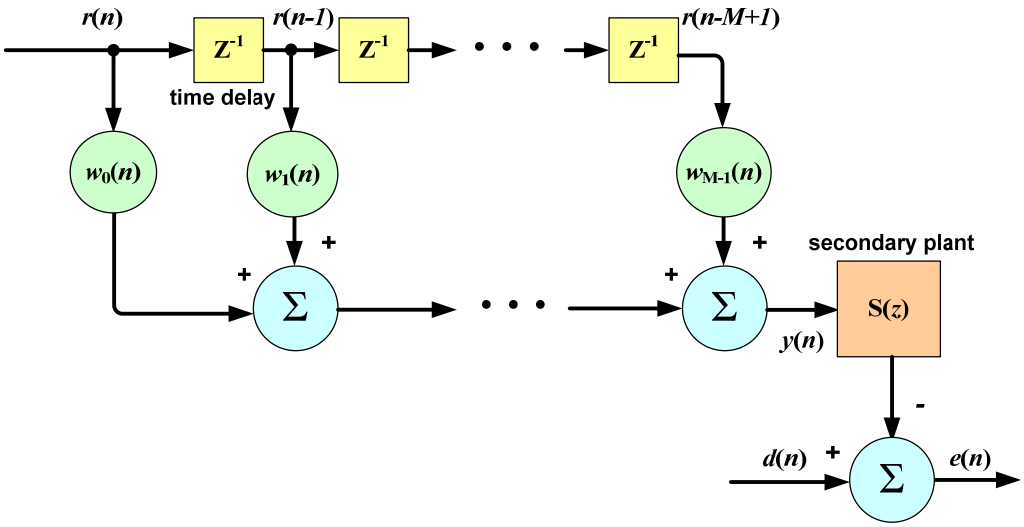

Figure 12. Block diagram of digital FIR transversal filter.

A discrete FIR filter consists of two distinct parts: a digital filter (described above) and a method to calculate the weighting vector, $\boldsymbol{w}(n)$. As stated above, the objective of the filter is to minimize the error at the target [14]. This is usually quantified by minimizing the mean square of the error signal, $\xi = \mathrm{E}[e^2(n)]$. If the disturbance is stationary and its characteristics are known, the optimal weighting vector can be calculated a priori. This filter is referred to as the *Wiener filter*. If the disturbance is time-varying and/or its characteristics are unknown, an adaptive algorithm is necessary to constantly update the weighting vector to minimize ξ. The goal of an adaptive filter is to update the weighting vector so that ξ approaches the minimum or optimal Wiener filter value. The standard form of an adaptive filter is shown in Figure 13. The least-mean-square (LMS) and recursive-least-square (RLS) adaptive filter techniques are two adaptive algorithms for updating the weighting vector [15].

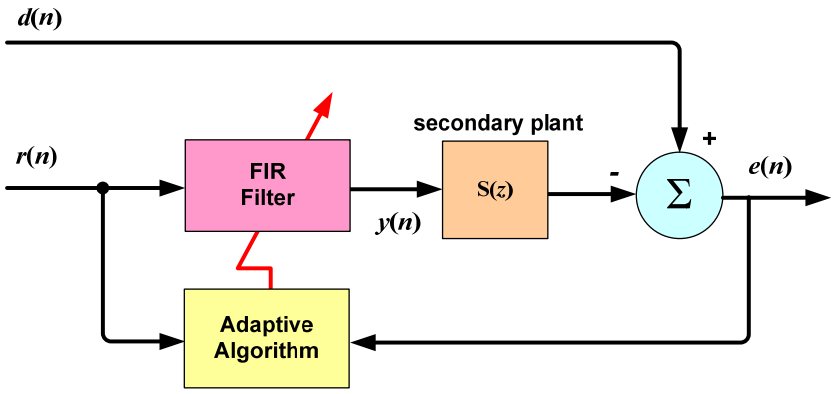

Figure 13. Block diagram of standard adaptive filter.

C. WIENER FILTER

The Wiener filter is the optimum linear discrete-time filter for estimating the disturbance in the case when the disturbance is both stationary and the spectral properties are known [15]. The Wiener filter is not adaptive, and therefore not practical for jitter control because of the unknown and time-varying nature of the jitter. Nevertheless, we can use the Wiener filter solution, a posteri, as a best case scenario comparison to the LMS and RLS methods under study. Both the LMS and RLS algorithms approach the optimal Wiener filter weightings. In [15], Haykin shows that the optimal Wiener weighting vector is the following:

$$\mathbf{w}_{optimal}(n) = \mathbf{R}^{-1}\mathbf{p} \tag{5}$$

Where $\mathbf{R}$ is the *autocorrelation matrix* of the reference signal, $\mathbf{R} = \mathrm{E}[\mathbf{r}(n)\mathbf{r}^{\mathrm{T}}(n)]$ and $\mathbf{p}$ is the *cross-correlation vector* between the reference signal and the disturbance, $\mathbf{p} = \mathrm{E}[\mathbf{r}(n)d(n)]$ [15]. E[ ] represents the expected value or, by the *mean ergodic theorem*, the mean value as the number of samples approaches infinity [15]. The reference signal and disturbance signal are assumed to have a zero mean [15]. Haykin also shows that the minimum Wiener controlled jitter is:

$$\xi_{\min} = \sigma^2_{\min} = \mathrm{E}[d^2(n)] - \mathbf{p}^{\mathrm{T}}\mathbf{R}^{-1}\mathbf{p} \tag{6}$$

When the disturbance signal has a zero mean, the mean square error, ξ, is equivalent to the variance, σ^2. Throughout this thesis, we use the value of one standard deviation, σ, of the beam position at the target to evaluate the "tightness" of the beam. Where $\sigma_{\min}$ is the minimum (or best achievable) beam spread according to Wiener theory. As a tool for measuring the quality of the reference signal, we define the ratio between the optimal Wiener disturbance rejection and total disturbance:

$$\gamma_{optimal} = \frac{\sigma_d - \sigma_{\min}}{\sigma_d} \tag{7}$$

Where σ_d is the standard deviation of the beam position at the target without control inputs. Therefore, $\gamma_{optimal}$ varies between 0 and 1, $\gamma_{optimal} = 0$ for no disturbance attenuation (no control) and $\gamma_{optimal} = 1$ for absolute attenuation (perfect jitter control). In order to compare $\gamma_{optimal}$ to experimental results in later chapters, we equivalently define the ratio between the controlled disturbance rejection and the total disturbance:

$$\gamma_{controlled} = \frac{\sigma_d - \sigma_{controlled}}{\sigma_d} \tag{8}$$

The value $\sigma_{controlled}$ is the standard deviation of the beam position at the target with control on.

D. FILTERED-X LEAST MEAN SQUARE ALGORITHM

The least-mean-square algorithm (LMS) is one of the simplest adaptive algorithms and has become a standard for comparison with more complex algorithms [4]. The algorithm uses the method of steepest descent to minimize ξ. In [14], Kuo shows that the LMS equation to update the weighting vector is the following, where μ is the convergence factor:

$$\mathbf{w}(n+1) = \mathbf{w}(n) - \mu \mathbf{r}(n) e(n) \tag{9}$$

The LMS algorithm takes steps, of size μ, towards the optimal weighting vector [4]. As a result, there is a tradeoff when choosing the convergence factor. When μ is too small, the weighting vector will converge too slowly and when μ is too large $\mathbf{w}(n)$ will

oscillate about the optimal value [14]. Therefore, the LMS algorithm can only be said to approximately approach the optimal Wiener weightings. For the LMS controllers in this thesis, we chose a conservative value of μ that slowly converges to a steady state while more precisely reaching the optimum weight vector to remove more of the disturbance.

1. Filtered-X Method

The output from the controller, $y(n)$, must pass through the secondary plant between the CFSM and the target sensor (OT-2) (shown in Figure 13). This causes gain and phase variations between the error and reference signal. To account for this, we place a copy of the secondary plant transfer function, $\hat{S}(z)$, in the reference signal path to the weight updating algorithm in Equation 9 [14].

$$\hat{\mathbf{r}}(n) = \hat{s}(n) * \mathbf{r}(n) \tag{10}$$

This method is referred to as the Filtered-X method in the literature (FX-LMS). Without this modification, the controller can become unstable. Figure 14 shows the Filtered-X method implemented in the controller. The reference signal, $r(n)$, is filtered on its path to the weight updating algorithm and not on the path to the transversal filter [14].

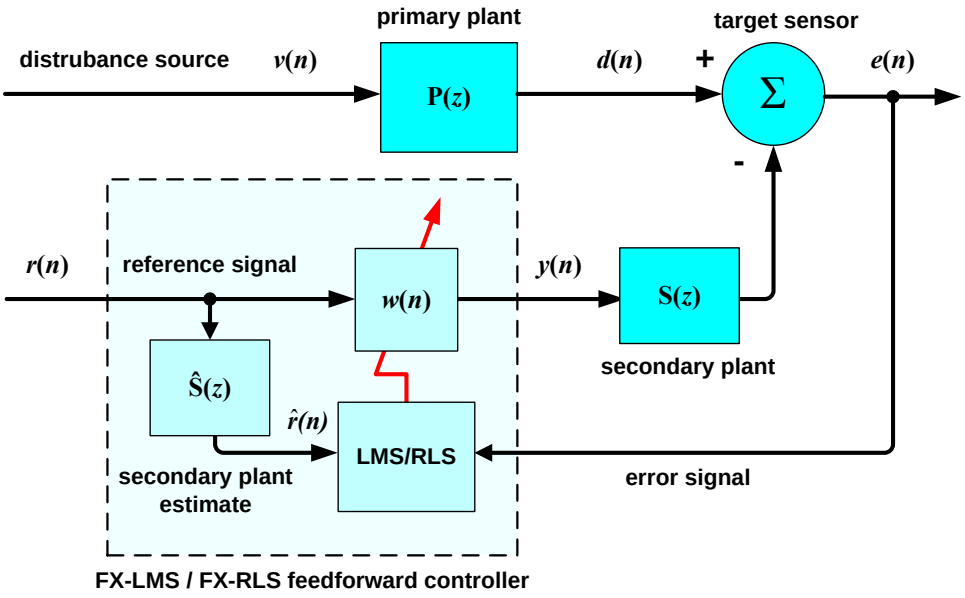

Figure 14. Feedforward FX-LMS/FX-RLS implementation.

To explain why this modification works, first assume the system is linear and the secondary plant block, S(z), can be equivalently analyzed on either side of the transversal filter. In the ideal case where S(z) = $\hat{S}(z)$ the block diagram can be rewritten as shown in Figure 15. Now the control signal, $y(n)$, no longer passes through the secondary plant, and therefore, eliminates the gain and phase variation problem. Figure 15 is only an equivalent representation of the system, not the actual implementation on the controller. However, it illustrates why the Filtered-X method works when implemented in the actual control law.

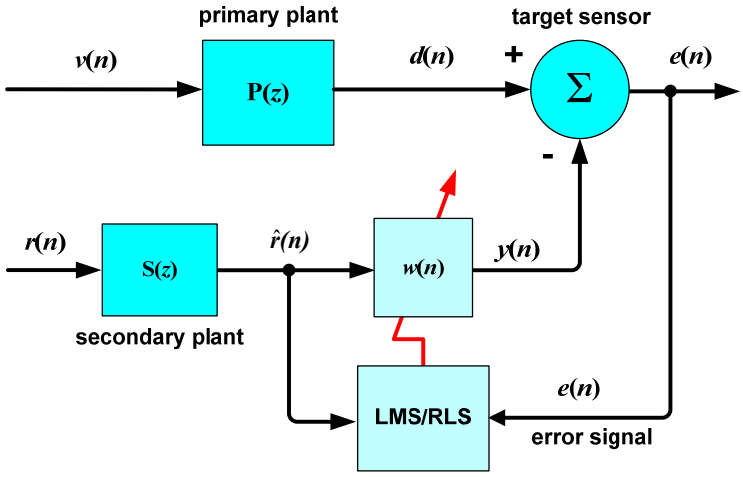

Figure 15. Equivalent Filtered-X representation.

2. Bias Estimation

Finally, we slightly modify our definition of the reference signal and weighting vector to take into account the presence of a DC component in the error signal. This is referred to as *bias estimation* and requires the addition of a constant element to the reference signal vector and a corresponding weight to track the bias [13].

$$\mathbf{r}_b(n) = [1, \mathbf{r}^{\mathrm{T}}(n)]^{\mathrm{T}} = [1, r(n), r(n-1), \cdots, r(n-M+1)]^{\mathrm{T}} \tag{11}$$

$$\mathbf{w}_b(n) = [w_b(n), \mathbf{w}^{\mathrm{T}}(n)]^{\mathrm{T}} = [w_b(n), w_1(n), w_2(n), \cdots, w_{M-1}(n)]^{\mathrm{T}} \tag{12}$$

E. FILTERED-X RECURSIVE LEAST SQUARE ALGORITHM

The recursive-least-square (RLS) algorithm provides faster convergence and smaller steady state error than the LMS algorithm [14]. The transversal filter structure of the RLS controller is identical to that of LMS; the difference is the weight updating algorithm. The RLS algorithm's cost function has a memory of errors with a forgetting factor of $0 < \lambda \leq 1$, while the LMS cost function (ξ) does not have memory [14]. The LMS method only uses the current error in the updating equation.

Instead of minimizing the mean square error like the LMS filter; the RLS algorithm minimizes the summation of the squares (least-squares) of all past error signal inputs augmented by the forgetting factor, λ [14].

$$C(n) = \sum_{i=1}^{n} \lambda^{n-i} e^2(i) \tag{13}$$

By applying the forgetting factor, recent data is weighted more heavily in order to accommodate nonstationary disturbances [15]. The Wiener optimal weight solution from Equation 5 is used to calculate the weighting vector. The correlation matrix, $\mathbf{R}(n)$, and cross-correlation vector, $\mathbf{p}(n)$, are modified to take into account the memory of errors. They are referred to as the *sample correlation matrix* and *sample cross-correlation vector* because of their time dependence [14].

$$\mathbf{R}(n) = \sum_{i=1}^{n} \lambda^{n-i} \mathbf{r}(i)\mathbf{r}^{\mathrm{T}}(i), \qquad \mathbf{p}(n) = \sum_{i=1}^{n} \lambda^{n-i} d(i)\mathbf{r}^{\mathrm{T}}(i) \tag{14}$$

It is theoretically possible to directly calculate the optimal weighting vector, $\mathbf{w}_{optimal}(n)$, at each time step using Equation 5 from Wiener theory. This method is referred to as the least-squares method, but would be extremely computationally expensive as n becomes large. Equation 5 requires the correlation matrix be calculated and inverted at each time step [14]. For a practical system, the way out of this problem is to recursively calculate the inverse correlation matrix, $\mathbf{Q}(n) = \mathbf{R}^{-1}(n)$ [14]. The recursive-least-square method eliminates the need to continuously recalculate $\mathbf{Q}(n)$ and greatly reduces the computational burden. The derivation to recursively calculate $\mathbf{Q}(n)$ requires a fair amount

of linear algebra and is explained in great detail by both Kuo [14] and Haykin [15]. The result is FX-RLS algorithm to update the weighting vector $\mathbf{w}(n)$ at each instance [14].

$$\mathbf{k}(n) = \frac{\lambda^{-1}\mathbf{Q}(n-1)\hat{\mathbf{r}}(n)}{1+\lambda^{-1}\hat{\mathbf{r}}^{\mathrm{T}}(n)\mathbf{Q}(n-1)\hat{\mathbf{r}}(n)} \tag{15}$$

$$\mathbf{w}(n) = \mathbf{w}(n-1) + \mathbf{k}^{\mathrm{T}}(n)e(n) \tag{16}$$

$$\mathbf{Q}(n) = \lambda^{-1}\mathbf{Q}(n-1) - \lambda^{-1}\mathbf{k}(n)\hat{\mathbf{r}}^{\mathrm{T}}(n)\mathbf{Q}(n-1) \tag{17}$$

Where $\mathbf{k}(n) \in R^{M}$ is the time-varying gain vector, and $\mathbf{Q}(n) \in R^{M\times M}$. Unlike the LMS method, RLS exactly approaches the optimal Wiener filter weightings [14]. Note that the use of $\hat{\mathbf{r}}$ indicates that the reference signal is filtered through the secondary plant dynamics just as in the FX-LMS algorithm [14].

Also, as in the FX-LMS algorithm, the reference signal and weight vectors are augmented with a constant element to track the DC component of the error signal (Equations 11 and 12) [13]. Therefore, the time-varying gain vector and inverse correlation matrix are actually: $\mathbf{k}(n) \in R^{M+1}$, and $\mathbf{Q}(n) \in R^{(M+1)\times(M+1)}$.

F. ADAPTIVE FILTERS WITH MULTIPLE REFERENCE SIGNALS

In [2], [3], [4] and [13] the FX-LMS and FX-RLS algorithms described above have a standard transversal filter structure that uses a single-channel reference signal. In this thesis, we are provided two reference signals that are each correlated with only components of the total beam jitter. We will now develop two methods for implementing the controllers with multiple reference signals. The reference signals are provided by the on-board accelerometer and the on-board PSD (OT-1). When using two reference signals, we give distinction between the numbers of accelerometer stages (*M*) and PSD stages (now denoted as *S*).

1. Method 1: Summation of Filter Outputs

Method 1 uses two separate control blocks (an accelerometer block and a PSD block). The individual outputs are summed and sent to the CFSM. Therefore, the RLS

algorithm will manipulate two inverse correlation matrices per axis: $\mathbf{Q}_{Accel}(n) \in R^{(M+1)\times(M+1)}$, $\mathbf{Q}_{PSD}(n) \in R^{(S+1)\times(S+1)}$. The RLS algorithm requires on the order of L^2 operations per time step, where L is the filter order [14]. As a result, method 1 requires $O\{(M+1)^2 + (S+1)^2\}$ operations. A difficulty with parallel adaptive filters is that their performance characteristics have not been proved mathematically as opposed to an individual adaptive filter. Placing the adaptive filters in parallel may cause unexpected interactions. Consequently, the optimum Wiener solution cannot be calculated for this algorithm (this is manifested in Chapter VII).

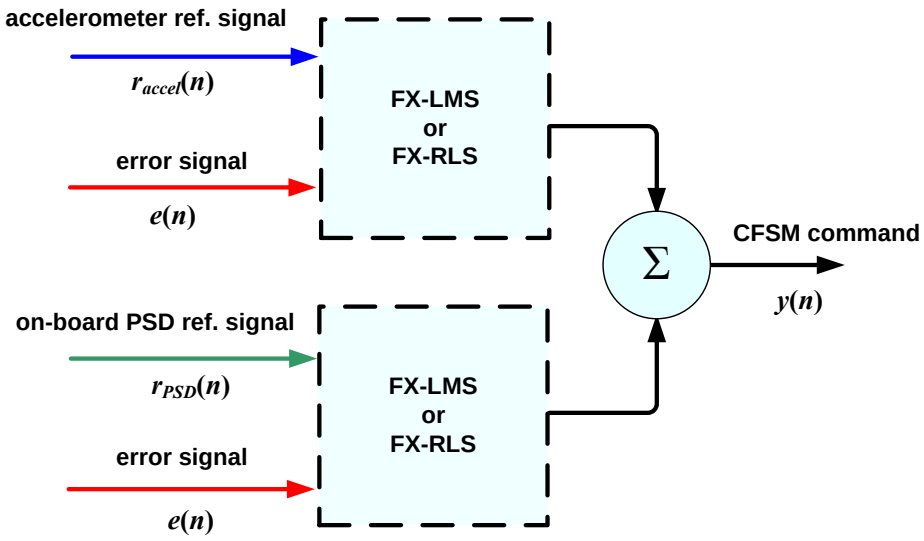

Figure 16. Multiple reference signals using method 1.

2. Method 2: Augmentation of Reference Signals

For method 2, the reference signals are combined inside a single control block. The reference signal and weight vectors are modified to contain both accelerometer and PSD stages.

$$\mathbf{r}(n) = [1, r_{Accel}(n), r_{Accel}(n-1), \cdots, r_{Accel}(n-M+1), r_{PSD}(n), r_{PSD}(n-1), \cdots, r_{PSD}(n-S+1)]^{\mathrm{T}} \quad (18)$$

$$\mathbf{w}(n) = [w_b(n), w_1(n), w_2(n), \cdots, w_{M+S}(n)]^{\mathrm{T}} \quad (19)$$

The rest of the algorithm is implemented as described is Chapters IV.D and IV.E. Method 2 has a simpler structure compared to method 1 because it only requires one filter. The RLS algorithm will manipulate one very large inverse correlation matrix per axis: $\mathbf{Q}(n) \in R^{(M+S+1)\times(M+S+1)}$ and requires $O\{(\mathrm{M+S+1})^2\}$ operations per time step. Method 2 is, therefore, more computationally expensive than method 1.

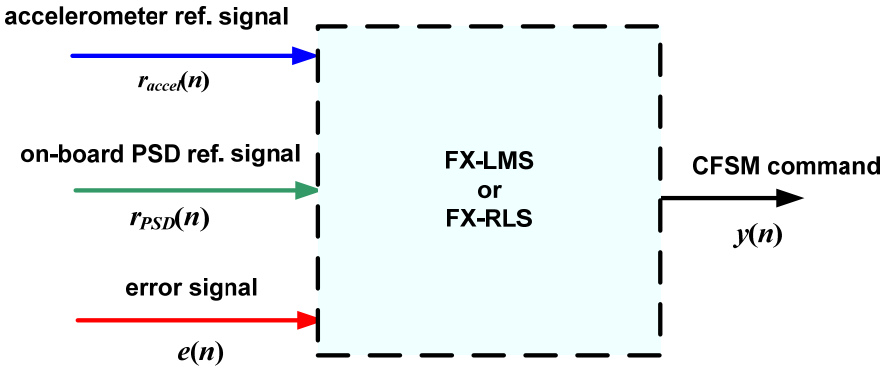

Figure 17. Multiple reference signals using method 2.

G. FEEDBACK ADAPTIVE FILTERS

In this section we will develop a method for pure feedback jitter control with adaptive filters. These methods do not require a reference signal like the feedforward case. Feedback control is necessary in situations when obtaining a reference signal is not practical. The presence of numerous jitter sources is an example of such a situation [14]. As discussed in Chapter III, depending on the quality of the reference signal, feedback control may be superior to the feedforward method.

Feedback adaptive filters use the same single channel transversal filter structure as the feedforward controllers. The error sensor (OT-2 for our experiment) always contains a residual noise signal that is utilized in feedback control to create a reference signal [14]. This technique is similar to the feedforward controller, however it internally generates its own reference signal using the adaptive filter output, $y(n)$, and the error signal, $e(n)$, as described by Equation 20 [14].

$$r(n) = \hat{d}(n) = e(n) + \hat{s}(n) * y(n) \tag{20}$$

Comparing the feedforward and feedback algorithms in Figures 14 and 18, respectively, shows their near identical structure. The filter output, $y(n)$, is filtered by the secondary plant estimate and then added to the error signal, $e(n)$. The secondary plant estimate, $\hat{S}(z)$, is the same that is employed for the Filtered-X method. The generated reference signal, $r(n)$, is an estimate of the primary noise signal, $d(n)$, from Equation 4 in Chapter IV.B, and therefore, given the distinction $\hat{d}(n)$ [14]. Kuo shows that under ideal conditions, when $\hat{S}(z) = S(z)$, the feedback method is transformed into the feedforward method [14]. Therefore, the performance of the feedback controller compared to the feedforward controller depends only on obtaining an accurate secondary plant model with our system identification methods.

The feedback controller uses the same Filtered-X method and bias estimator as described in the previous sections.

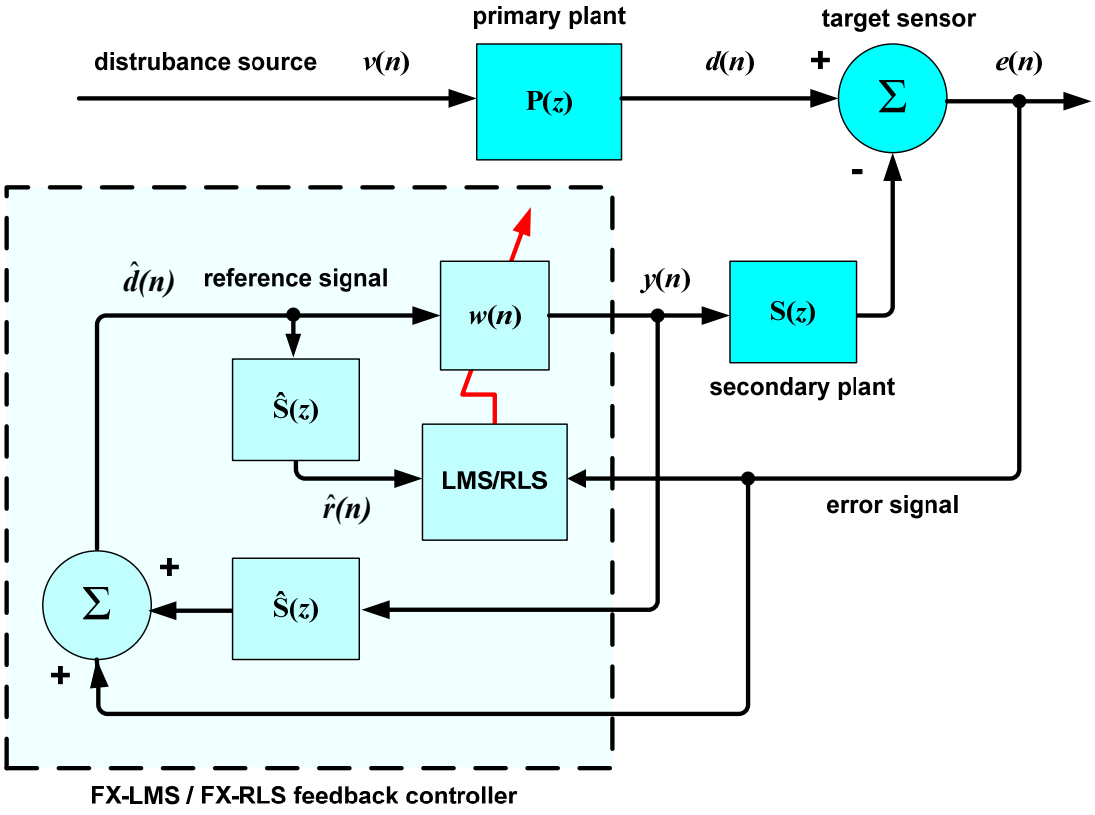

Figure 18. FX-LMS / FX-RLS feedback implementation.

1. Parallel PI Controller

Initial testing with the feedback controller consisting only of an adaptive filter showed instability when the DC component of the error signal was large. In other words, when the beam was given a large initial bias error in addition to the DFSM and shaker disturbances, the feedback controller would behave erratically. The internal bias estimator in the adaptive filter seemed to not work as anticipated. However, when the bias error was small, the feedback controller behaved as expected.

It is difficult to fully explain this instability; however, it is thought to be caused by a large initial transition of the reference signal, $\hat{d}(n)$, when the controller is switched on. The reference signal in a feedforward controller remains stationary even as control input is applied because the reference sensor is upstream of the control actuator. Experiments with a downstream feedforward reference sensor gave similar results to the feedback instability seen here. The downstream reference signal contained a large change in the DC component when the controller was turned on due to the initial bias error being corrected. This appeared to initiate instability in the system. Inspection of the feedback reference signal, from Equation 20, reveals that a large initial transition is expected because the reference signal is derived from the downstream error (target) sensor.

As a solution to improve the robustness of the control method to allow for large DC biases, a proportional-integral (PI) controller was placed in parallel with the adaptive filter. This technique is similar to the feedback adaptive filter research done in [5]-[11].

An error PI controller applies fixed gains (K_p and K_i) to the error signal and the integral of the error signal. The following is the PI control law in discrete-time where T_s is the sample time [16]:

$$y_{PI}(n) = K_p \cdot e(n) + K_i \cdot T_s \sum_{k=0}^{n} e(k) \tag{21}$$

This a classical linear time-invariant control technique which works to push the error signal towards zero. With the PI controller placed in parallel with the adaptive filter, it removes the initial bias error so that the feedback adaptive filter may perform correctly.

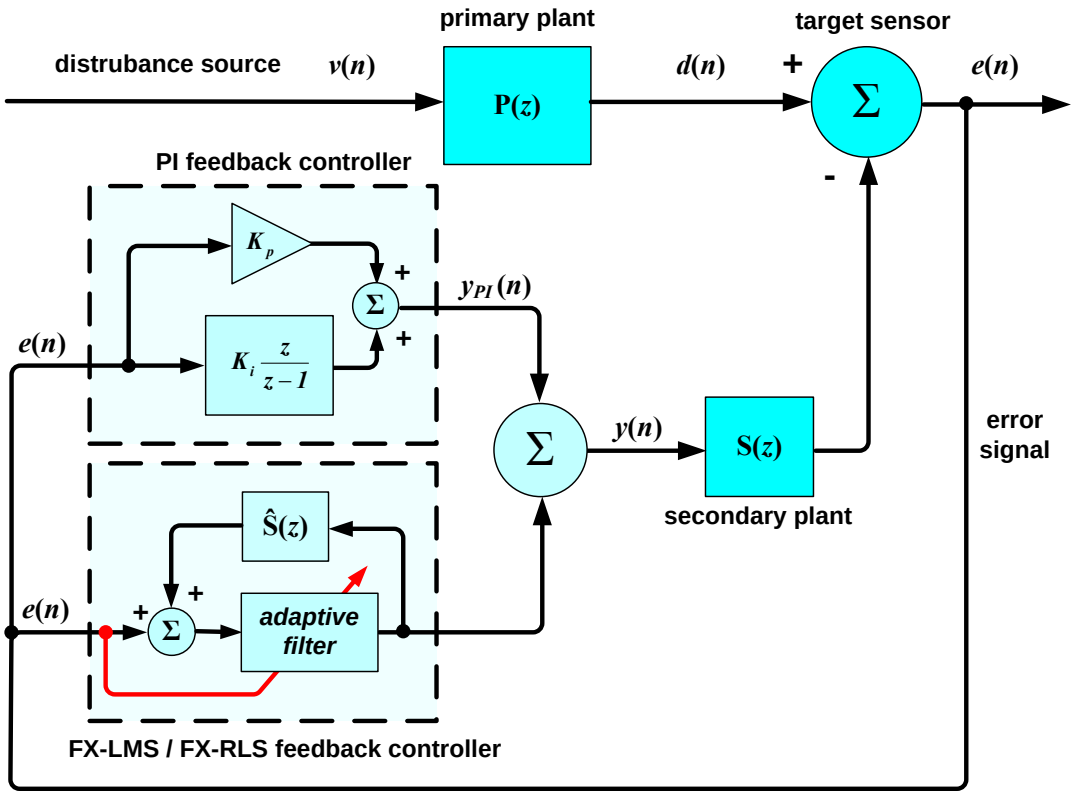

Figure 19. Feedback adaptive filter with parallel PI controller.

H. HYBRID FEEDBACK - FEEDFORWARD ADAPTIVE FILTER

A combination of the feedback and feedforward methods is refereed to in the literature as a hybrid adaptive filter [14]. In such a system, the canceling signal, $y(n)$, is generated from both a reference sensor (or sensors) and the error sensor. To accomplish this we simply place feedback and feedforward adaptive filters in parallel [14]. This method utilizes both the reference signal(s) and the internally generated reference signal. Kuo mentions that this approach is the most popular in noise canceling headphone technology [14]. For the same reasons mentioned in the previous section, a PI controller was placed in parallel with the hybrid controller for the experiments. The hybrid controller uses parallel adaptive filters, and therefore, as mentioned in Chapter IV.F.2, cannot be mathematically analyzed. A diagram of the hybrid adaptive filter is shown in Figure 20.

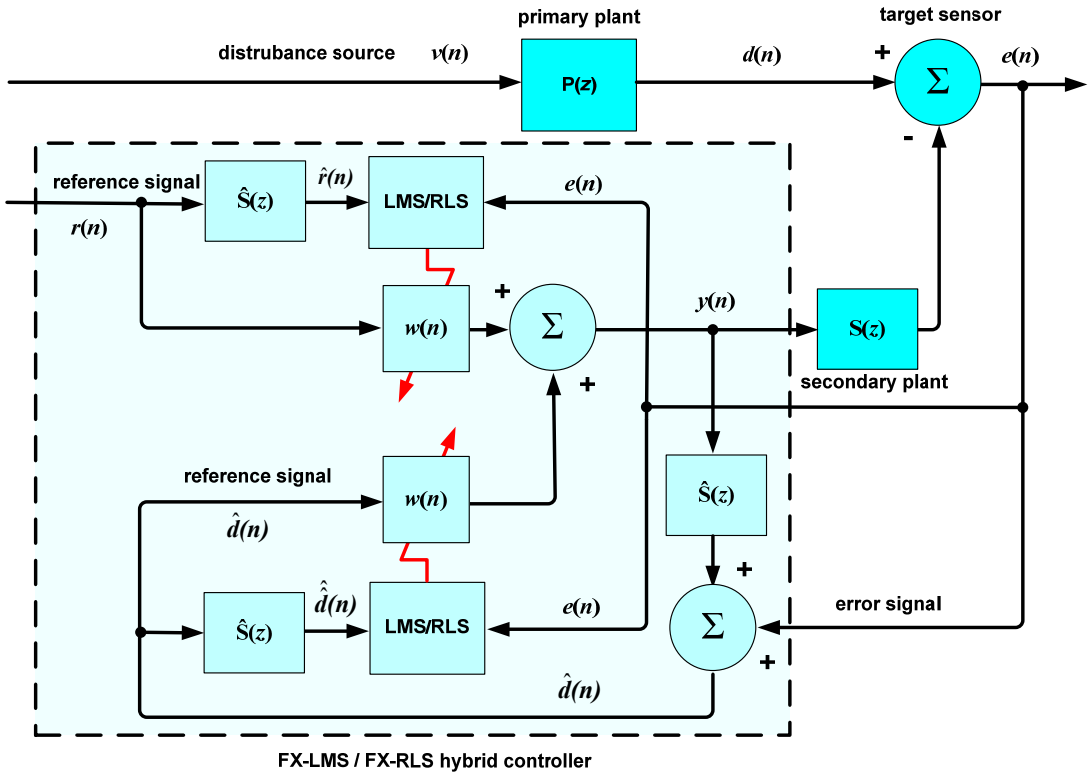

Figure 20. FX-LMS / FX-RLS hybrid adaptive filter implementation, parallel PI controller not shown.

V. SYSTEM IDENTIFICATION

The adaptive filter control methods require a model of the secondary plant dynamics on the system. More precisely, we must identify an open-loop model from the control input (applied to the CFSM) to the measurement signal of the beam position at the target sensor (OT-2). This secondary plant model, $\hat{S}(z)$, is required for the Filtered-X method in order to account for variations between the reference and error signals paths. It is also needed for estimating the primary noise source, $d(n)$, in adaptive feedback control. Experimental results showed negligible coupling between the two axes of the CFSM. An input to one axis of the mirror yielded less than 10 percent movement in the other axis for typical amplitudes used in the experiments [3]. Therefore, system identification is preformed for each axis separately.

A single-input single-output (SISO) black-box model is identified by a subspace method using MATLAB's System Identification Toolbox. The subspace method of system identification (SI) consists of exciting the system with a signal of sufficient distinct frequencies and then analyzing the data to determine the best model [4]. Typical input signals are filtered Gaussian white noise, a random binary signal or a chirp sinusoid. This method of SI has the advantage of directly providing a discrete-time state-space model that can be easily applied to digital control systems. The MATLAB toolbox also recommends the optimal model order for the system.

A pseudo-random binary signal was chosen for the input signal to the CFSM [13]. Figure 21 shows the input signal and the resultant output signal from the target PSD (OT-2).

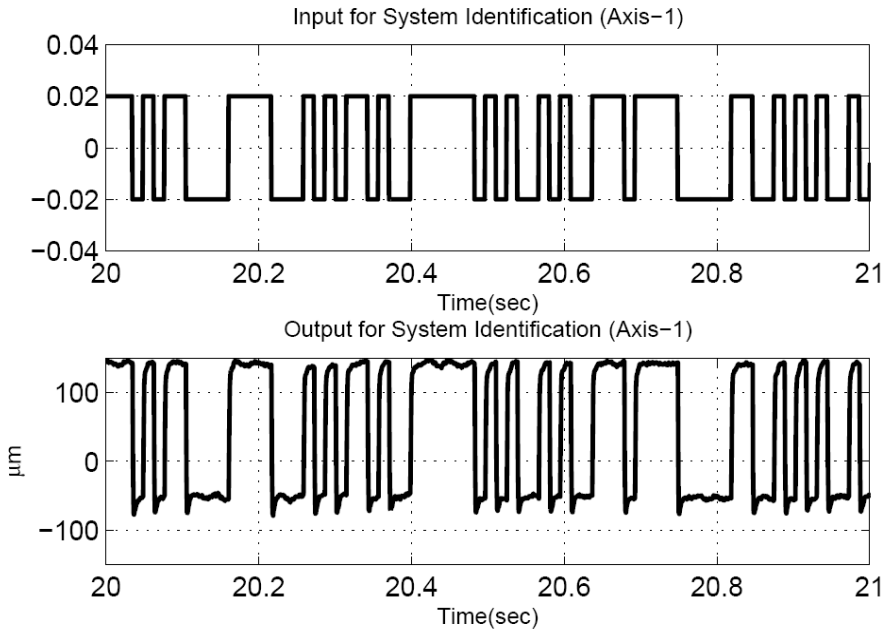

Figure 21. Input and output signals for system identification. From Yoon [13].

The SI Toolbox provided a 3rd-order, discrete-time, state-space model for each axis. Secondary plant models were created for the target sensor (OT-2) in both its on-board and off-board positions on the testbed. Figures 22 and 23 show the frequency response plots.

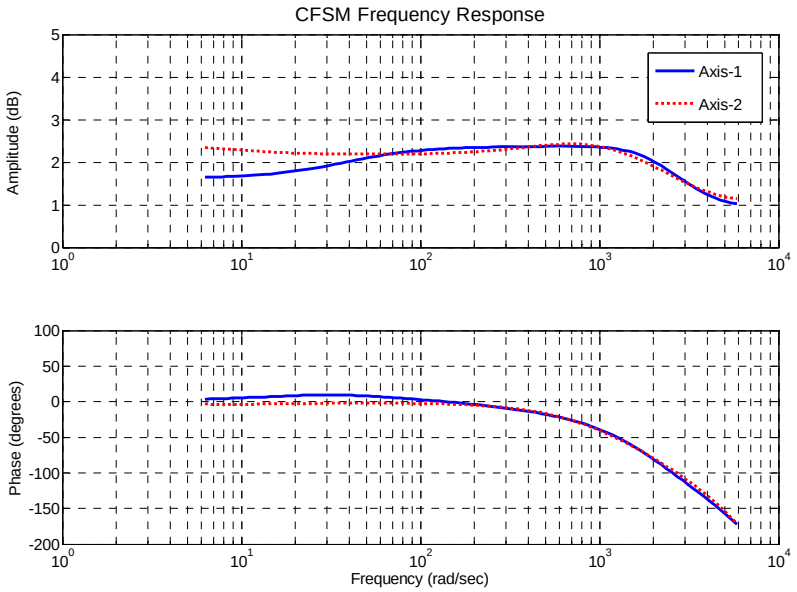

Figure 22. Frequency response of open-loop system. Target positioned off-board.

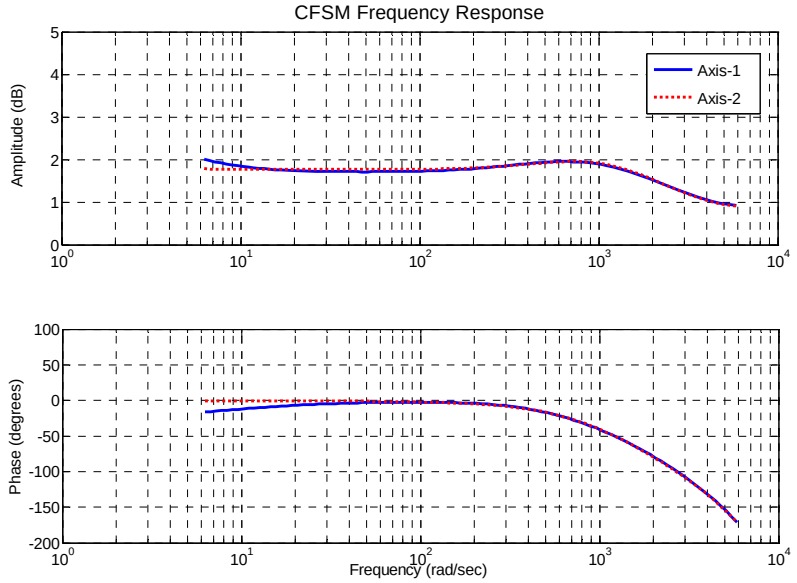

Figure 23. Frequency response of open-loop system. Target positioned on-board.

THIS PAGE INTENTIONALLY LEFT BLANK

VI. DISTURBANCE SOURCES AND REFERENCE SIGNAL CORRELATION

A. DISTURBANCE SOURCES

In the following chapter, several experiments with various configurations were run on the JCT to explore the capabilities of the proposed control techniques. Table 1 summarizes the characteristics of the disturbances and their individual contributions to the beam position error at the target. The data is reported as the standard deviation, σ, of the jitter radius. Experiments were conducted with the target sensor in two different positions (on and off the vibration platform). The effects of the disturbances vary between the two positions.

Target	Bias (DC)	Narrowband (Shakers)	Broadband (DFSM)	Total Jitter
Off-board	≈1000 μm	40 Hz, $\sigma \approx$ 40 μm 60 Hz, $\sigma \approx$ 30 μm	0 - 200Hz band-limited white noise, $\sigma \approx$ 51 μm	$\sigma \approx$ 71 μm
On-board	≈1000 μm	40 Hz, $\sigma \approx$ 18 μm 60 Hz, $\sigma \approx$ 17 μm	0 - 200Hz band-limited white noise, , $\sigma \approx$ 48 μm	$\sigma \approx$ 52 μm

Table 1. Jitter disturbance characteristics.

Considering the control bandwidth of the CFSM (800 Hz) and initial testing, it was decided that 0 to 200 Hz band-limited white noise would be an appropriate range to attempt to control [3]. Asking the CFSM to control disturbances above 200 Hz risked exceeding the mirrors current limitations [3]. The frequencies for the two narrowband shaker disturbances were chosen arbitrarily. The frequencies, which are representative of aircraft/spacecraft vibrational environments, are far enough apart that they are easily deciphered on a power spectral density plot.

For all experiments in this thesis, the developed control techniques are tested against all the above disturbance sources simultaneously. The power spectral density plot (PSD) of the beam position at the target in the presence of the disturbances is shown in

Figure 24. The individual contributions to the total beam jitter are shown by additionally plotting the DFSM and shaker disturbances separately. The shaker frequencies at 40 Hz and 60 Hz can be clearly seen.

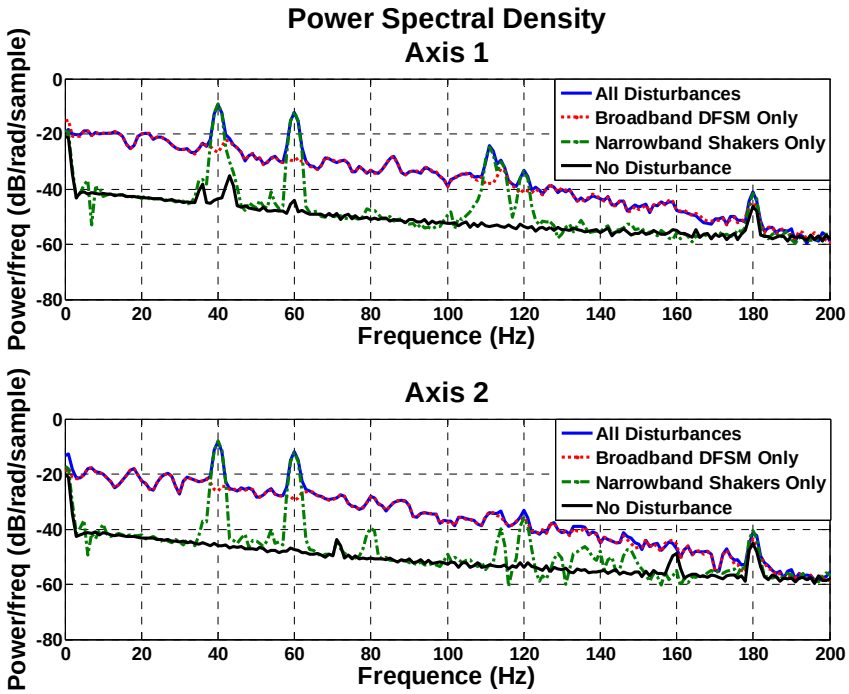

Figure 24. PSD plot of beam jitter from combined and individual disturbance sources

B. REFERENCE SIGNAL CORRELATION EXAMPLES

For the feedforward methods, where a reference signal is required, appreciating the consequences of choosing a proper reference signal is helpful for understanding the system. For example, if we attempt to use only an accelerometer reference signal, the result will be that only the disturbances correlated with the accelerometer signal (the shakers) will be rejected. The accelerometer signal is said to be semi-coherent with the total disturbance. This example is demonstrated in Figure 25 which shows a power spectral density plot for an FX-RLS controller with an accelerometer reference signal. It is obvious that only the shaker disturbances (at 40 Hz and 60 Hz) are attenuated while the broadband disturbance remains uncontrolled. Also, notice that not only are the shaker disturbances removed, but the 40 Hz and 60 Hz components of the broadband disturbance.

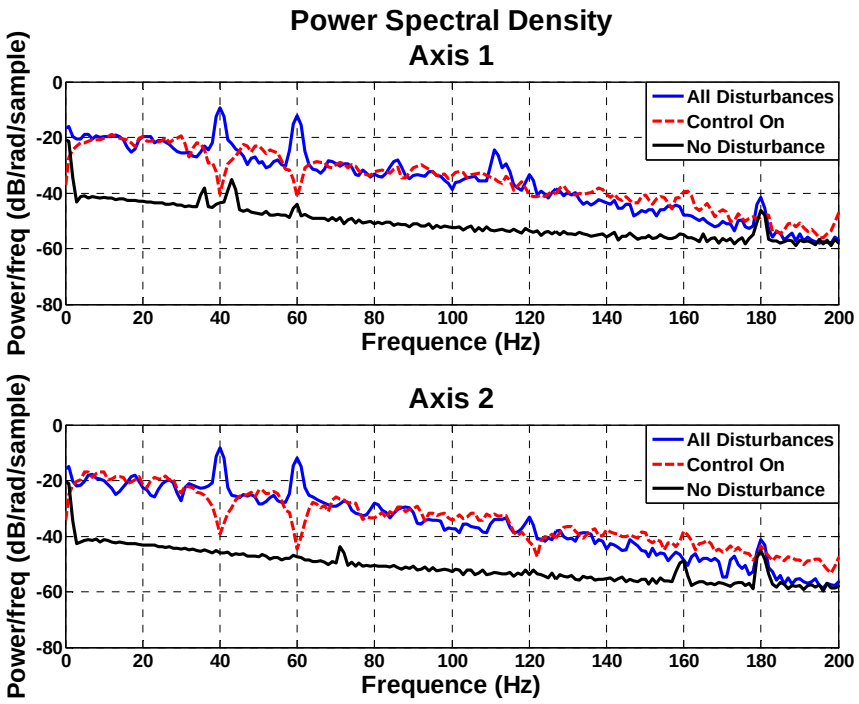

Figure 25. Jitter rejection experiment using 45 stage feedforward FX-RLS controller with accelerometer reference signal.

Another similar example is using a reference signal from an on-board PSD. When the on-board PSD is subjected to shaker vibrations its signal is no longer well correlated with the shaker disturbances. Therefore, the on-board PSD reference signal controller cannot reject the narrowband jitter from the shakers. This example is demonstrated in Figure 26. In the power spectral density plot, it is also apparent that the controller has difficulty rejecting the broadband jitter above 40 Hz. Figure 26 is a good example of why methods for using multiple reference signals are necessary.

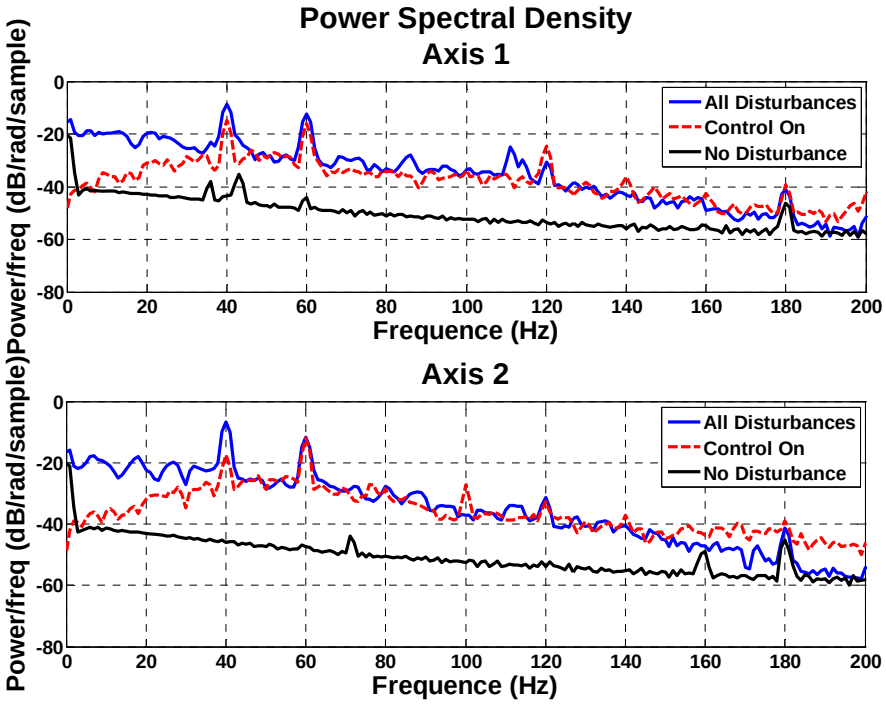

Figure 26. Jitter rejection experiment using 45 stage feedforward FX-RLS controller with an on-board PSD reference signal.

C. REFERENCE SIGNAL CORRELATION EXPERIMENT

In order to give more insight into the performance of the developed controllers an experiment was conducted to characterize the degree of correlation (or coherence) between the various reference signals and the disturbances. Using experimental data, the optimal amount of jitter rejection, $\gamma_{optimal}$ from Equation 7, was calculated comparing each individual reference signal and disturbance source. Therefore, the results in Table 2 represent the best possible jitter rejection for a given reference signal in an adaptive filter. Included in Table 2, is the internally generated reference signal used in the feedback controller, $\hat{d}(n)$. The target sensor (OT-2) was mounted in its off-board position for this experiment.

Reference Signal:	Primary noise estimate, $\hat{d}(n)$ 45 stgs.		Off-board PSD (coherent) 45 stgs.		On-board PSD (semi-coherent) 45 stgs.		Accel. X-axis 45 stgs.		Accel. Y-axis 45 stgs.		Accel. Z-axis 45 stgs.	
PSD Axis:	Axis		Axis		Axis		Axis		Axis		Axis	
	1	2	1	2	1	2	1	2	1	2	1	2
DFSM	0.932	0.914	0.958	0.959	0.958	0.957	0.081	0.144	0.098	0.151	0.093	0.120
Shaker 1	0.965	0.953	0.958	0.953	0.950	0.938	0.568	0.684	0.825	0.850	0.951	0.928
Shaker 2	0.953	0.947	0.954	0.946	0.624	0.933	0.923	0.893	0.915	0.893	0.953	0.913
Both Shakers	0.951	0.954	0.951	0.944	0.636	0.889	0.553	0.663	0.875	0.853	0.951	0.933
All Dist.	0.946	0.931	0.833	0.841	0.578	0.692	0.290	0.275	0.342	0.408	0.411	0.402

Table 2. Optimal Wiener jitter rejection, $\gamma_{optimal}$ from Equation 7

Table 2 quantitatively demonstrates the statements made in Chapter II about the correlation of the reference signals. For attenuating all disturbances, the off-board PSD reference signal performs significantly better than the on-board PSD. As shown in Figure 25, the accelerometer reference signals are successful at controlling the shaker disturbances but completely ineffective for control of the DFSM disturbance. The primary noise estimate reference signal, used in the feedback techniques, shows the best performance for controlling all of the disturbances.

D. CHOOSING THE ACCELEROMETER REFERENCE SIGNAL

Due to the two orthogonally mounted shakers, the vibrational disturbance is complex and along all three axes of the platform. Choosing a proper signal from the 3-axis accelerometer to use as a reference is not arbitrary. For this research, the accelerometer signal that produced in best results in Table 2 was used in the jitter rejection experiments in the following chapters. Therefore, the Z-axis accelerometer signal was used for both axes of the control law (Axis-1 and Axis-2).

In a more complex system with many sources of vibration this technique may not be appropriate. In such a system, the signals from all three axes of the accelerometer could be used in the control law.

VII. DISTURBANCE REJECTION EXPERIMENTS

A. PERFORMANCE METRICS

The goal of the disturbance rejection experiments is to evaluate the various control methods for pointing the beam to the static target center position (0,0) in the presence of both the DFSM and shaker disturbances, as well as a bias error. A detailed explanation of the disturbance characteristics was given the previous chapter. For each experiment, the testbed was run for a total of 15 seconds. The controller turns on after an elapsed time of 5 seconds and attempts to push the beam to the target center and remove the jitter. The standard deviation is calculated for the beam position (in μm) as a measure of the "tightness" or spread of the beam [3]. Using Equation 8, from Chapter IV, $\gamma_{controlled}$ is calculated to determine the amount of disturbance rejection achieved. The following sections give details of other performance metrics used in the analysis of the control laws.

1. Beam Intensity Increase Factor

The obvious consequence of optical beam jitter is the diminished ability to point the beam at a target. A slightly less obvious, but equally detrimental effect of beam jitter is to reduce the beam intensity (W/m^2) at the receiving sensor or target. This effect, for example, could dramatically decrease the signal to noise ratio of the laser communication system or the lethality of a high energy laser weapon. To illustrate the benefit of jitter control, the *beam intensity increase factor* is calculated. This metric is a ratio of the beam intensity at the target with and without jitter control:

$$\eta = \frac{I_{controlled}}{I_{uncontnrolled}} \tag{22}$$

The beam intensity (irradiance) is given by Equation 23 where P is the total beam power and r_{eff} is the effective beam radius [17].

$$I = \frac{P}{\pi \cdot r_{eff}^2} \tag{23}$$

When the beam contains jitter, the effective beam radius becomes the sum of the stationary beam radius, r_0, and beam position deviation from the target (standard deviation).

$$I = \frac{P}{\pi \cdot (r_0 + \sigma)^2} \tag{24}$$

Where σ is the standard deviation of the beam position radius: $\sigma^2 = \sigma_{Axis-1}^2 + \sigma_{Axis-2}^2$. Plugging into Equation 22 yields the following:

$$\eta = \frac{(r_0 + \sigma_{uncontrolled})^2}{(r_0 + \sigma_{controlled})^2} \tag{25}$$

In order to define η in more general terms, we convert the amount of beam jitter from standard deviation of beam position, σ (μm), to standard deviation of beam deflection angle, σ_θ (microradians):

$$\sigma(x) = \sigma_\theta x \tag{26}$$

Where x is the path distance to the target. In other words, we find σ_θ by normalizing the beam position deviation with the beam path length on the JCT, l_{JCT}.

$$\sigma_\theta = \frac{\sigma(l_{JCT})}{l_{JCT}} \tag{27}$$

Assuming the beam is Gaussian, diffraction limited and focused on the target, the beam radius at the target, r_0, is also a function of path length, x [17]:

$$r_0(x) = \frac{\lambda}{\pi \cdot w_0} x \tag{28}$$

Where λ is the optical wavelength and w_0 is the radius of the beam (defined by the $1/e^2$ intensity point) at the source [17]. Plugging into Equation 25 yields the following result.

$$\eta(\lambda, w_0) = \frac{(\frac{\lambda}{\pi \cdot w_0} + \sigma_{\theta,\, uncontrolled})^2}{(\frac{\lambda}{\pi \cdot w_0} + \sigma_{\theta,\, controlled})^2} \tag{29}$$

For a normal run on the JCT, $\sigma_{\theta,uncontrolled}$ is calculated with the data taken between 0 and 5 seconds (no control), and $\sigma_{\theta,controlledd}$ is calculated from the data with control on between 10 and 15 seconds. The transient data (from 5-10 seconds) is not used to allow the controller to reach a steady state. For this calculation, we plug in a wavelength of λ = 1064 nm and a 20 cm diameter beam, which is representative of directed energy beam control applications.

2. Convergence Time

The convergence time for an adaptive filter controller is the amount of time necessary for the weight updating algorithm to converge to a steady state weighting vector. The amount of jitter rejection will also reach a steady state at this time. Instead of reporting the convergence time for the two axes separately, the standard deviation of the radius beam position is used. We define the convergence time, τ_c, as the amount of time needed to reach 99 percent of the final jitter rejection.

$$\sigma(\tau_c) \cdot 99\% = \sigma(t_{final}) \tag{30}$$

3. Calculating $\gamma_{optimal}$

When possible, $\gamma_{optimal}$, from Equation 7, is computed and compared with the experimental result, $\gamma_{controlled}$. As discussed in Chapter IV, it is only possible to calculate $\gamma_{optimal}$ when a single control block is used.

Comparing the theoretical $\gamma_{optimal}$ with the experimental result is not as straightforward as first expected by the author. The secondary plant dynamics are not included in the Wiener filter derivation like they are in the adaptive filter algorithms (using the Filtered-X modification). As a result, the Wiener filter theory was modified to use the filtered reference signal, $\hat{\mathbf{r}}(n)$. Therefore, the autocorrelation matrix in Equations 5 and 6 becomes: $\mathbf{R} = \mathrm{E}[\hat{\mathbf{r}}(n)\hat{\mathbf{r}}^{\mathrm{T}}(n)]$ and the cross-correlation vector is: $\mathbf{p} = \mathrm{E}[\hat{\mathbf{r}}(n)d(n)]$.

To justify this modification, Figure 27 shows the theoretical weight vector, $\mathbf{w}_{optimal}(n)$, from Equation 5 using both a filtered and unfiltered reference signal. Also

shown in the plot is an actual weight vector, $\mathbf{w}(n)$, that was calculated on-line by an FX-RLS controller. A 55 stage filter was used with 10 PSD stages and 45 accelerometer stages.

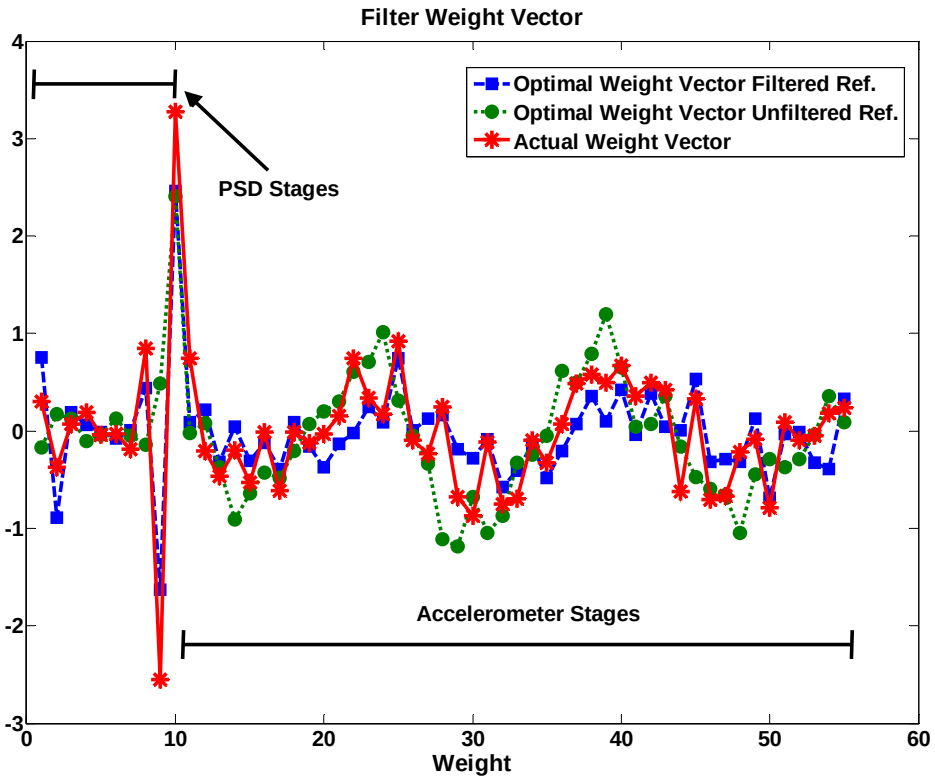

Figure 27. Comparison of weight vector, w(n).

Although the actual weight vector does not converge exactly to either $\mathbf{w}_{optimal}(n)$ variation, it more closely matches the filtered reference signal vector.

Even with the above modification to the Wiener equation, $\gamma_{optimal}$ and $\gamma_{controlled}$ are still not directly comparable. This is because while a Filtered-X adaptive filter uses a filtered reference signal in the weight updating algorithm, it uses an unfiltered reference signal when calculating the output command: $y(n) = \mathbf{w}^{\mathrm{T}}(n)\mathbf{r}(n)$ from Equation 3. This nuance of the Filtered-X method is not captured in the Wiener filter theory. Essentially, our $\gamma_{optimal}$ calculation uses the ideal Filtered-X model from Figure 15, where $S(z) = \hat{S}(z)$

and the secondary plant dynamics are assumed linear. Therefore, we will presume the $\gamma_{optimal}$ calculation to be an approximation of the theoretical best case $\gamma_{controlled}$.

Adaptive filter theory is a very complex topic and predicting a controller's performance on a real world system is not trivial. Experimental results, like the ones in this thesis, are always necessary to validate the performance of proposed control systems. This section illustrates the great difficulty to determine valid theoretical predictions of performance. In fact, it was debated whether to include the $\gamma_{optimal}$ analysis at all. However, the author believes theoretical predictions (even if they are only approximations) are important in the thorough understanding of the control system.

4. Power Spectral Density Analysis

For every experiment, two plots are produced to measure the effectiveness of the control law. A power spectral density plot shows the beam position at the target in the frequency domain. The uncontrolled data (0-5 seconds of a test) is displayed in reference to the controlled data (10-15 seconds). The transient data (5-10 seconds) is not used in the power spectral density analysis. The power spectral density plot highlights the controller's ability to reject disturbances at specific frequencies.

5. Standard Deviation of Beam Position Error

To observe the rate of convergence, the standard deviation of the beam position is plotted in the time domain. This plot illustrates the controller's ability to quickly converge to the optimal gains. Instead of plotting the two axes separately (Axis-1 and Axis-2) the radius beam position is used.

6. Organization of Analysis

A total of five adaptive filter techniques are discussed in this thesis: single reference feedforward, multiple reference feedforward (methods 1 and 2), feedback and hybrid feedback/feedforward. Two weight updating algorithms are covered: FX-LMS and

FX-RLS. In addition, these control techniques are tested with the target sensor mounted both on and off the vibration platform. Consequently, there are 20 different configurations to test and analyze.

The purpose of this paper is not to compare system performance versus target position, but to demonstrate that these control techniques work in both target position scenarios. Therefore, the analysis of the two target positions is treated separately. Similarly, the FX-LMS and FX-RLS algorithms have been studied in great detail in the literature and their differences are well understood. FX-RLS generally has a faster rate of convergence and smaller steady state error than FX-LMS, at the cost of being more computationally expensive. Therefore, the two methods will also be examined separately except for a brief analysis in the conclusion.

B. FEEDFORWARD ADAPTIVE FILTERS USING MULTIPLE REFERENCE SIGNALS

In this section we compare the multiple reference methods for feedforward control to the single reference method from [2], [3], [4] and [13]. The Filtered-X method with a bias estimator is used for all experiments. The single reference method uses an off-board PSD as a reference sensor, which we know is reasonably well correlated with all disturbances (from Chapter VI). For the multiple reference signal controllers, both methods 1 and 2 for combining the reference signals in the control law are tested. The multi-reference controllers use an on-board PSD and accelerometer reference sensors. Chapter VI showed that the on-board PSD was only well correlated with the DFSM while the accelerometer was correlated with the shakers. Chapter VI also showed that using the Z-axis accelerometer signal would produce the best results for both axes of the system.

Choosing the filter parameters (convergence factor, number of stages etc.) was primarily done by trial and error. In [4], Bateman et al. found that when using a PSD reference signal, the FX-LMS controller performs best with a single stage. This was confirmed, however when using an accelerometer reference signal, many filter stages had better performance. The FX-LMS controller in this experiment used a single stage for the PSD, 45 stages for the accelerometer and a convergence factor of 0.5 ***(S = 1, M = 45, μ =***

0.5*)**. For the FX-RLS controller, the best performing forgetting factor was found to be $\lambda = 0.99$. Multiple stages performed best for both the PSD and accelerometer reference signals. The FX-RLS controller needed more accelerometer stages than PSD stages to effectively attenuate the jitter. **(*S = 10, M = 45).

1. Off-Board Target

With the target sensor off-board the platform, the testbed simulates scenarios such as a free-space laser communications transmitter or an optical relay spacecraft.

a. FX-LMS

All of the FX-LMS controllers were able to attenuate approximately 90 percent of the jitter. The controllers using multiple reference signals preformed as well as the single (off-board PSD) reference type for steady state jitter control. The multiple reference signal controller using method 1 showed the best steady state performance with an intensity increase factor of 30.2. The multiple reference signal methods, however, took much longer to converge to a steady state than the single reference controller.

Table 3 summarizes the results of the experiment. The power spectrum plot in Figure 29 reveals that all of the FX-LMS controllers effectively removed the broadband disturbance, but had some difficulty with the narrowband shaker disturbances (40 Hz and 60 Hz). The power spectrum plot shows an interesting harmonic effect at 120 Hz and 180 Hz. This is likely caused by higher harmonics of the 60 Hz shaker disturbance.

The single reference controller performance was actually better than its $\gamma_{optimal}$ estimate, which is believed to be due to the uncertainty in the $\gamma_{optimal}$ calculation.

Controller					Performance Metrics					
Weight Update	PSD Stgs.	Accel Stgs.	Target Pos.	Ref. Signal	Intensity Factor, η	Converge Time, τ_c	Jitter Rejection $\gamma_{conrolled}$ Axis		Wiener Theory $\gamma_{optimal}$ Axis	
							1	2	1	2
FX-LMS	1-Off	0	Off	Single	31.5	0.8 s	0.893	0.864	0.810	0.776
FX-LMS	1-On	45	Off	Mult.(1)	30.2	12.5 s	0.914	0.878	n/a	n/a
FX-LMS	1-On	45	Off	Mult.(2)	20.2	12.4 s	0.892	0.842	0.896	0.881

Table 3. Disturbance rejection results, feedforward FX-LMS with off-board target.

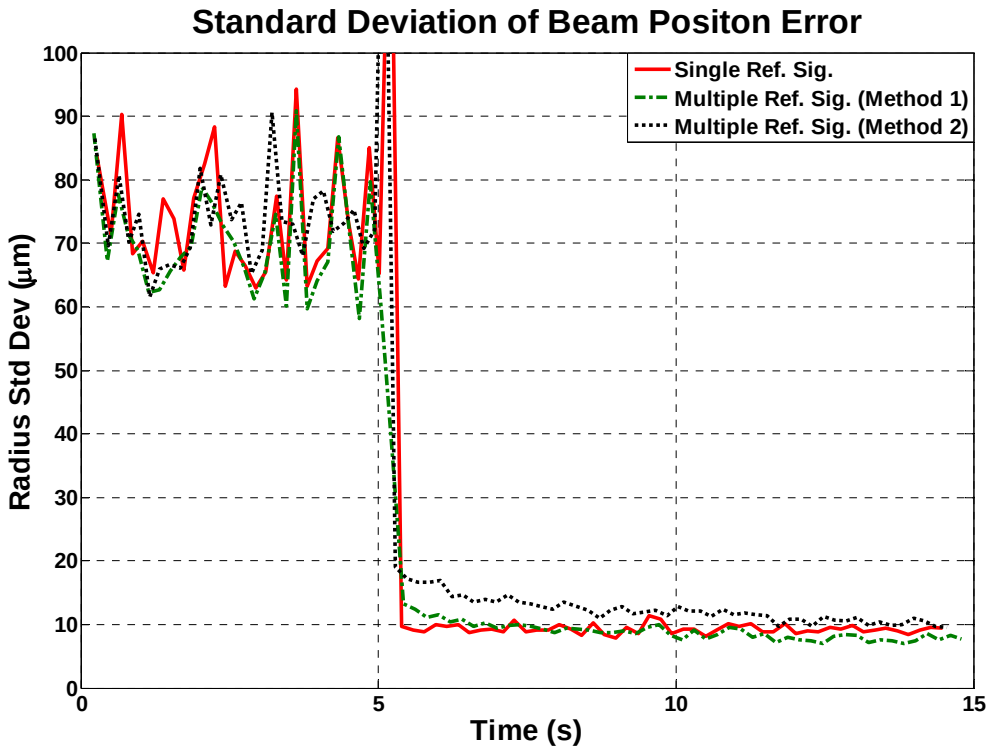

Figure 28. Standard deviation of beam position, feedforward FX-LMS with off-board target.

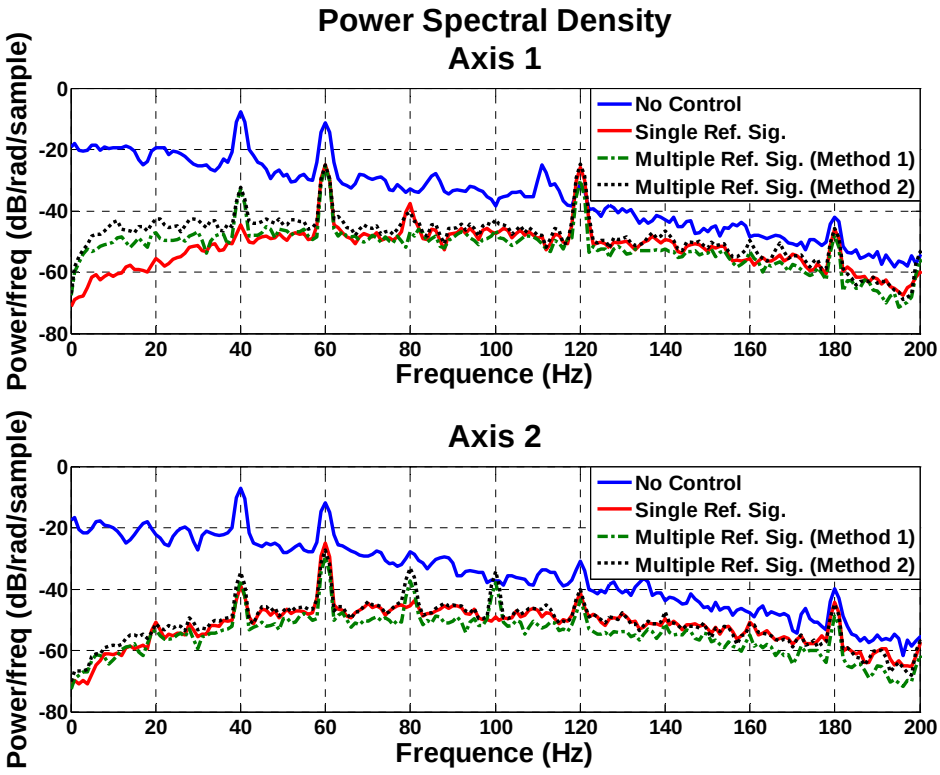

Figure 29. Power spectrum of beam position, feedforward FX-LMS with off-board target.

b. FX-RLS

Using the FX-RLS method, the multiple reference controllers preformed better than the off-board PSD reference signal. Methods 1 and 2 for combining the two reference signals in the control law worked equally well. All FX-RLS methods had very fast convergence times. The power spectrum plot in Figure 31 shows that the CFSM removes both the broadband and narrowband disturbances effectively. The single reference controller had difficulty with the 60 Hz shaker. With the help of the feedforward accelerometer signal, both shaker disturbances were completely removed using the multiple reference method.

The multi-reference signal controller is not only more practical for real systems but achieves superior performance over the single reference. This, however, should not come as a complete surprise. Using multiple reference signals essentially provides more information about the disturbances to the controller than a single reference signal.

While the majority of the jitter is removed from the beam, the same harmonic effect is present in the power spectrum plot in Figure 31. The controller failed to attenuate the disturbance at 20 Hz intervals above 80 Hz.

Controller					Performance Metrics					
Weight Update	PSD Stgs.	Accel Stgs.	Target Pos.	Ref. Signal	Intensity Factor, η	Converge Time, τ_c	Jitter Rejection $\gamma_{conrolled}$ Axis		Wiener Theory $\gamma_{optimal}$ Axis	
							1	2	1	2
FX-RLS	55-Off	0	Off	Single	15.6	0.8 s	0.785	0.799	0.835	0.850
FX-RLS	10-On	45	Off	Mult.(1)	48.1	0.6 s	0.895	0.919	n/a	n/a
FX-RLS	10-On	45	Off	Mult.(2)	49.5	0.7 s	0.895	0.921	0.918	0.911

Table 4. Disturbance rejection results, feedforward FX-RLS with off-board target.

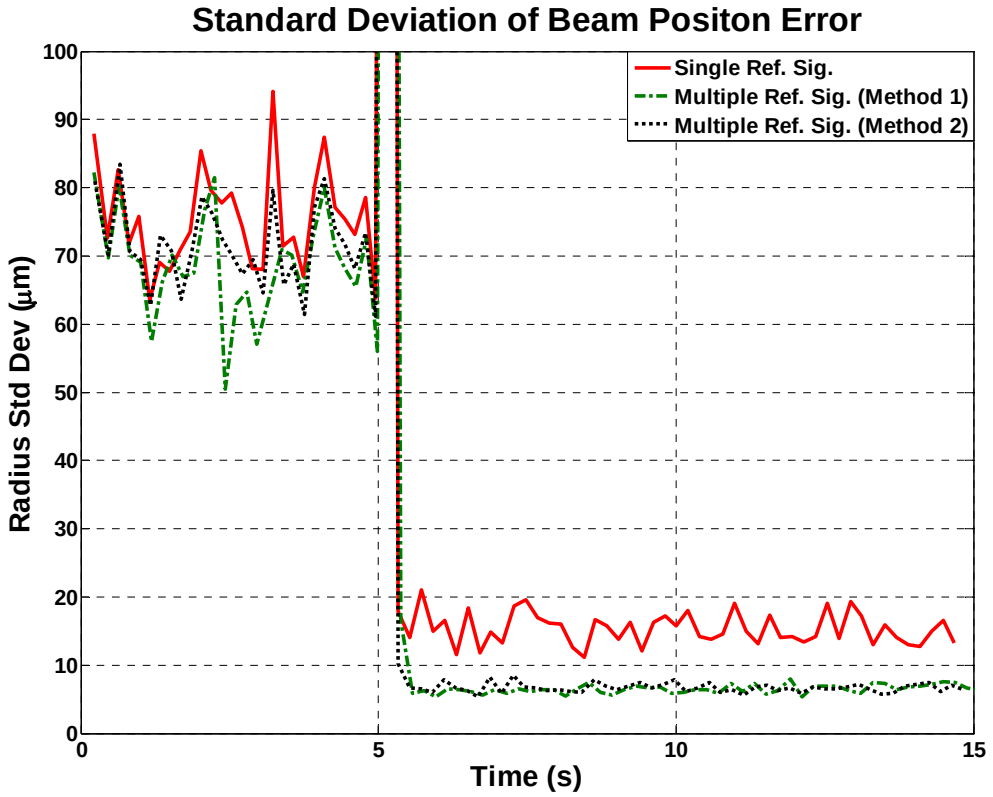

Figure 30. Standard deviation of beam position, feedforward FX-RLS with off-board target.

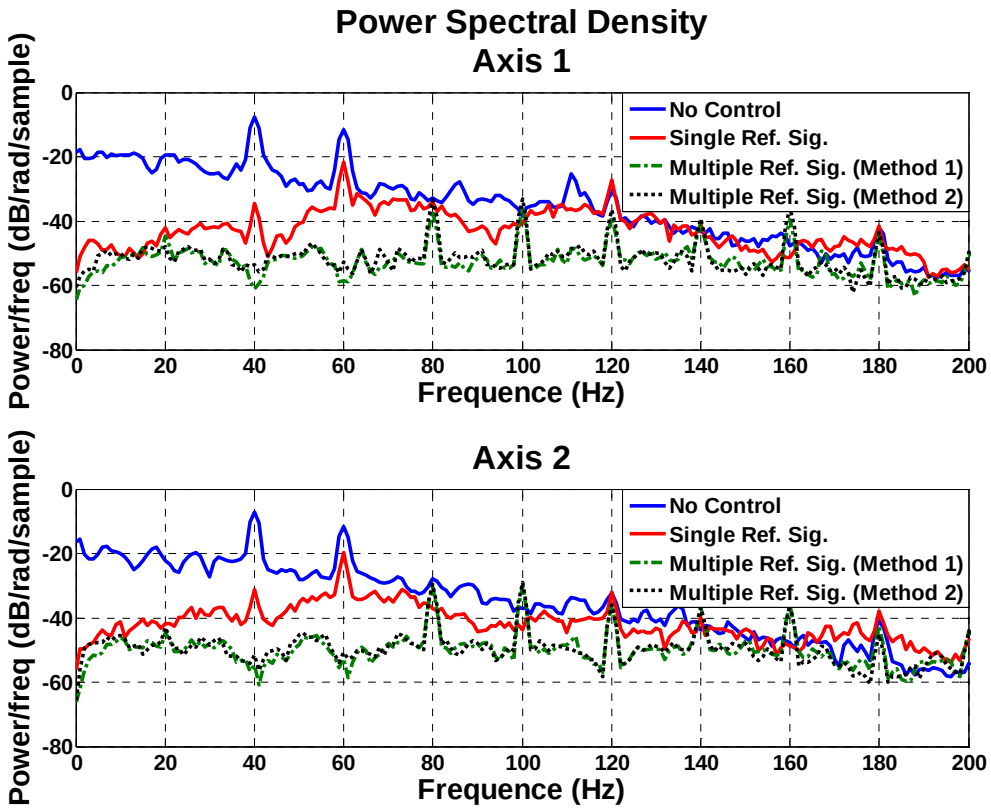

Figure 31. Power spectrum of beam position, feedforward FX-RLS with off-board target.

2. On-Board Target

By mounting the target sensor on the vibration platform it is subjected to the shaker disturbances. Early in the development in the JCT, it was questioned whether the developed control techniques would work in such a situation. Therefore, it was decided to repeat all experiments in the on-board target configuration. When the target sensor is located on-board the platform, the testbed simulates a scenario such as a free-space laser communications receiver, or a jitter control system in a laser resonator.

a. FX-LMS

The FX-LMS controllers successfully attenuated the jitter with the target mounted in the on-board position. The multiple reference signal controllers preformed significantly better than the single reference type. The power spectral density plot reveals that the single reference controller was unable to control the 40 Hz shaker disturbance. In

fact, the controller added jitter to the beam in Axis-1 at 40 Hz. The method 1 multi-reference signal controller achieved the best steady state performance. Similar to the off-board experiment, the multiple reference signal controllers had very long convergence times.

Controller					Performance Metrics					
Weight Update	PSD Stgs.	Accel Stgs.	Target Pos.	Ref. Signal	Intensity Factor, η	Converge Time, τ_c	Jitter Rejection $\gamma_{conrolled}$ Axis		Wiener Theory $\gamma_{optimal}$ Axis	
							1	2	1	2
FX-LMS	1-Off	0	On	Single	7.34	0.3 s	0.770	0.595	0.760	0.456
FX-LMS	1-On	45	On	Mult.(1)	31.0	6.5 s	0.895	0.892	n/a	n/a
FX-LMS	1-On	45	On	Mult.(2)	23.7	8.7 s	0.871	0.858	0.882	0.846

Table 5. Disturbance rejection results, feedforward FX-LMS with on-board target.

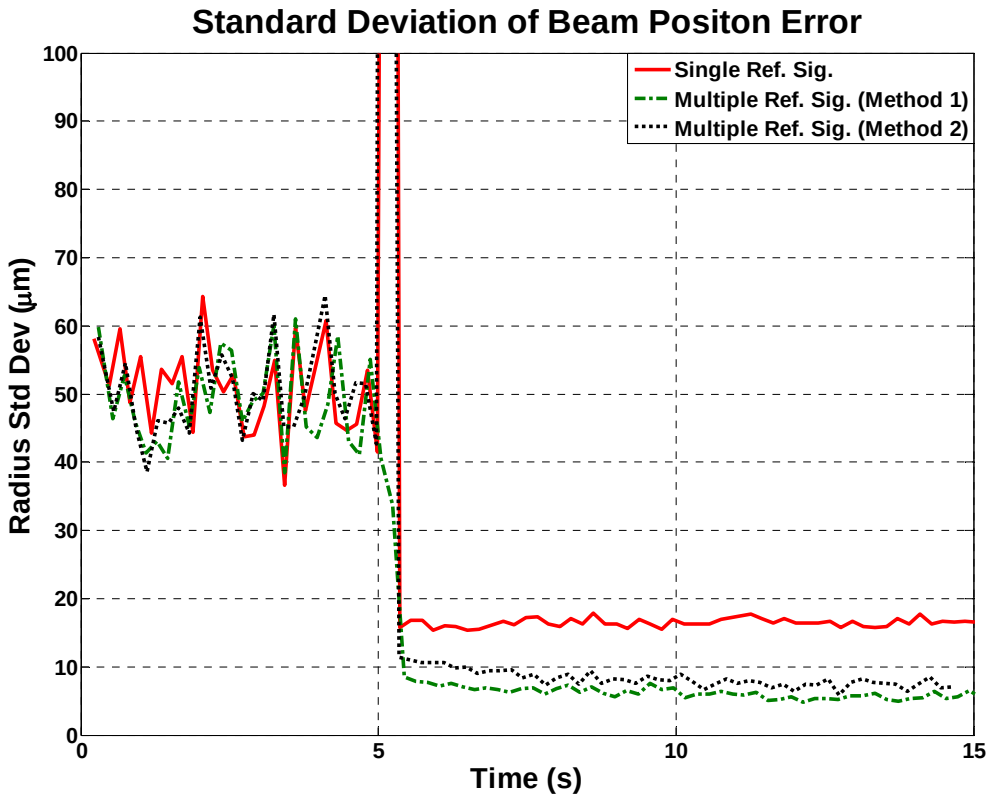

Figure 32. Standard deviation of beam position, feedforward FX-LMS with on-board target.

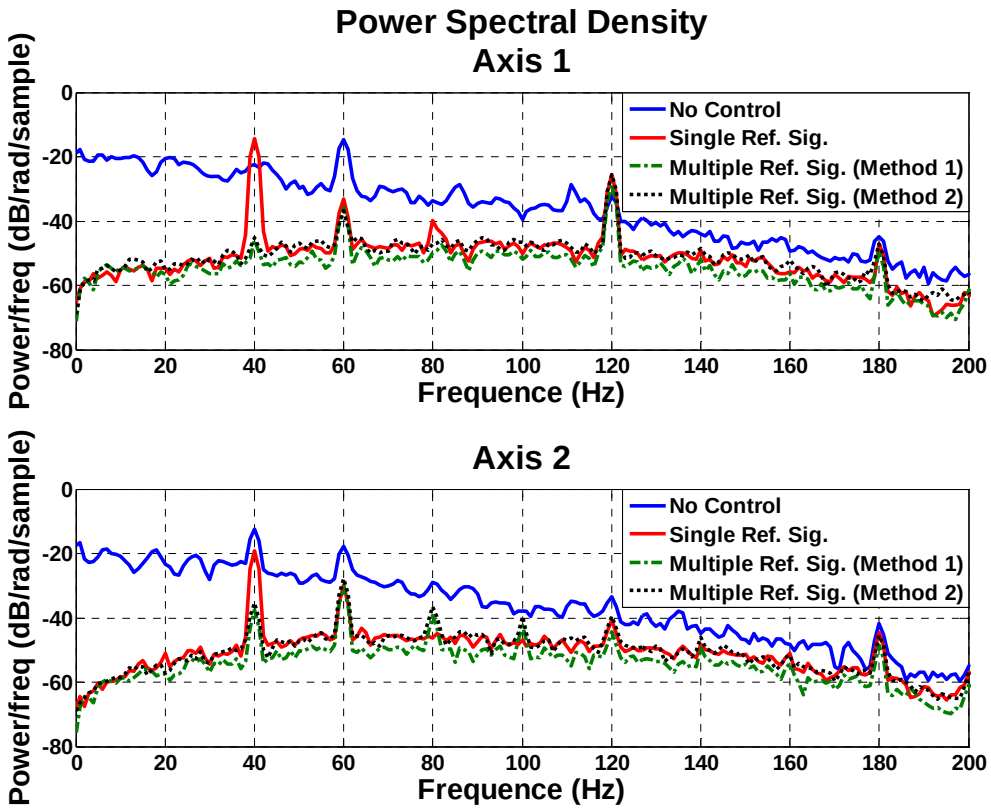

Figure 33. Power spectrum of beam position, feedforward FX-LMS with on-board target.

b. FX-RLS

The on-board target FX-RLS results are very similar to the off-board case. The multiple reference signal controllers were superior at attenuating both the broad and narrowband disturbances. All FX-RLS techniques converged quickly to their steady state performance.

Controller					Performance Metrics					
Weight Update	PSD Stgs.	Accel Stgs.	Target Pos.	Ref. Signal	Intensity Factor, η	Converge Time, τ_c	Jitter Rejection $\gamma_{conrolled}$ Axis		Wiener Theory $\gamma_{optimal}$ Axis	
							1	2	1	2
FX-RLS	55-Off	0	On	Single	7.39	0.3 s	0.771	0.606	0.813	0.674
FX-RLS	10-On	45	On	Mult.(1)	30.9	0.7 s	0.885	0.900	n/a	n/a
FX-RLS	10-On	45	On	Mult.(2)	29.5	0.5 s	0.892	0.896	0.927	0.890

Table 6. Disturbance rejection results, feedforward FX-RLS with on-board target.

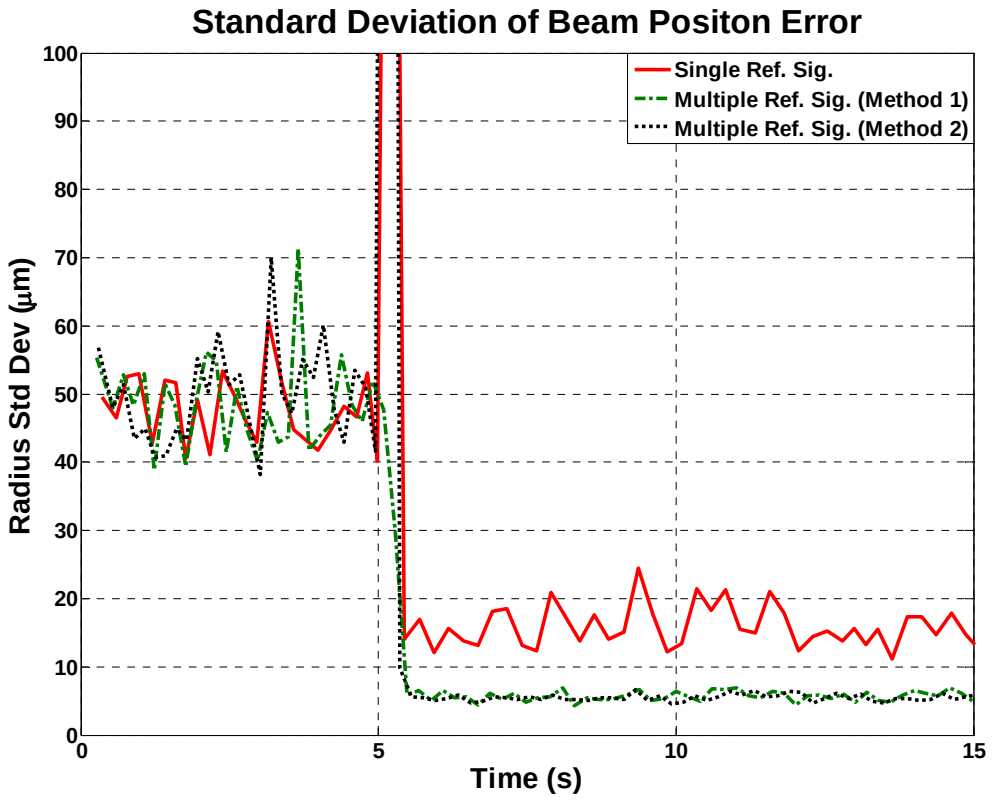

Figure 34. Standard deviation of beam position, feedforward FX-RLS with on-board target.

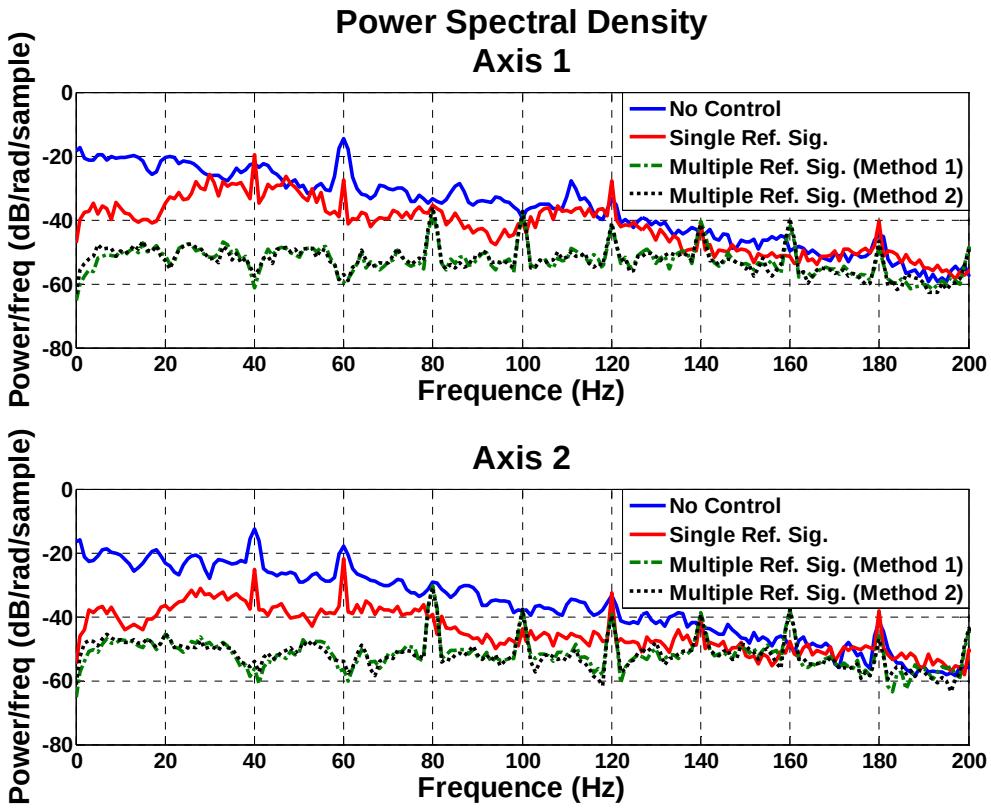

Figure 35. Power spectrum of beam position, feedforward FX-RLS with on-board target.

C. FEEDBACK AND HYBRID ADAPTIVE FILTERS

This section compares the developed feedback and hybrid adaptive filters with the best performing feedforward technique from the previous section. Feedback adaptive filter control has the great advantage of not requiring a reference signal. In addition, analysis in Chapters III and IV gave evidence that the feedback technique may, in fact, perform better than the feedforward method. Chapter IV argued that feedback vs. feedforward performance depends on obtaining a quality model of the secondary plant dynamics and the degree of correlation of the feedforward controller's reference signal(s). Due to the complexity of the algorithms and system dynamics, a comparison of the control methods is difficult to model mathematically and experimental tests are essential for comparing the techniques.

For this test, the feedforward filter was run with the same parameters as in the previous section, $\mu = 0.5$, $S = 1$, $M = 45$ for the FX-LMS controller and $\lambda = 0.99$, $S = 10$, $M = 45$ for the FX-RLS controller. The feedback controller uses an estimate of the primary noise source as a reference signal, $\hat{d}(n)$, with a convergence factor of $\mu = 0.5$ and single stage, $S_{FB} = 1$, for FX-LMS. For the FX-RLS feedback controller, a forgetting factor of $\lambda = 0.99$ and $S_{FB} = 50$ stages was used.

The hybrid adaptive filter requires a reference signal because it is a combination of the feedback and feedforward techniques. Both the FX-LMS and FX-RLS variations of the hybrid controller use a feedback adaptive filter control block in parallel with a feedforward multi-reference controller using method 2 to combine the reference signals. The FX-LMS hybrid controller uses a single feedback stage, a single feedforward on-board PSD stage and 30 feedforward accelerometer stages. ($\mu = 0.5$, $S_{FB} = 1$, $S_{FF} = 1$, $M = 30$) The FX-RLS hybrid controller uses 10 feedback stages, 10 feedforward on-board PSD stages and 30 accelerometer stages ($\lambda = 0.99$, $S_{FB} = 10$, $S_{FF} = 10$, $M = 30$).

A PI controller was placed in parallel with the feedback and hybrid adaptive filters. The PI control gains were tuned manually to $K_p = 0.05$ and $K_i = 200$. With this implementation, the PI controller removes the initial bias from the error signal. Therefore, the bias estimator in the adaptive filter is not necessary. Testing showed that the controller preformed the same with or without the bias estimator.

1. Off-Board Target

a. FX-LMS

The feedback and hybrid methods both preformed well against the feedforward controller. The power spectrum plot in Figure 37 reveals that the feedback type methods controlled the broadband disturbance better than the feedforward method, while control of the narrowband disturbance was essentially equal. Although the convergence times for the feedback and hybrid methods were still relatively slow (compared to FX-RLS) they were an improvement over the feedforward controller. The feedback method showed slightly better performance over the hybrid method.

Inspection of the power spectrum plot in Figure 37 shows that the harmonic effect observed in the feedforward controllers is much less prevalent in the feedback and hybrid controllers.

Controller						Performance Metrics					
Weight Update	$\hat{d}(n)$ Stgs.	PSD Stgs.	Acc. Stgs.	Trgt. Pos.	Cont. Type	Intensity Factor, η	Converge Time, τ_c	Jitter Rejection $\gamma_{conrolled}$ Axis		Wiener Theory $\gamma_{optimal}$ Axis	
								1	2	1	2
FX-LMS	0	1-On	0	Off	FF	30.2	12.5 s	0.914	0.878	n/a	n/a
FX-LMS	1	0	0	Off	FB	50.1	3.8	0.916	0.912	0.862	0.844
FX-LMS	1	1-On	30	Off	Hybrid	46.8	3.8	0.908	0.909	n/a	n/a

Table 7. Disturbance rejection results, feedback/hybrid FX-LMS with off-board target.

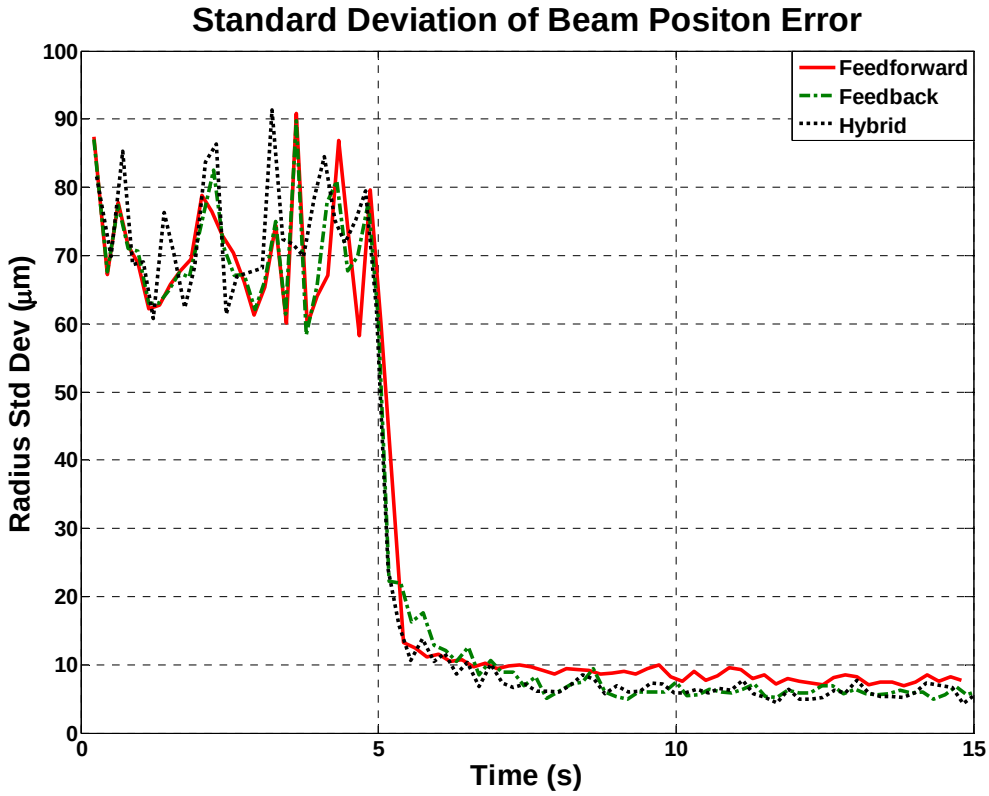

Figure 36. Standard deviation of beam position, feedback/hybrid FX-LMS with off-board target.

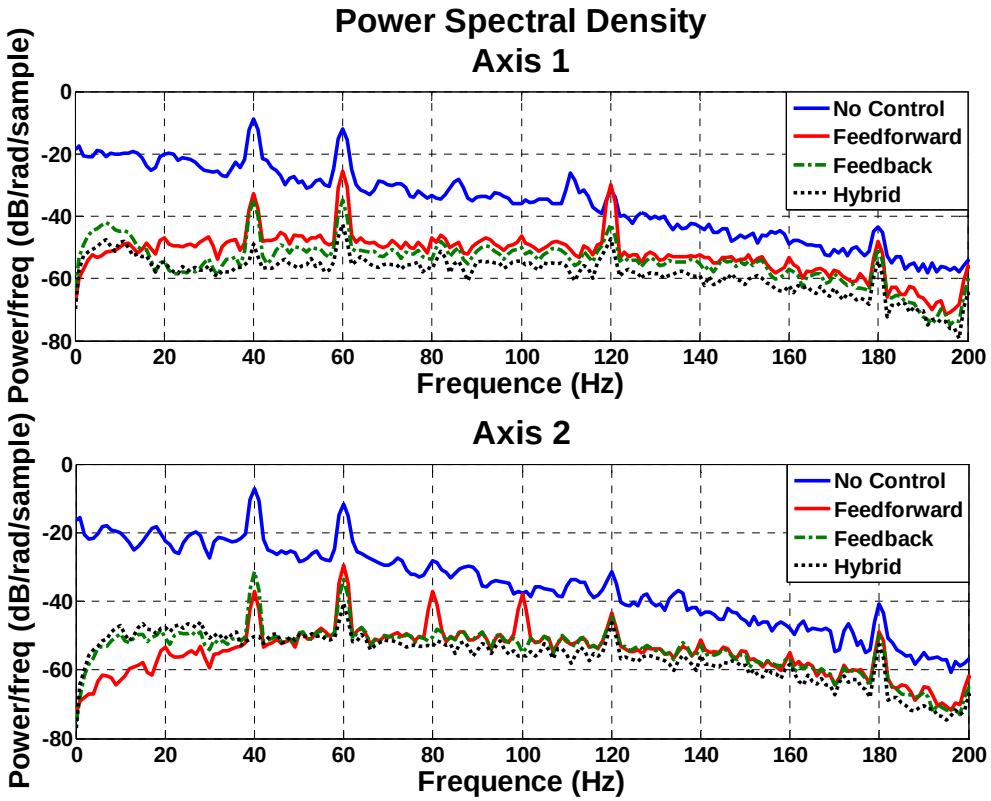

Figure 37. Power spectrum of beam position, feedback/hybrid FX-LMS with off-board target.

b. FX-RLS

Using the FX-RLS weight updater, the feedback and hybrid methods preformed superiorly to the feedforward method. All three methods converged very quickly to their steady state values. The hybrid method had the best overall performance and was able to attenuate approximately 93 percent of the jitter.

Controller						Performance Metrics					
Weight Update	$\hat{d}(n)$ Stgs.	PSD Stgs.	Acc. Stgs.	Trgt. Pos.	Cont. Type	Intensity Factor, η	Converge Time, τ_c	Jitter Rejection $\gamma_{conrolled}$ Axis		Wiener Theory $\gamma_{optimal}$ Axis	
								1	2	1	2
FX-RLS	0	1-On	45	Off	FF	49.5	0.7 s	0.895	0.921	0.918	0.911
FX-RLS	50	0	0	Off	FB	57.3	0.5 s	0.928	0.917	0.944	0.932
FX-RLS	10	10-On	30	Off	Hybrid	65.7	0.4 s	0.935	0.931	n/a	n/a

Table 8. Disturbance rejection results, feedback/hybrid FX-RLS with off-board target.

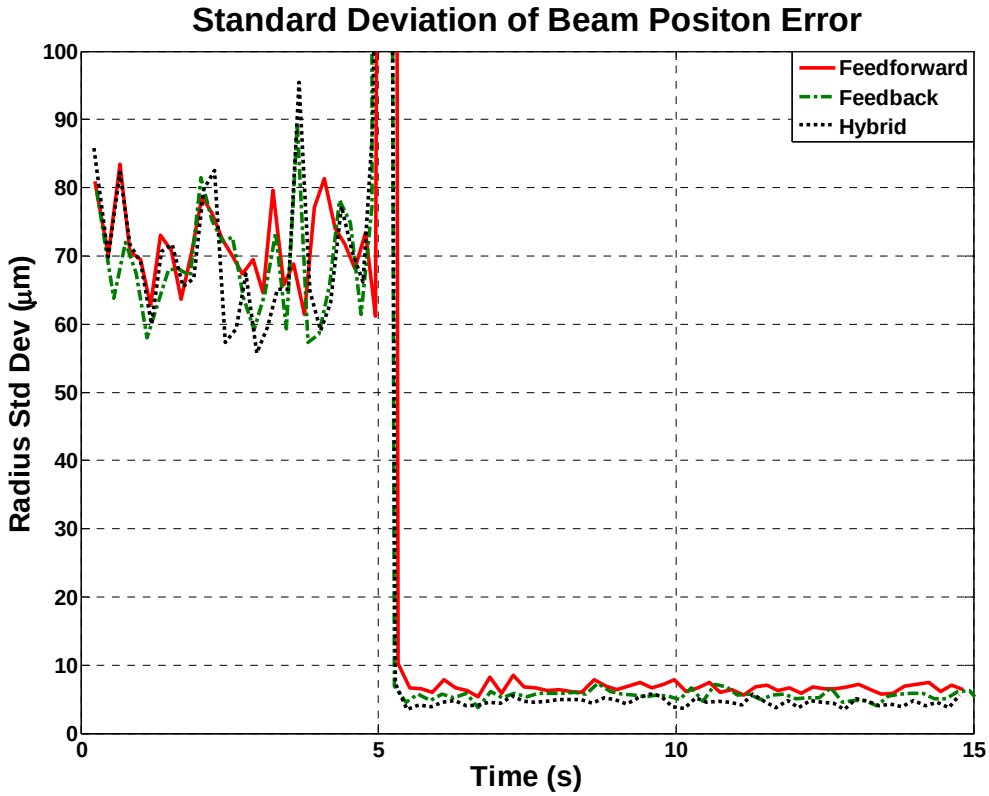

Figure 38. Standard deviation of beam position, feedback/hybrid FX-RLS with off-board target.

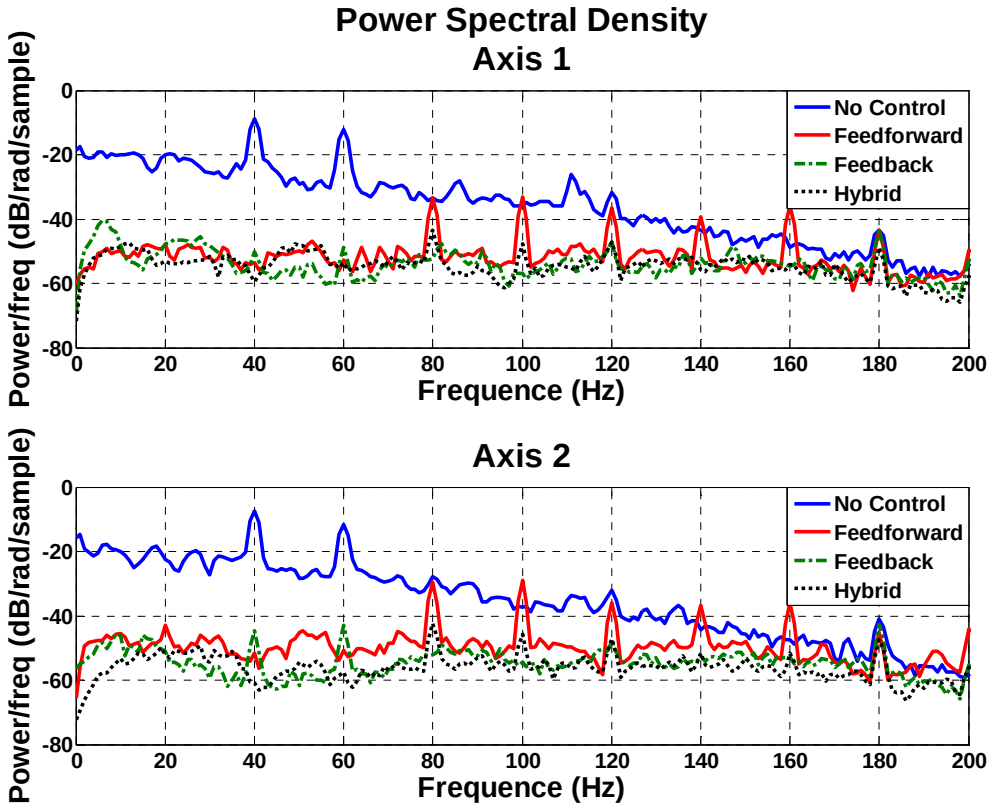

Figure 39. Power spectrum of beam position, feedback/hybrid FX-RLS with off-board target.

2. On-Board Target

a. FX-LMS

The on-board target experiment results were very similar to the off-board results. The feedback and hybrid methods preformed equally to the feedforward method. All three methods had slow convergence times.

Controller						Performance Metrics					
Weight Update	$\hat{d}(n)$ Stgs.	PSD Stgs.	Acc. Stgs.	Trgt. Pos.	Cont. Type	Intensity Factor, η	Converge Time, τ_c	Jitter Rejection $\gamma_{conrolled}$ Axis		Wiener Theory $\gamma_{optimal}$ Axis	
								1	2	1	2
FX-LMS	0	1-On	0	On	FF	31.0	6.5 s	0.895	0.892	n/a	n/a
FX-LMS	1	0	0	On	FB	30.6	4.9 s	0.849	0.893	0.862	0.822
FX-LMS	1	1-On	30	On	Hybrid	31.1	6.5 s	0.896	0.905	n/a	n/a

Table 9. Disturbance rejection results, feedback/hybrid FX-LMS with on-board target.

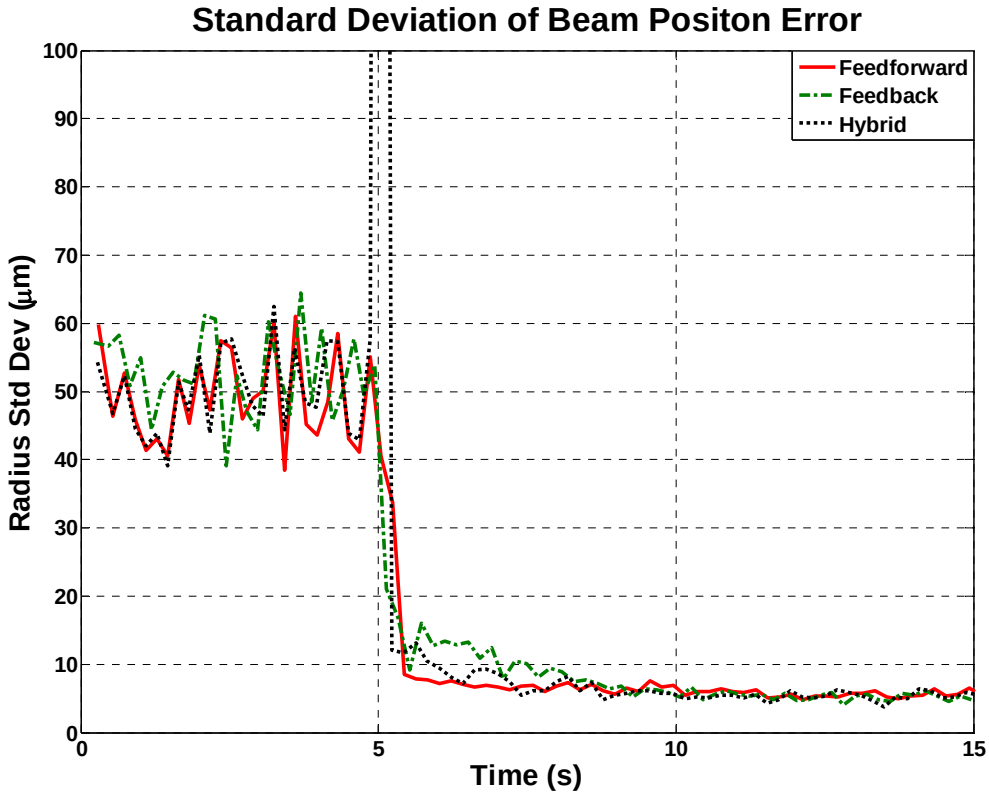

Figure 40. Standard deviation of beam position, feedback/hybrid FX-LMS with on-board target.

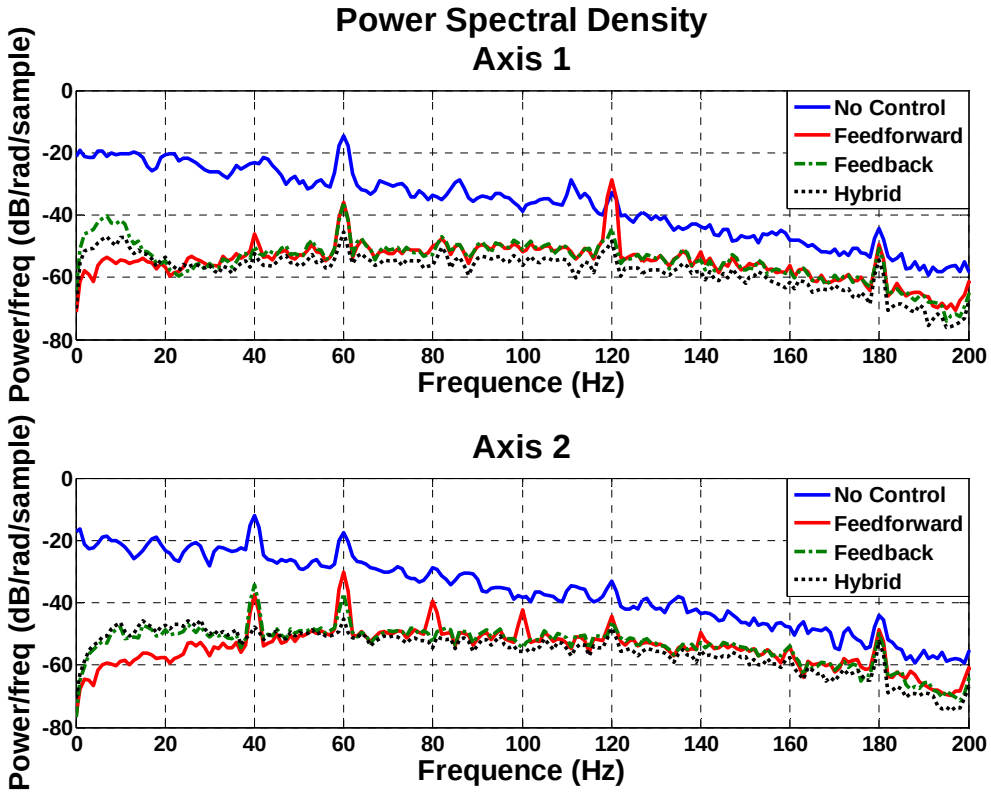

Figure 41. Power spectrum, feedback/hybrid FX-LMS with on-board target.

b. FX-RLS

The FX-RLS on-board target experiments showed that the feedback method preformed equally to the feedforward method. The hybrid controller showed the best overall performance.

Controller						Performance Metrics					
Weight Update	$\hat{d}(n)$ Stgs.	PSD Stgs.	Acc. Stgs.	Trgt. Pos.	Cont. Type	Intensity Factor, η	Converge Time, τ_c	Jitter Rejection $\gamma_{conrolled}$ Axis		Wiener Theory $\gamma_{optimal}$ Axis	
								1	2	1	2
FX-RLS	0	1-On	45	On	FF	30.9	0.7 s	0.885	0.900	n/a	n/a
FX-RLS	50	0	0	On	FB	31.2	0.3 s	0.897	0.887	0.933	0.912
FX-RLS	10	10-On	30	On	Hybrid	41.2	0.5 s	0.922	0.916	n/a	n/a

Table 10. Disturbance rejection results, feedback/hybrid FX-RLS with on-board target.

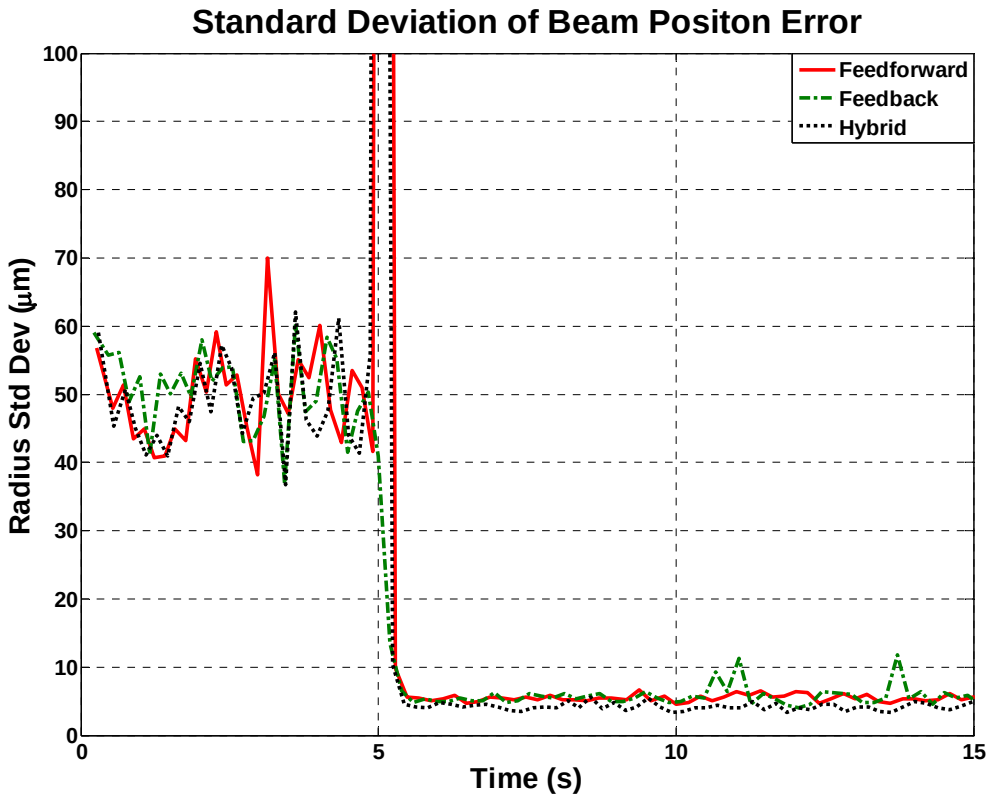

Figure 42. Standard deviation of beam position, feedback/hybrid FX-RLS with on-board target.

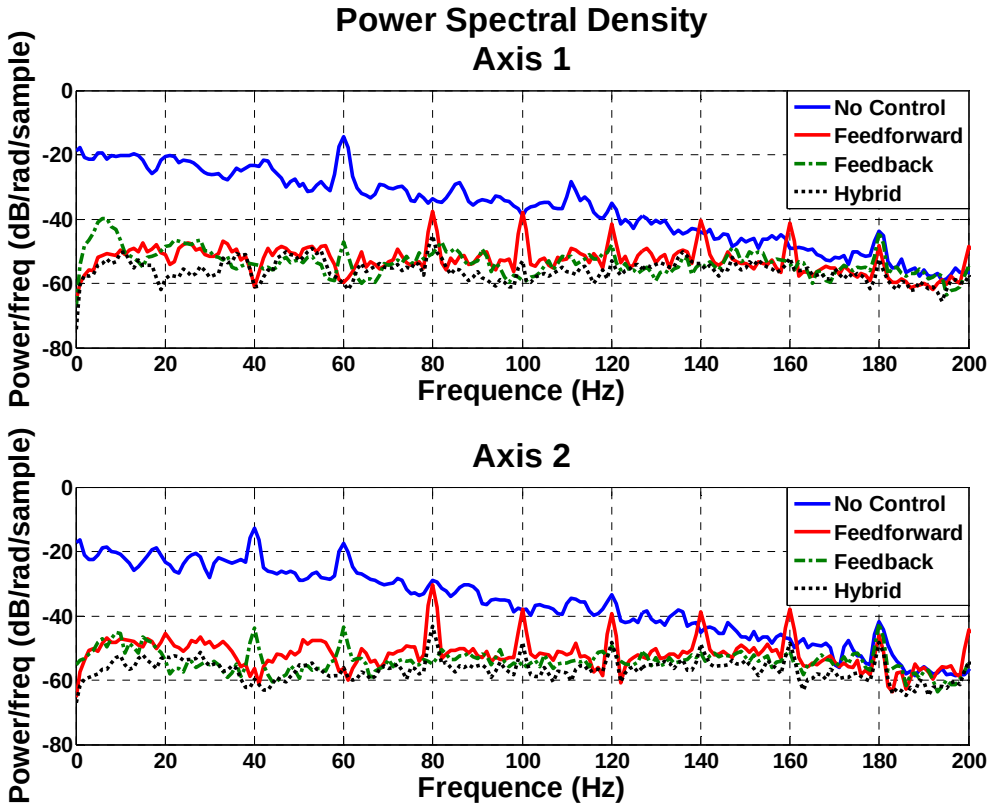

Figure 43. Power spectrum of beam position, feedback/hybrid FX-RLS with on-board target.

D. CONCLUSIONS

The jitter rejection experiments detailed in this chapter have the very simple objective of pointing the laser beam accurately at a static target while rejecting jitter using a fast-steering mirror. The experiments in this chapter took 10 variations (20 if you count off-board/on-board target) of adaptive filter controllers and compares them using several performance metrics. The overall lessons learned are given in the following sections.

1. FX-LMS vs. FX-RLS

During the jitter rejection experiments, the FX-LMS and FX-RLS controllers often preformed equally well in terms of steady state jitter rejection. Overall, the FX-RLS controller was able to remove slightly more disturbance than FX-LMS. The simpler LMS

algorithm was able to achieve this high performance because the LMS convergence factor, μ, was chosen to increase steady state performance at the cost of slower convergence. The FX-RLS method achieved far better convergence times (as much as 20 times better) than FX-LMS.

2. Multiple Feedforward Reference Signals

In past JCT experiments at NPS ([2], [3], [4], [13]) a single reference sensor was used to demonstrate feedforward beam control techniques. When the feasibility of obtaining such a signal in practice was questioned, it became a goal of this thesis to demonstrate feedforward jitter control using more practically attainable reference signals. This lead to the development of the multiple reference signal methods.

The jitter rejection experiments showed that multiple semi-coherent reference signals preformed as well as or better than the single off-board PSD reference sensor. This proved the overall feasibility of feedforward jitter control for situations when obtaining a fully coherent reference signal is not possible. Two methods were created to combine the semi-coherent reference signals in the control law. Experiment showed that the methods have generally equal performance for both steady state jitter rejection and convergence times. It was shown in Chapter IV that method 1 has a lower computational cost, and therefore, this method is considered the overall best technique.

The power spectrum plots revealed that a harmonic effect was present in the position of the controlled beam. Comparison with the feedback controller experiments indicated that this effect was due to higher harmonics of the shaker disturbances in the feedforward accelerometer reference signal.

3. Feedback Adaptive Filters

The requirement of an auxiliary reference sensor(s) in the feedforward adaptive filter inspired the development of a pure feedback adaptive filter that internally generates its own reference signal. Further analysis indicated that the feedback technique may perform better than feedforward. The jitter rejection experiments confirmed this speculation. In most cases, the feedback technique had better steady state jitter rejection

and convergence times than feedforward. The hybrid technique had the best overall performance. The harmonic effect seen in the feedforward controllers was not as present in the hybrid controller and completely absent in the feedback controller.

VIII. TARGET TRACKING AND BEAM POINTING WITH ADAPTIVE FILTERS

In the previous chapter, adaptive filter methods were demonstrated to point the beam at a static target, the (0, 0) position on the target PSD. While the experiments in Chapter VII are directly applicable to many beam control applications, other beam control scenarios exist such that the target is dynamic. This control challenge is sometimes referred to in the literature as Acquisition, Tracking and Pointing (ATP). This chapter addresses the application of adaptive filters for target tracking and beam pointing.

A. TRACKING CONTROL ALGORITHMS

1. PI Controller

The proportional integral (PI) controller is the classical target tracking algorithm. A PI controller is a negative feedback technique that applies fixed gains to the error signal (difference between the beam position and the desired position) and integral of the error signal [16]. Refer back to Chapter IV.G.1 for more detail. The controller's performance can be adjusted by manually tuning the control gains. As discussed in Chapter IV, the PI controller is linear time-invariant and cannot adapt to the disturbance characteristics. The PI controller is used for comparison with the adaptive filter methods.

2. Adaptive Filter Trackers

The adaptive filter algorithms developed in Chapter IV can be modified to track a target by simply modifying the error signal definition from Equation 4. The desired position is no longer the target center, but the tracking signal, $t(n)$. Therefore, we modify Equation 4 to include the tracking signal:

$$e(n) = d(n) - s(n) * y(n) - t(n) \tag{31}$$

The adaptive filter always minimizes the error signal, and by subtracting the tracking signal, $t(n)$, from the output of the target sensor, the controller will track $t(n)$. Figure 44 illustrates the implementation of the adaptive filter tracker.

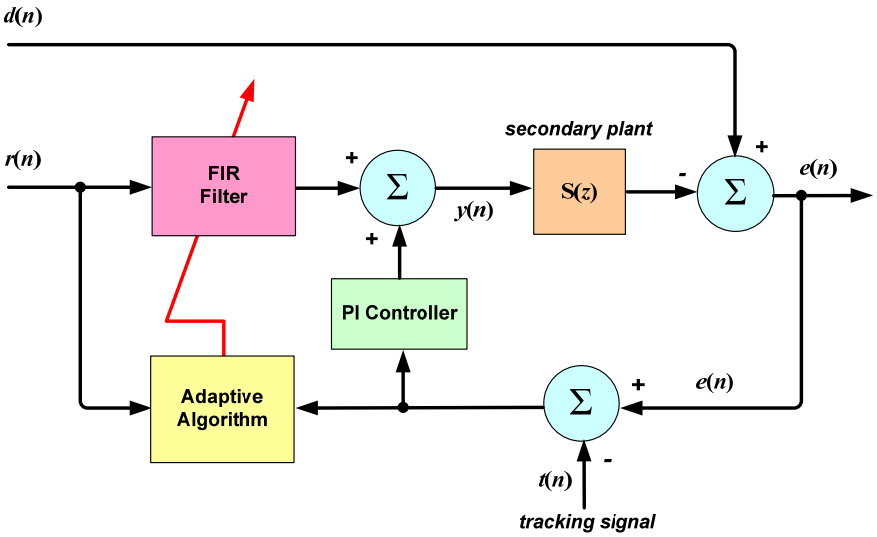

Figure 44. Adaptive filter tracking algorithm.

Initial testing with the adaptive filter tracker showed instability with the dynamic target. To compensate for this problem, the adaptive filters were placed in parallel with a PI controller. Recall, that the feedback and hybrid adaptive filters from Chapter IV already included a parallel PI controller. Therefore, now all three filter types (feedforward, feedback and hybrid) use parallel PI controllers. An example of a parallel PI / adaptive filter controller is shown Figure 44 as well as Figure 19 from Chapter IV.

B. PERFORMANCE METRICS

The adaptive filter controllers were asked to track a small circle on the target PSD while being subjected to the same narrow and broadband disturbances as in Chapter VII. The beam tracks a 200 μm radius (or ~ 160 microradian half-angle) circle on the detector at a rate of 20 Hz. The tracking signal is created by feeding two 20 Hz sine waves with a 90 degree phase shift to the two axes of the controller.

The experiments were conducted with the target sensor in the off-board position only. This configuration imitates actual target tracking applications. Each experiment is run for 15 seconds, 0-5 seconds is open-loop (or no control). The PI controller turns on at t = 5 seconds; and at t = 10 seconds, the adaptive filter controller turns on and runs in parallel with the PI controller.

1. RMS Track Error

The primary quantitative performance metric for target tracking is the RMS track error. The root-mean-square (RMS) is calculated for the track error or the difference between the beam position and the tracking signal (desired position). This value is analogous to using the standard deviation in the previous chapter to represent beam spread. The RMS error is also plotted against time to compare the performance of the PI controller (5-10 seconds) and the adaptive filter controller (10-15 seconds).

2. Beam Trace Plot

A beam trace plot is also provided for one of the experiments as a qualitative measure of performance. The beam position is plotted on an Axis-1/Axis-2 grid to compare the PI controller to the adaptive filter. By tracing a circle for 5 seconds at 20 Hz, the beam makes 100 rotations of the 200 μm radius.

C. TARGET TRACKING EXPERIMENTS

The results from the target tracking experiments are summarized in Table 11. The addition of adaptive filter control, parallel to the PI controller, improved the trackers performance in all cases. A PI controller alone achieved 57.8 μm RMS track error while tracking the 200 μm radius circle. Adding a feedback or hybrid adaptive filter improved performance by up to 10 times. The feedforward adaptive filter achieved relatively poor results.

Controller						Performance Metrics
Weight Update	$\hat{d}(n)$ Stgs.	PSD Stgs.	Acc. Stgs.	Target Position	Controller Type	RMS Radius Tracking Error (μm)
---	---	---	---	---	PI Feedback	57.8
FX-LMS	0	1-On	45	Off	Adaptive Feedforward	47.8
FX-LMS	1	0	0	Off	Adaptive Feedback	7.5
FX-LMS	1	1-On	30	Off	Adaptive Hybrid	7.8
FX-RLS	0	10-On	45	Off	Adaptive Feedforward	51.2
FX-RLS	50	0	0	Off	Adaptive Feedback	5.8
FX-RLS	10	10-On	30	Off	Adaptive Hybrid	5.2

Table 11. Summary of target tracking results

Figure 45 shows a beam trace plot comparing the PI tracker to the FX-RLS hybrid tracker. The figure dramatically demonstrates the improvement of performance achieved by using the adaptive filter tracker. Not only does the PI controller trace a different path at each revolution, but also the mean path is not circular. The adaptive filter tracker closely traces the 200 μm circle. Beam trace plots for the other experiments were very similar to Figure 45.

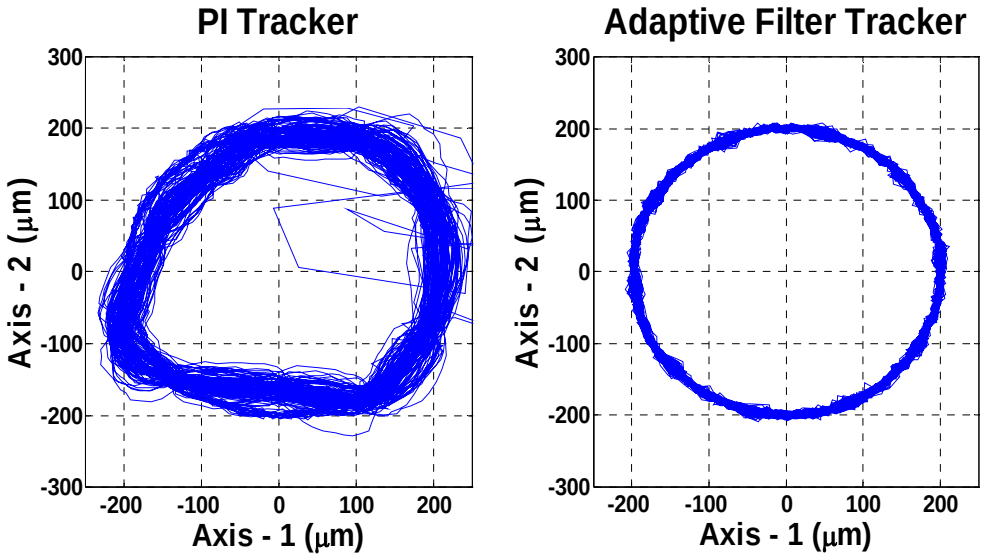

Figure 45. Beam Trace Plot, PI Tracker vs. FX-RLS Hybrid Tracker

The FX-RLS feedback and hybrid controllers achieved slightly better performance than FX-LMS. Similar to the Chapter VII results, FX-LMS showed a much slower convergence time which is visible in the RMS track error plot in Figures 45 (FX-LMS) and 46 (FX-RLS).

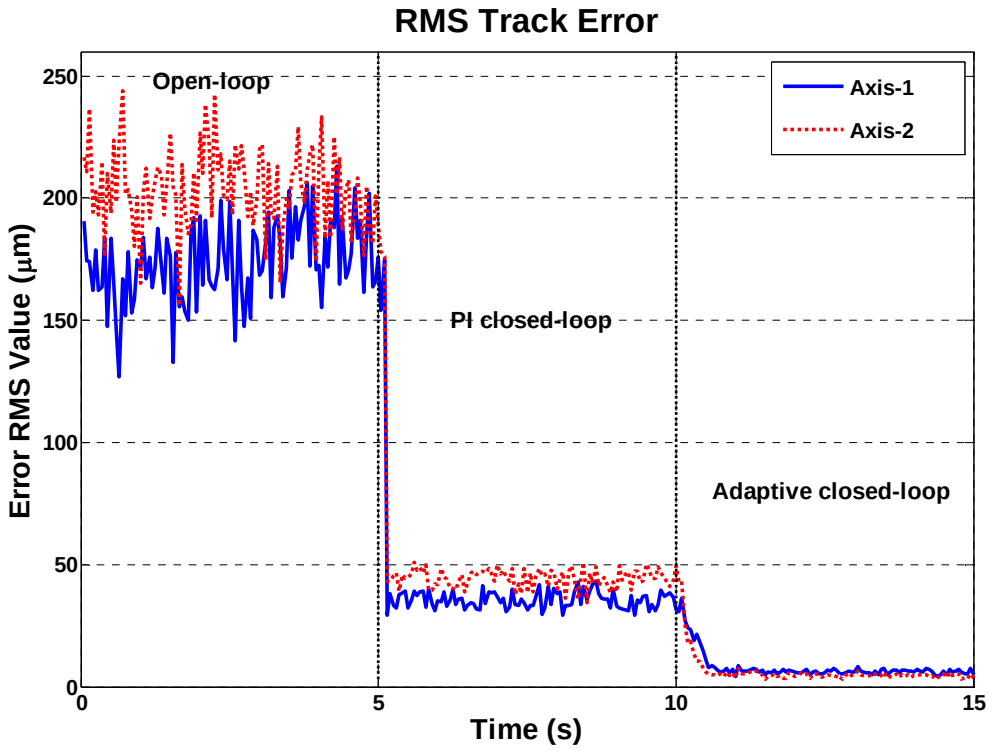

Figure 46. RMS Track Error for FX-LMS Hybrid Tracker

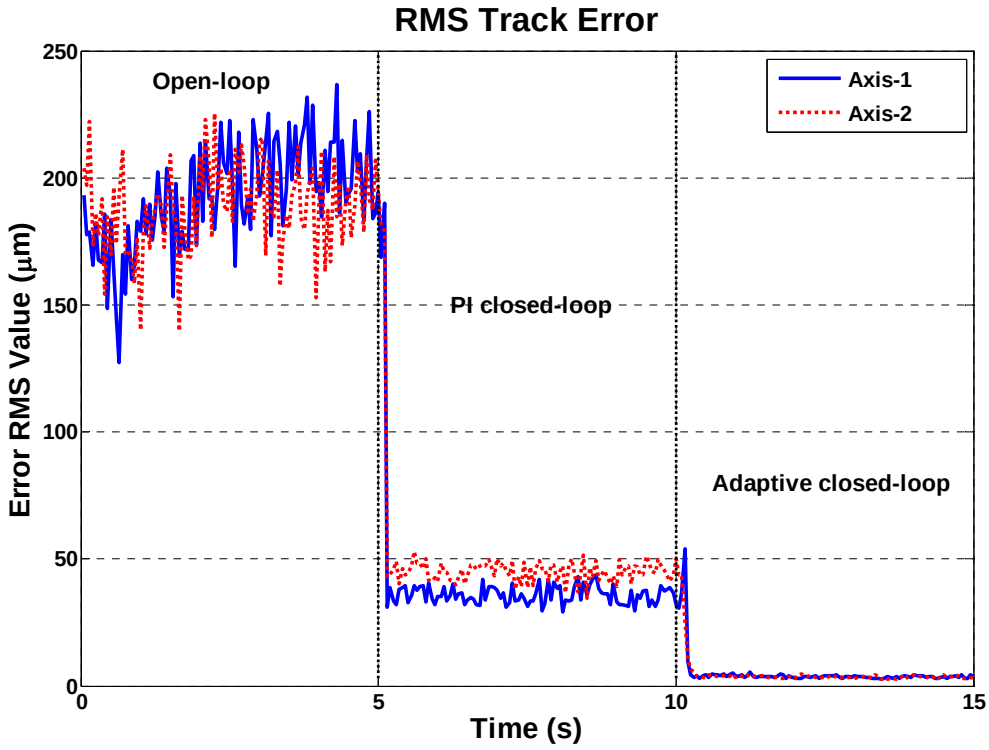

Figure 47. RMS Track Error for FX-RLS Hybrid Tracker

IX. CONCLUSIONS

A. SUMMARY

This research was conducted as a follow on to research preformed on the JCT by Professor Brij Agrawal, Dr. Joseph Watkins, Brett Bateman and Dr. Hyungjoon Yoon [2], [3], [4], [13]. In their research, feedforward adaptive filter algorithms that used a single off-board PSD reference sensor were developed and successfully tested on the JCT. The original inspiration for the present research came when the feasibility of obtaining a fully coherent reference signal in a practical beam control application was questioned. The goal was to develop feedforward jitter control methods using multiple semi-coherent reference signals. As the research progressed, it became another goal of this thesis to demonstrate the use of feedback adaptive filter techniques that had previously only been studied by other research groups (Professor Gibson at UCLA). An additional objective was to apply adaptive filter methods to a target tracking control algorithm.

In order to implement feedforward jitter control, methods for using multiple reference signals in the control law were developed. The reference sensors used (on-board PSD and accelerometer) were practically attainable in beam control applications. A feedback adaptive filter method was introduced that used only the error signal to estimate the primary noise source for use as a reference. A hybrid method, which used both feedforward and feedback techniques, was also tested.

In order for this research to be applicable to many beam control systems, the computationally economic FX-LMS algorithm and the higher performing FX-RLS algorithm were both tested. The JCT was configured with the target sensor both on and off the vibration platform to imitate various beam control scenarios. In addition, the adaptive filter controllers were tested while tracking both a static target (classical jitter control) and a dynamic target (target tracking).

Due to the complexities of adaptive filter algorithms, mathematical predictions of performance are difficult to produce accurately. Experiment on a testbed, like the JCT at

NPS, is vital for designing these advanced control techniques. In this thesis, some mathematical approximations of performance using optimal Wiener filter theory were attempted. These predictions were helpful in choosing the proper accelerometer reference signal.

Experimental results showed that the multi-reference feedforward adaptive filter preformed as well as or better than the single reference methods used in previous JCT research. The feedback and hybrid adaptive filter techniques had the best overall performance. The FX-LMS algorithm measured up very well against the more complex FX-RLS method in terms of steady state jitter rejection. The FX-LMS method did, however, take much more time to converge to a steady state.

Adaptive filter methods were successfully demonstrated for tracking a dynamic target. The feedback and hybrid controllers had as much as 10 times greater performance than a classical PI target tracker.

In many cases, instability was an issue with the adaptive filters, especially when a large DC bias was attempted to be rejected. To increase the stability and overall robustness of the controller, a classical PI controller was often used in parallel with the adaptive filter.

B. SUGGESTIONS FOR FUTURE RESEARCH

As a result of the research done on the JCT, several other interesting topics of study have arisen. These are suggestions for future research:

- Thus far, all controllers on the jitter control testbed have been single-input single-output or single channel in adaptive filter terms. Kuo develops methods for multi-channel adaptive filters in [14] which could be implemented on the jitter control testbed. This technique would couple the control between the axes of the CFSM and could possibly further improve performance.

- The adaptive filters in this thesis are all of the transversal filter type. The research team at UCLA has primarily studied the more advanced adaptive lattice filter. Implementation of this technique on the JCT is needed, as well as a thorough study of its performance versus the transversal filter.

- One of the new developments on the JCT during the course of this research was the acquisition of a second shaker. This second shaker could possibly be used as a control actuator instead of the fast-steering mirror. In fact, the CSA shaker is intended to be used as an inertial actuator in active vibration control applications. One shaker could be used as a disturbance source while the other attempts to attenuate the motion. Theoretically, the same adaptive filter methods can be used for this application.

- The accelerometer used as feedforward reference sensor was always mounted in the same location on the testbed. An interesting experiment would be to move the location of the accelerometer and observe the controllers performance. It has yet to be proved experimentally how important the accelerometer location is on the testbed.

THIS PAGE INTENTIONALLY LEFT BLANK

APPENDIX: EQUIPMENT SPECIFICATIONS

A. NEWPORT FAST-STEERING MIRROR

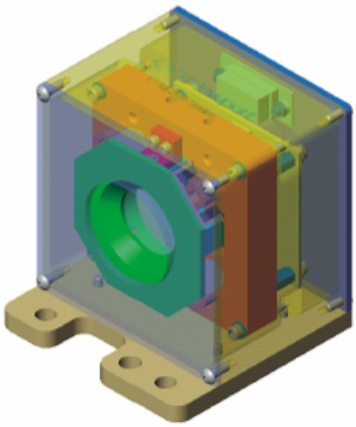

FSM Housing

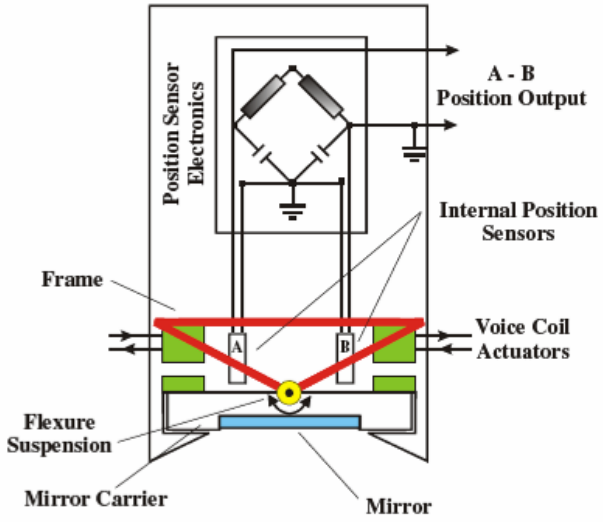

Figure 9 Typical FSM assembly showing the eight basic components

Figure 48. Newport FSM assembly.

3. Specifications

3.1 FSM-200 / FSM-CD100 Controller / Driver System

Number of Axes	2 (tip-tilt)
Angular Range from ±10 V	±26.2 mrad (±1.5°), mechanical[1]
Resolution	≤ 1 µrad rms, mechanical[1]
Repeatability	≤ 3 µrad rms, mechanical[1]
Accuracy From ±26.2 mrad, 25°C[1,2]	≤ 0.262 mrad (0.015°), mechanical[1]
Linearity From ±26.2 mrad, 25°C[1,2]	≤ 1.0%
Peak Angular Velocity	10 rad/sec
Peak Angular Acceleration	3500 rad/sec^2
Closed-Loop Amplitude Bandwidth[2] (-3 dB)	1 KHz at 10 mV (typical)
Closed-Loop Phase Bandwidth[2] (60° lag)	400 Hz (typical)
Gain Margin	≥ 10 dB
Phase Margin	≥ 45°
Response Flatness[2]	Peaking ≤3 dB
Large Angle Step Response, 26.2 mrad steps, mechanical[1]	3.5 ms rise time to 90% 12 ms settling time to 5%
Cross-axis Coupling, Static	≤ 0.1%
Cross-axis Coupling, Dynamic	≤ 0.1%
Powered Null Offset (Closed-Loop)	±1 mrad, mechanical[1]
Noise Equivalent Angle (1 Hz to 10 kHz)	≤ 3 µrad rms
Resolution of Local Position Sensor	≤ 0.5 µrad
Quiescent Power at FSM Assembly	≤ 5 W at any angle ±26.2 mrad
Operating Temperature[2]	0 to 50°C (32 to 122°F)
Storage Temperature	-20 to 55°C (-4 to 131°F)
Installation Category	II
Pollution Degree	2
Use Location	Indoor use only

Figure 49. Newport FSM specifications.

Relative humidity	< 95%, non-condensing
Operating altitude	< 3,000 m (10,000 ft)
Warm-up Time for Mirror Stability[2] at 25°C	≤ 10 minutes
Mirror Thermal Drift[2]	≤ 5 µrad/°C, mechanical[1]
Optical Axis Location Without Base	1.5 in. (38.1 mm) high, centered left-to-right
Mass with base	1.1 lb (0.5 kg)
FSM-200 Envelope Without Base [w × h × d]	3.0" × 3.0" × 2.3" (76.2 × 76.2 × 58.7 mm)
Interconnect Cable Length	9.8 ft (3 m)

Table 1 FSM-200/FSM-CD100 System Specifications

3.2 Dielectric Mirror Option

Mirror Substrate Material	Fused silica, BK7, Zerodur, or Pyrex
Mirror Retaining Mechanism	Bonded dielectric mirror, factory replaceable
Pivot Point of Axes (centered on mirror)	Gimbaled at mirror surface
Mirror Diameter	25.4 mm
Mirror Thickness	6.35 mm
Mirror Wedge	≤ 5 arc min
Clear Aperture (at 0° angle of incidence)	≥ 20.3 mm
Clear Aperture (at 45° angle of incidence)	≥ 14.4 mm
Reflectivity[3]	Common mirror coatings are available
Surface Flatness[3] (after coating & bonding)	≤ λ/10 at 632.8 nm over clear aperture
Surface Quality[3]	15-5 scratch-dig

Table 2 Dielectric Mirror Option Specifications

Figure 50. Newport FSM specifications.

3.3 Aluminum Mirror Option

Mirror Substrate	Diamond turned aluminum
Mirror Retaining Mechanism	Integral mirror, factory replaceable
Pivot Point of Axes (centered on mirror)	6.58 mm behind mirror surface
Mirror Diameter	50.8 mm
Clear Aperture (at 0° angle of incidence)	≥ 45.7 mm
Clear Aperture (at 45° angle of incidence)	≥ 32.3 mm
Reflectivity[4]	R > 90%, 0.5-11 µm
Surface Flatness[4]	≤ λ/4 P-V at 632.8 nm over clear aperture
Surface Roughness[4]	≤ 70 Å
Surface Quality[4]	60-40 scratch-dig

Table 3 Aluminum Mirror Option Specification

(1) Optical angular range is equal to twice the mechanical angular range.
(2) Measured under DIT control. Optical closed-loop performance is also determined by external feedback electronics.
(3) Optical parameters apply to central 80% of mirror aperture.
(4) Optical parameters apply to central 90% of mirror aperture.

3.4 FSM-CD100 Controller/Driver

Command Input and DIT Output	Analog, ±10 V = ±26.2 mrad
Peak Operating Power to Mirror	30 W
Continuous Max Operating Power to Mirror	15 W
Thermal Protection	60 °C at mirror coil
Current Protection	3 A
Operating Temperature[2]	0 to 50 °C (32 to 122 °F)
Storage Temperature	-20 to 55 °C (-4 to 131 °F)
Installation Category	II
Pollution Degree	2
Use Location	Indoor use only

Figure 51. Newport FSM and Controller/Driver specifications.

Relative humidity	< 95%, non-condensing
Operating altitude	< 3,000 m (10,000 ft)
Power	100-240 Vac ±10%, 47-63 Hz
Current consumption (typical)	0.40 A @ 100 Vac 0.25 A @ 240 Vac
Fuses	2 ea, 5 x 20 mm, slow-blow (T), rated 2.5 A, 250 Vac
Weight (with rack mounting flanges)	10.64 lb (4.83 kg)
Case Dimensions (excluding connectors & mounting flanges)	3.94" x 17.0" x 11.6" [h x w x d] (100 x 432 x 285 mm)

Table 4 FSM-CD100 Controller/Driver Specifications

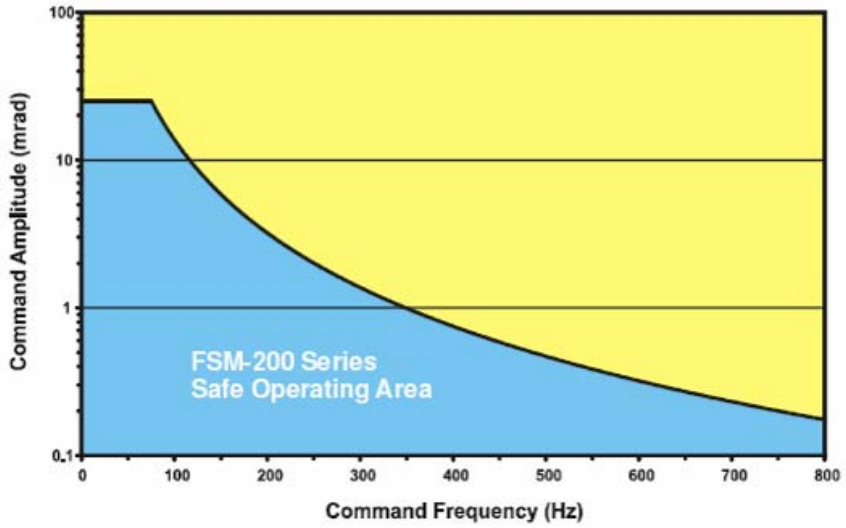

Figure 10 Safe Operating Area for FSM-200 Series fast steering mirrors.

Figure 52. Newport FSM and Controller/Driver specifications.

B. BAKER FAST-STEERING MIRROR

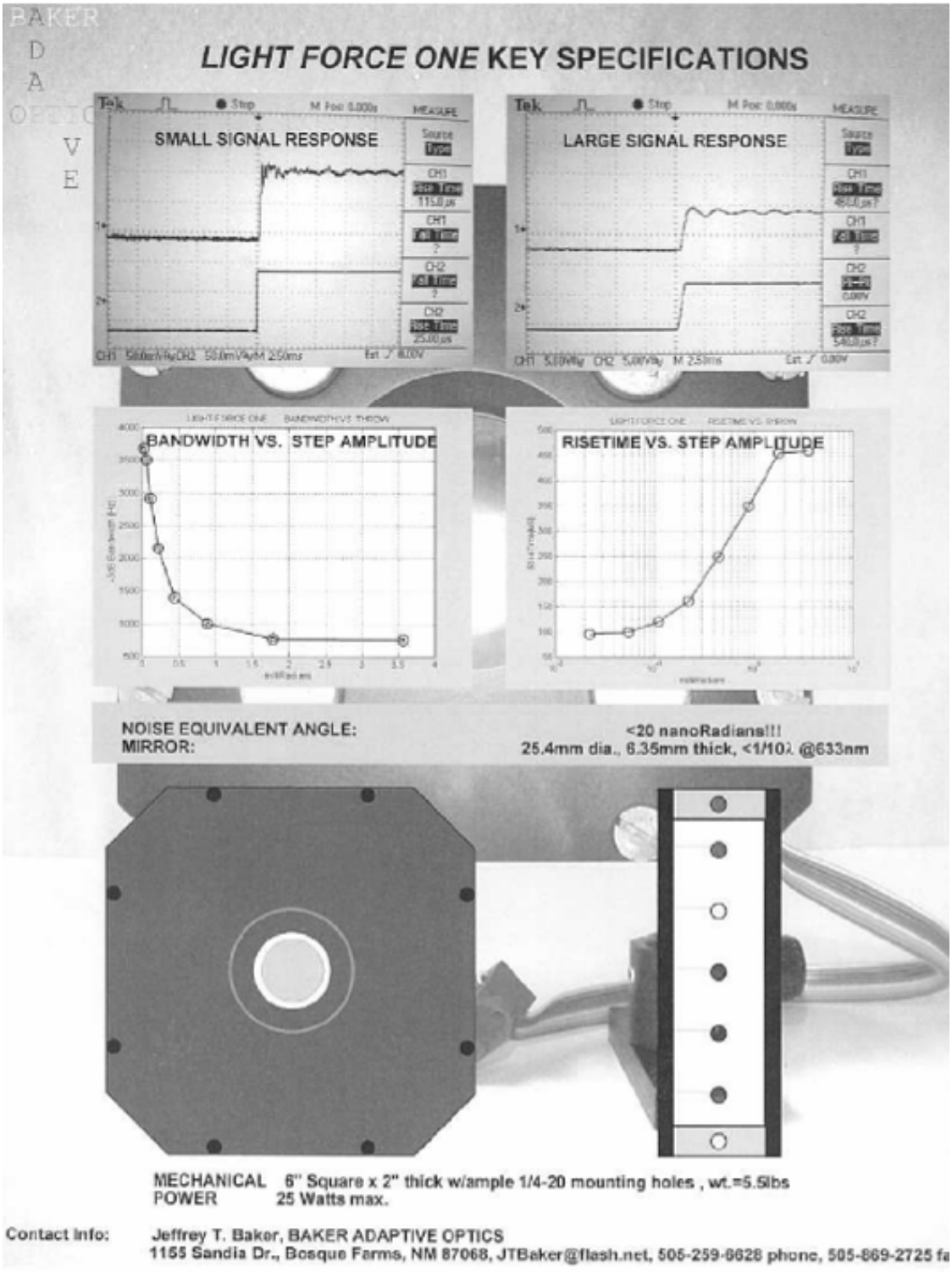

Figure 53. Baker Fast-Steering Mirror specifications. From Watkins [3]

C. AURA PRO-BASS SHAKER (SHAKER 1)

Specifications:	*Bass Shaker*	*Pro Bass Shaker*
Model Number	AST-1B-4	AST-2B-4
Suggested Retail Price Per Pair	$199	$239
Frame Size	5.4" W x 2.2" H	5.4" W x 2.2" H
Force, Peak	20 Lbf (89 N)	30 Lbf (132 N)
Effective Impedance	4 Ohms	4 Ohms
Power, Continuous	25 Watts RMS	50 Watts RMS
Power, Max	50 Watts RMS	75 Watts RMS
Height	2.2"	2.2"
Diameter	5.1"	6.2"
Weight	3.0 lb.	3.0 lb.
Resonance Frequency (fo)	40 Hz	40 Hz
Usable Frequency Range	20-80 Hz	20-80 Hz
UPC Code	7-94002-30750-1	7-94002-30770-9
QTY/Master Carton	8 Pairs	8 Pairs
Wt./Master Carton	53 Lbs.	55.24 Lbs.
Dimension of Master Carton	13.5" L x 13.0625" W x 11.375" H	15.75" L x 15.8125" W x 9.75" H
Master Carton/Pallet	36 M/C (288 Pairs)	24 M/C (192 Pairs)

Bass Shaker Frequency Response

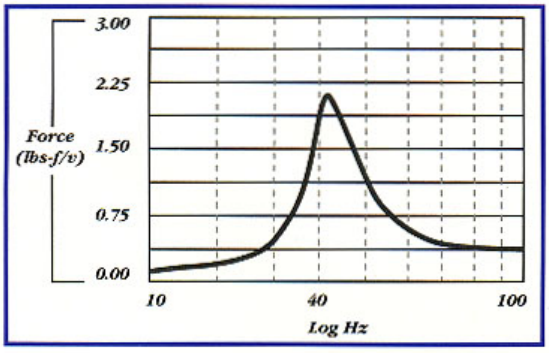

- A two-channel 50-100 Watt RMS/channel amplifier is recommended with one Bass Shaker operating from each channel.
- LPF (low pass filter), if used, should be set to 100 Hz.
- For best results, drive both Bass Shakers with same mono signal.
- Both Bass Shakers in an installation should be wired in phase. The Bass Shaker wiring is coded for phasing.
- Bass Shakers perform best when mounted rigidly to a compliant surface in the vehicle. The pan beneath the seats is usually an ideal location for mounting.
- Bass Shakers can be combined with a subwoofer.
- The 25 Watt RMS/channel Bass Shaker and 50 Watt RMS/channel Pro Bass Shaker are sold in pairs and are available with or without an optional two-channel Aura 50 Watt RMS/channel amplifier.

For additional information contact Aura Systems Interactive Division.

AURA
INTERACTIVE

A division of AURA SYSTEMS, INC.
2335 Alaska Avenue
El Segundo, CA 90245

Phone: 310-643-5300 Fax: 310-643-9463 800-909-AURA

Figure 54. Aura Pro Bass Shaker specifications.

D. CSA INERTIAL ACTUATOR (SHAKER 2)

SA Series Inertial Actuators

CSA Engineering, Inc.

- Inertial force generator
- 1-10 lbf broadband output (0 - peak)
- Peak outputs greater than 100 lbf
- Wide bandwidth (20 to 1000 Hz)
- Self contained

SA series actuators deliver inertial force over a wide bandwidth in compact, rugged, electromagnetically efficient forms. The actuators use an electromagnetic circuit with a moving magnet that allows the coil to be thermally grounded to the housing. Magnets are suspended by specially designed long life flexures. The force is generated along the axis of the cylindical units.

Typical applications include active damping or vibration cancellation, mounts for active vibration isolation, or disturbance generation. Dynamic amplification at frequencies near the actuator resonance results in large force outputs. A rigid housing enables direct insertion of the SA into structural load paths.

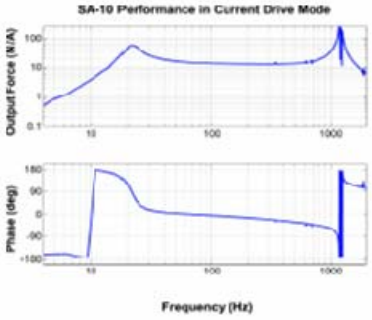

Actuators are specified by force capacity and internal suspension resonance. Standard options/accessories include alternative end caps, coils of specified impedance, a variety of cable interfaces, and current or voltage drive mode amplifiers. The overall design is easily customizable to meet the requirements of mounting configurations, drive electronics, or mass budgets.

The SA1, SA5, and SA10 are standard products. Also available are the SA2, SA35 and other non-standard models. Actuators are specified as SA*x*-*f* where *x* is the zero-peak force output at high frequency in pounds and *f* is the primary resonant frequency in Hz. For example, the SA5-60 produces 5 pounds force and has a 60 Hz resonance.

SPECIFICATIONS				
	SA1	SA5	SA10	Units
Rated Force Output*	1	5	10	lbf (0-peak)
Bandwidth	40-1000	20-1000	20-1000	Hz
Motor Constant**	0.5	2	5	lbf/Amp
Resonant Frequency***	30-200	30-200	30-200	Hz
Resistance**	2	2	2	Ohm
Total Mass	0.25	2.9	5.5	lbm
Diameter	35	76	93	mm
Height	30	66	92	mm

* Significantly greater forces possible with good heatsinking
** Typical values
*** User-specified. Manufactured to ± 2-3%

For more information, email *actuators@csaengineering.com*

Figure 55. CSA Inertial Actuator specifications.

E. KISTLER ACCELEROMETER

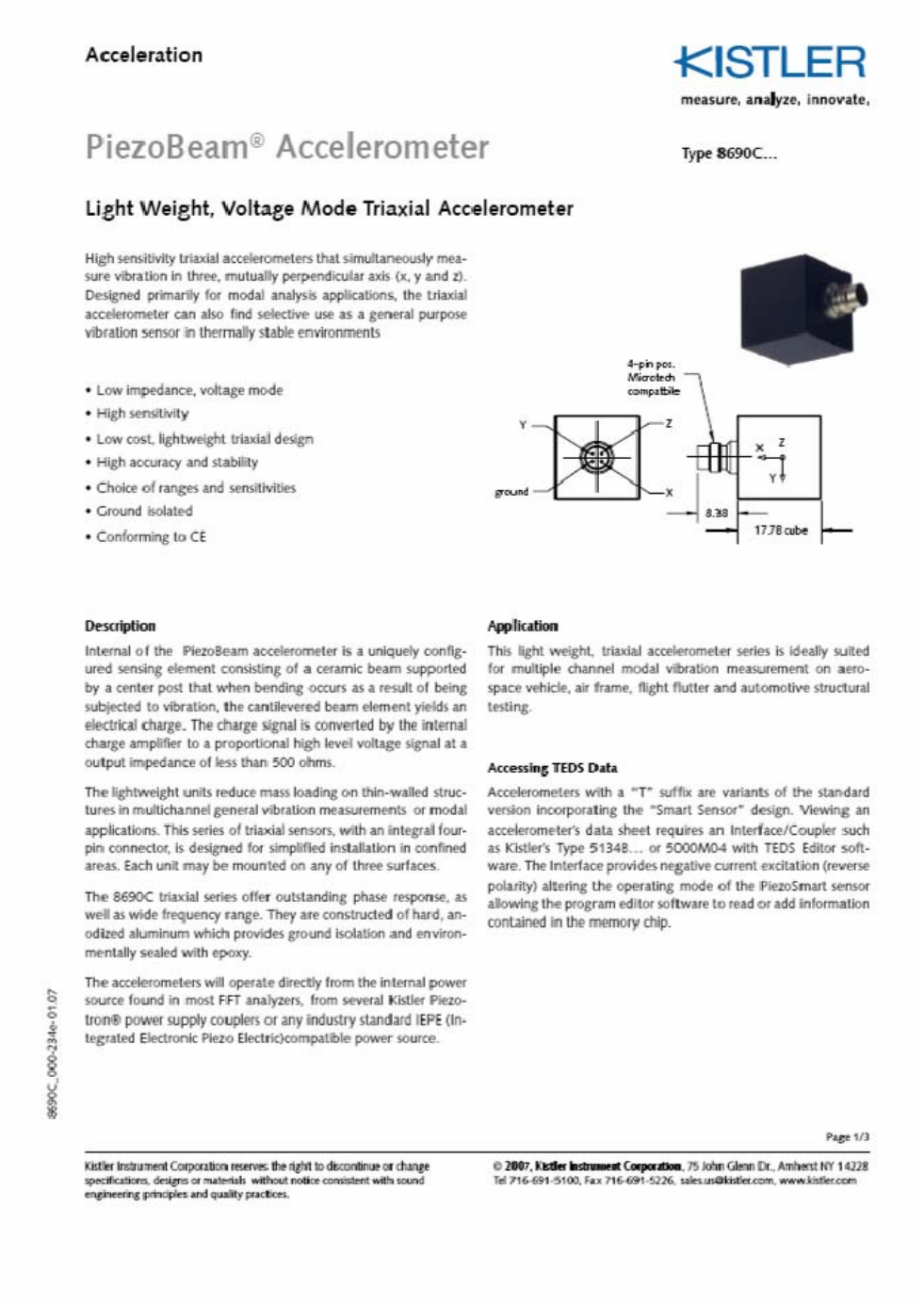

Acceleration

KISTLER
measure, analyze, innovate.

PiezoBeam® Accelerometer

Type 8690C...

Light Weight, Voltage Mode Triaxial Accelerometer

High sensitivity triaxial accelerometers that simultaneously measure vibration in three, mutually perpendicular axis (x, y and z). Designed primarily for modal analysis applications, the triaxial accelerometer can also find selective use as a general purpose vibration sensor in thermally stable environments

- Low impedance, voltage mode
- High sensitivity
- Low cost, lightweight triaxial design
- High accuracy and stability
- Choice of ranges and sensitivities
- Ground isolated
- Conforming to CE

4-pin pos. Microtech compatible
Y
Z
ground
X
8.38
17.78 cube

Description

Internal of the PiezoBeam accelerometer is a uniquely configured sensing element consisting of a ceramic beam supported by a center post that when bending occurs as a result of being subjected to vibration, the cantilevered beam element yields an electrical charge. The charge signal is converted by the internal charge amplifier to a proportional high level voltage signal at a output impedance of less than 500 ohms.

The lightweight units reduce mass loading on thin-walled structures in multichannel general vibration measurements or modal applications. This series of triaxial sensors, with an integral four-pin connector, is designed for simplified installation in confined areas. Each unit may be mounted on any of three surfaces.

The 8690C triaxial series offer outstanding phase response, as well as wide frequency range. They are constructed of hard, anodized aluminum which provides ground isolation and environmentally sealed with epoxy.

The accelerometers will operate directly from the internal power source found in most FFT analyzers, from several Kistler Piezotron® power supply couplers or any industry standard IEPE (Integrated Electronic Piezo Electric)compatible power source.

Application

This light weight, triaxial accelerometer series is ideally suited for multiple channel modal vibration measurement on aerospace vehicle, air frame, flight flutter and automotive structural testing.

Accessing TEDS Data

Accelerometers with a "T" suffix are variants of the standard version incorporating the "Smart Sensor" design. Viewing an accelerometer's data sheet requires an Interface/Coupler such as Kistler's Type 5134B... or 5000M04 with TEDS Editor software. The Interface provides negative current excitation (reverse polarity) altering the operating mode of the PiezoSmart sensor allowing the program editor software to read or add information contained in the memory chip.

8690C_000-234e-01.07

Page 1/3

Figure 56. Kistler Accelerometer specifications.

KISTLER
measure, analyze, innovate.

Technical Data

Type	Unit	8690C5	8690C10	8690C50
Acceleration Range	g	±5	±10	±50
Acceleration Limit	gpk	±8	±16	±80
Threshold nom.	grms	0,00012	0,00028	0,001
Sensitivity, ±5%	mV/g	1000	500	100
Resonant Frequency mounted, nom.	kHz	9	22	22
Frequency Response, ±5%	Hz	1 ... 3000	1 ... 5000	1 ... 6000
Phase Shift, <5°	Hz	4 ... 2000	4 ... 2000	4 ... 4000
Amplitude Non-linearity	%FSO	≤1	≤1	≤1
Time Constant nom.	s	1	1	1
Transverse Sensitivity max.	%	1	1	1
Long Term Stability	%	≤1	≤1	≤1
Environmental:				
Base Strain Sensitivity @ 250με	g/με	<0,001	<0,001	<0,001
Shock Limit (0,2ms pulse)	gpk	5000	10000	10000
Temperature Coeff. of Sensitivity	%/°C	-0,04	0,08	0,08
Temperature Range Operating	°C	0 ... 65	0 ... 65	0 ... 65
Temperature Range Storage	°C	-23 ... 95	-23 ... 95	-23 ... 95
Output:				
Bias nom.	VDC	11	11	11
Impedance	Ω	<500	<500	<100
Voltage full scale	V	±5	±5	±5
Current	mA	2	2	2
Source:				
Voltage	VDC	20 ... 30	20 ... 30	20 ... 30
Constant Current	mA	2 ... 18	2 ... 18	2 ... 18
Impedance min.	kΩ	>100	>100	>100
Construction:				
Sensing Element	type	Ceramic Bimorph/Bender	Ceramic Bimorph/Bender	Ceramic Bimorph/Bender
Housing/Base	material	Al. Hard Anodized	Al. Hard Anodized	Al. Hard Anodized
Sealing-housing/connector	type	Epoxy	Epoxy	Epoxy
Connector	type	4-pin pos.	4-pin pos.	4-pin pos.
Ground Isolated min.	MΩ	10	10	10
Weight	grams	11,2	11,2	11,2
Mounting (thread/stud)	type	Wax/Adhesive	Wax/Adhesive	Wax/Adhesive

1 g = 9,80665 m/s², 1 inch = 25,4 mm, 1 gram = 0,03527 oz, 1 lbf-in = 0,1129 Nm

8690C_000-234e-01.07

Figure 57. Kistler Accelerometer specifications.

F. NEWPORT VIBRATION ISOLATION PLATFORM

BenchTop™

Compact Pneumatic Vibration Isolation Platform with Self-Leveling

- Hybrid chamber/laminar flow design maximizes isolation bandwidth
- Integrated leveling values improve repositioning accuracy after disturbance
- Low profile, compact design minimizes footprint

BenchTop™ Compact Vibration Isolation Platforms provide the rock solid performance and ultra-small packaging that is so critical to today's life science and disk drive applications.

Exclusive Stabilizer™ vibration isolation technology, adapted from our acclaimed Stabilizer Model I-2000 Vibration Isolators, is at the heart of the system. This technology is renowned for compact size, faster settling times, superior high-center-of-mass stability, lower natural frequency, and a patented, self-centering piston mechanism.

Four isolator modules recessed into the bottom of the platform achieve top-notch table top vibration isolation. Each contains a pneumatic, flexible rolling diaphragm that supports the load, thereby decoupling vibrations from the isolated platform. If the platform is disturbed, the modules automatically relevel the platform using compressed air.

No more bulky canisters to impede instrument access, restrict arm positioning or crowd workspaces. Newport's hybrid-chamber design allows all vibration modules to be completely hidden within the platform.

The BenchTop also minimizes fatigue. That's because its low profile design adds only about two inches of height to your support surface. Add optional padded armrests - and you can work for hours with unparalleled ease.

Video image of human spinal cord neurons acquired through a camera/microscope system placed on a BenchTop™ unit. Available with either plastic laminate or stainless steel tops, the BenchTop is ideal for providing vibration isolation in applications involving time lapse photography, videomicroscopy, probing and manipulation of cells under high magnification.

Specifications

	Sizes (W x L) [In. (cm)]	Maximum Recommended CG Height [In. (mm)]
	20 (50.8) x 24 (61.0)	8 (203.2)
	24 (61.0) x 36 (91.4)	11.0 (279.4)
Platform Thickness:		
Thickness, BenchTop, Standard Laminate [In. (mm)]		2.0 (51)
Thickness, BenchTop, Stainless [In. (mm)]		2.2 (56)
Thickness, BenchTop Stainless, w/holes [In. (mm)]		3.0 (75)
Mounting Holes		1/4-20 on 1 In. centers (M6-1.0 on 25 mm centers)
Max. Load Range (lb)		175 (80)

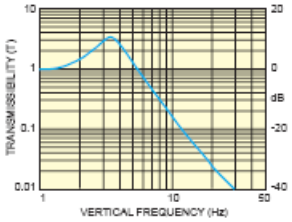

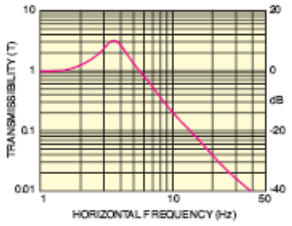

Newport

Phone: 1-800-222-6440 · Fax: 1-949-253-1680

Figure 58. Newport Vibration Isolation Platform specifications.

BenchTop Isolation Performance

Model	Vertical Isolation* Res (Hz)	Vertical Isolation* 10Hz (%)	Horizontal Isolation* Res (Hz)	Horizontal Isolation* 10Hz (%)	Amplification at Resonance Vert (dB)	Amplification at Resonance Horz (dB)	Maximum Load per Isolator [lb (kg)]	Re-leveling Accuracy [in. (mm)]	Self Centering
CM-225	3.2	90	3.6	96	12	10	60 (27)	0.025 (0.6)	Yes

* Nominal resonance peak, isolation and damping at full rated load

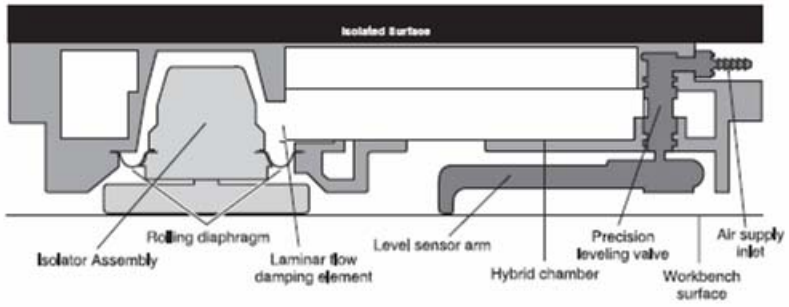

Ordering Information

Model	w/ Cleanroom prep. Model	Size (W x L) [in. (cm)]
BT-2024	BTC-2024	20 (50.8) x 24 (61.0)
BT-2436	BTC-2436	24 (61.0) x 36 (91.4)

Options and Accessories

Append these codes to the BenchTop model number. For example, the order number for a 24 in. x 36 in. (61.0 x 91.4 cm) BenchTop with a sealed mounting hole stainless steel work surface is BT-2436-OPT 02.

Option Code	Description
01	Stainless steel work surface (no mounting holes)
02	Stainless steel work surface (mounting holes)

For metric M6-1.0 sealed mounting holes, add an M- prefix to the order number, for example, M-BT-2436-OPT 02

Accessories

Model (Metric)	Description
ACGP	Air Compressor, high throughput
ACMP (ACMP-02)	Air Compressor, low noise
ARF	Air Regulator/Filter
BT-A	Armrest
BT-C	Cable Manager™

Figure 59. Newport Vibration Isolation Platform specifications.

LIST OF REFERENCES

[1] E. H. Anderson, R. L. Blankinship, L. P. Fowler, R. M. Glaese, P. C. Janzen, "Adaptive Filtering and Feedforward Control for Suppression of Vibration and Jitter," in Proceedings of SPIE Defense and Security Symposium, Orlando, Florida, April 2007.

[2] R. J. Watkins and B. N. Agrawal, "Use of least means squares filter in control of optical beam jitter," Journal of Guidance, Control, and Dynamics, vol. 30, no. 4, pp. 1116–1122, July-August 2007.

[3] R. J. Watkins, "The adaptive control of optical beam jitter," Ph.D. dissertation, Naval Postgraduate School, Monterey, CA., December 2004.

[4] B. E. Bateman, "Experiments on laser beam jitter control with applications to a shipboard free electron laser," Master's thesis, Naval Postgraduate School, Monterey, CA., December 2007.

[5] P. K. Orzechowski, J. S. Gibson, and T.-C. Tsao, "Optimal disturbance rejection by LTI feedback control in a laser beam steering system," in Proceedings of the 43th IEEE Conference on Decision and Control, Atlantis, Paradise Island, Bahamas, December 2004, pp. 2143– 2148.

[6] P. K. Orzechowski, N. Chen, S. Gibson, and T.-C. Tsao, "Optimal jitter rejection in laser beam steering with variable-order adaptive control," in Proceedings of SPIE, vol. 6569, 2007, 65690V.

[7] P. K. Orzechowski, N. Y. Chen, J. S. Gibson, and T.-C. Tsao, "Optimal Suppression of Laser Beam Jitter by High-Order RLS Adaptive Control," IEEE Transactions on Control Systems Technology, vol. 16, no. 2, pp. 255-267, March 2008.

[8] P. K. Orzechowski, J. S. Gibson, and T.-C. Tsao, "Adaptive Control of Jitter in a Laser Beam Pointing System," in Proceedings of the American Control Conference, Minneapolis, Minnesota, USA, June 2006, pp. 2700– 2705.

[9] N. O. P´erez Arancibia, N. Y. Chen, J. S. Gibson, and T.-C. Tsao, "Variable-order adaptive control of a microelectromechanical steering mirror for suppression of laser beam jitter," Optical Engineering, vol. 45, no. 10, October 2006, 104206.

[10] N. O. P´erez Arancibia, N. Chen, S. Gibson, and T.-C. Tsao, "Adaptive control of jitter in laser beam pointing and tracking," in Proceedings of SPIE, vol. 6304, 2006, 63041G.

[11] S.-B. Jiang and J. S. Gibson, "An unwindowed multichannel lattice filter with orthogonal channels," IEEE Transactions on Signal Processing, vol. 43, no. 12, pp. 2831–2842, December 1995.

[12] M. A. McEver, D. G. Cole, and R. L. Clark, "Adaptive feedback control of optical jitter using Q-parameterization," Optical Engineering, vol. 43, no. 4, pp. 904–910, April 2004.

[13] H. Yoon, "Laser Beam Jitter Control Using Recursive-Least-Square Adaptive Filters," Submitted to Optical Engineering.

[14] S. M. Kuo and D. R. Morgan, Active Noise Control Systems: Algorithms and DSP Implementations. New York: Wiley-Interscience, 1996.

[15] S. Haykin, Adaptive Filter Theory, 4th Ed., Prentice-Hall, Upper Saddle River, NJ, 2002.

[16] K. Ogata, Modern Control Engineering, 4th Ed., Prentice-Hall, Upper Saddle River, NJ, 2002.

[17] R. S. Quimby, Photonics and Lasers, Wiley-Interscience, Hoboken, New Jersey, 2006.

INITIAL DISTRIBUTION LIST

1. Defense Technical Information Center
   Ft. Belvoir, Virginia

2. Dudley Knox Library
   Naval Postgraduate School
   Monterey, California

3. Physics Department
   Naval Postgraduate School
   Monterey, California

4. Mechanical and Astronautical Engineering Department
   Naval Postgraduate School
   Monterey, California

5. Professor Brij Agrawal
   Naval Postgraduate School
   Monterey, California

6. Professor Andres Larraza
   Naval Postgraduate School
   Monterey, California

7. Dr. Hyungjoo Yoon
   Naval Postgraduate School
   Monterey, California

8. Mr. Charles Staley
   771 TS / EWAP
   Edwards AFB, California

9. Mr. Michael Beerer
   771 TS / EWAP
   Edwards AFB, California